Discharge Measurement in Streams Using a Large-Scale Particle Image Velocimetry Prototype

Adrian A. Harpold

Thesis submitted to the Faculty of the
Virginia Polytechnic Institute and State University
In partial fulfillment of the requirements for the degree of

Masters of Science in Biological Systems Engineering

Saied Mostaghimi, Chair
Theo Dillaha
David Vaughan
Pavlos Vlachos

January 11, 2005
Blacksburg, VA

KEYWORDS: LSPIV, stream, discharge, monitoring

Discharge Measurement in Streams Using a Large-Scale Particle Image Velocimetry Prototype

Adrian A. Harpold

ABSTRACT

Flow information is necessary in many diverse applications including water supply management, pollution control, irrigation, flood control, energy generation, and industrial use. New technologies have been developed for the establishment of stage-discharge relationships due to concerns about costs, accuracy, and safety of traditional discharge estimation methods. One emerging technology for measuring open-channel flow is Large-Scale Particle Image Velocimetry (LSPIV).

LSPIV is a system capable of measuring surface velocity by collecting and analyzing recorded images of the stream surface. LSPIV has several advantages over conventional discharge measurement techniques: LSPIV is safer, could be automated to reduce labor, and could produce 'real-time' discharge measurements. Therefore, the overall goal of this study was to evaluate the accuracy and feasibility of using LSPIV to measure discharge in low-order streams. The specific goals were to develop and test a prototype under varying conditions in a laboratory flume, adapt the prototype for field conditions, test the accuracy of the prototype in the field, and assess and recommend improvements for LSPIV operation as a stream discharge measuring device.

The laboratory experiments results indicated that LSPIV accuracy was influenced by camera angle, surface disturbances and flow regime (Froude number), and particle seeding density. Camera angle was optimum around 15 degrees, with larger camera angles producing more error due to image distortion. Conditions at high Froude numbers

likely produced out-of-plane displacement losses due to surface disturbances. Low Froude numbers also showed under-predictions, which were likely due to agglomeration of the tracer particles at low velocities. Finally, the laboratory results demonstrated that tracer seeding density should be maximized and that densities below three particles per interrogation window should significantly reduce LSPIV accuracy.

The LSPIV prototype was tested at two low-order streams after developing a field prototype and operating procedures. Under field conditions, the prototype acquired consistent images, performed the necessary image processing, and established rules for estimating input parameters. The accuracy of LSPIV was evaluated using a Flo-Mate 2000 current meter and a permanent weir. Overall, twenty discharge measurements were taken with each measuring device at Stroubles Creek and Crab Creek. The discharges measured ranged from 0.12 to 63 cfs, which corresponded to a large range of velocities, with both simple and complex flow patterns. Problems were encountered from surface glare reducing image quality at both sites.

The LSPIV prototype was accurate for most measuring conditions with a mean error of -1.7%, compared to the weir measurements. The LSPIV measurements tended to under-predict discharge at high stages and had greater error at moderate flows (up to 39%) compared to the weir. However, at low flow conditions LSPIV showed improved discharge accuracy over the current meter, in comparison to the weir measurements. The LSPIV discharge measurements were not statistically different from either the current meter or weir ($\alpha = 0.05$). Finally, the LSPIV discharge measurements had an uncertainty of approximately ±14% (at a 95% confidence interval).

In conclusion, LSPIV accuracy can be degraded by surface disturbances, inadequate illumination, and poor seeding densities. However, LSPIV showed adequate accuracy with the potential to become competitive with conventional discharge measurement techniques and therefore, has the potential to reduce costs and increase the geographic extent of surface water monitoring networks.

Acknowledgements

I would like to thank my advisor, Dr. Saied Mostaghimi, for his guidance, wisdom, and patience. I would also like to thank my other committee members, Dr. Theo Dillaha, Dr. David Vaughan, and Dr. Pavlos Vlachos. Additionally, Kevin Brannan spurred my interest in this field and provided me inexhaustible support and guidance. Next, I would like to thank Dr. Tamim Younos and the Virginia Water Resources Research Center for providing a seed grant. The NSF REU program also provided support and I would especially like to thank Cami Johnson, Sean Tolle, and Dr. David Vaughan for their help. There were also many people that made this project possible: Jeff Wynn, Dr. Christian Mariger, Laura Teany, Matt Habersack, Christine Bechtel, and Dave Borys. Lastly, I would like to thank Dr. Theresa Wynn who was my inspiration for pursuing a career in research. Most importantly, I would like to thank my parents for instilling in me a never ending thirst for knowledge (for better or worse).

TABLE OF CONTENTS

TABLE OF FIGURES

TABLE OF TABLES

CHAPTER 1: INTRODUCTION

Open channel flow is a component of the hydrologic cycle where measurements representing large geographic extents are economically feasible and can be achieved with reasonable accuracy (Herschy, 2002). Good water management is therefore founded on precise open channel flow measurements. Flow information is necessary in many diverse applications including water supply management, pollution control, irrigation, flood control, energy generation, and industrial use (Herschy, 2002). Flow information is dependent on obtaining field measurements in sometimes challenging conditions.

Stream gauging stations have been used as the standard method of measuring open channel flows for over 100 years (Costa et al., 2000). A gauging station is generally an automated system that measures the depth of flow in the channel (stage) and estimates flow using a stage-discharge relationship. If a calibrated control structure is not installed in the stream, the channel bathymetry is surveyed and discharge is measured using current meters, in difficult measuring conditions, Acoustic Doppler Velocimetry (ADV) (York and Oberg, 2002). Flow measurements, across a large range of conditions, are used to develop a channel specific stage-discharge relationship. Flow monitoring is generally labor intensive and a costly endeavor (Grant, 1997).

Due to funding constrains, state and federal agencies can employ only a limited number of field technicians for stream flow measurements (Melcher et al., 1999). As a result, the technicians can make only a limited number of individual flow measurements. In order to develop rating curves with a high level of accuracy, much of the technicians' time is devoted to a limited number of streams. Consequently, funding limits the capacity to expand the number of gauging stations.

New technology has been developed for the establishment of stage-discharge relationships due to concerns about costs, accuracy, and safety of traditional discharge estimation methods

during high flow conditions (Grant, 1997). The US Geological Survey (USGS) is investigating technologies for direct, continuous, non-contact measurement of open channel discharge (Melcher et al., 1999). During flood conditions, any instrument that must be placed in the water (e.g. current meter) could produce high measurement errors and would be a potential hazard to those operating the instrument (Melcher et al., 1999, Cheng et al., 2001). Both flood and pollution control techniques require accurate measurements, throughout the flow regime of a stream, especially during high flows (Costa et al., 2000).

Research by Costa et al. (2000) showed that it is possible to measure discharge with non-contact methods that maintain accuracy levels equivalent to those of conventional methods. Cruetin et al. (2003) demonstrated that large-scale particle image velocimetry (LSPIV) might be a viable method for collecting discharge measurements accurate enough for rating curve development. The USGS and other researchers have concluded that LSPIV is a promising technology for non-contact remote flow measurement (Bradley et al., 2002; Melcher et al., 1999).

Large-Scale Particle Image Velocimetry (LSPIV) is a system capable of measuring surface velocity by collecting and analyzing recorded images of the flow field (the stream surface). The LSPIV system tracks the movement of 'tracers' on the water surface through successive images using statistical correspondence. Cross-correlation algorithms divide the image into small interrogation areas; each producing one displacement vector. The velocity is the ratio of the particle displacement divided by the elapsed time between images. LSPIV is an offshoot of conventional PIV, classical flow visualization, and laser speckle velocimetry (Adrian, 1991).

Significant work has been done to refine methodologies and techniques involved in PIV, but its application to the measurement of open channel flows (LSPIV) is more recent. Therefore, only a limited amount of field data is available to verify the accuracy of LSPIV velocity measurements. For example, research conducted by Bradley and Kruger (2002) indicated that discharge

measurements determined with LSPIV are as accurate as discharge measured using conventional methods. Bradley and Kruger (2002) compared discharge measurements from LSPIV and current meter methods for a stream in Iowa with a drainage area of 150 km^2. The study found differences between current meter and LSPIV discharge measurements were within the estimated standard error of the current meter. In a more recent study, Creutin et al. (2003) measured discharge in a 70-m cross-section of the Iowa River (8470 mi^2 watershed). Their results indicate that LSPIV is capable of constructing a rating curve accurately and quickly with a stationary camera that is operated remotely.

Use of LSPIV for flow measurements in low-order streams has several advantages. LSPIV is not as labor intensive and does not present the safety concerns of the conventional methods during high-flow events. The technology used in LSPIV is relatively inexpensive, and will become even cheaper as the cost of information technology continues to decrease (Costa et al., 2000). Furthermore, LSPIV shows promise for remote monitoring applications (Bradley et al., 2002, Cruetin et al., 2003), which could also reduce labor and data management costs (Melcher et al., 1999). These cost-savings could allow for the expansion of stream flow monitoring network in a region or a state (Cheng et al., 2002). The increase in the geographic extent of stream monitoring would greatly enhance our understanding of the quantity and quality of our water resources.

Another potential benefit of the LSPIV technology could be enhancement of state's efforts to assess pollutant discharges and manage water resources. For example, the Commonwealth of Virginia is required by the Clean Water Act to develop a TMDL (Total Maximum Daily Load) for any waterbody that does not meet water quality standards. Stream discharge measurements are used to calibrate models that are in turn used to estimate the reductions in both point and nonpoint source pollution necessary to achieve water quality standards. Currently, there is considerable

uncertainty in the pollutant allocation process because of scarcity of observed flow data in some areas, particularly for upland watersheds dominated by nonpoint pollution (NRC, 2001). Furthermore, the recent extreme weather events in Virginia and the region (e.g. droughts and floods) have highlighted the value of stream flow monitoring. Quantifying the Commonwealth's water resources allows for better allocation of water for human consumption, irrigation, and aquatic habitat. Flow data are needed to better understand watershed dynamics, and for calibration and validation of hydrologic models, which are critical for efficient and equitable management of Virginia's water resources.

Previous applications of LSPIV to flow monitoring systems have been limited. Additionally, no work using LSPIV has been conducted in the streams of Virginia. Semi-automated LSPIV systems show promise as an inexpensive non-contact method for flow measurement in low-order streams within the small watersheds of Virginia. More efficient rating curve development could increase the number of streams that are monitored, and thereby help better manage water resources.

1.1 Goal

The overall goal of the study was to evaluate the accuracy and viability of using large-scale particle image velocimetry (LSPIV) to measure discharge rates in low-order streams of upland watersheds. The specific objectives were to:

- Construct a laboratory-scale LSPIV prototype for measuring discharge rates using surface velocities in a laboratory flume and test the accuracy of the prototype under various conditions.
- Adapt the laboratory prototype for measuring flow rates in low-order streams by constructing a field prototype, develop an operation procedure, and conduct an accuracy analysis of the prototype under varying field conditions.
- Assess and recommend improvements for LSPIV operation as a stream discharge measuring device in Virginia's upland watersheds.

1.2 Null Hypothesis

The LSPIV prototype will provide discharge measurements with accuracy comparable to those of current meters and control structures.

CHAPTER 2: LITERATURE REVIEW

Stream gauging stations are the conventional method of measuring open channel discharge (Costa et al., 2000). A gauging station is generally an automated system that measures the depth of flow in the channel (stage). Flow is then estimated using a stage-discharge relationship. If a calibrated control structure (e.g. weir) is not installed in the stream, the channel bathymetry is surveyed and flow is measured using current meters, pressure sensors or, in difficult measuring conditions, Acoustic Doppler Velocimetry (York and Oberg, 2002). However, these conventional flow monitoring techniques are generally labor intensive and costly (Grant, 1997). These limitations are the impetus behind the development of new discharge measurement techniques (Melcher et al., 2000).

Large-Scale Particle Image Velocimetry (LSPIV) is an emerging non-contact technology for measuring stream discharge. LSPIV uses a system that measures the surface velocity by collecting and analyzing recorded images of the flow field (the stream surface). The LSPIV system tracks the movement of 'tracers' on the water surface through successive images. Computer algorithms divide the image into small areas; each producing one displacement vector. The velocity is the ratio of the particle displacement divided by the elapsed time between images. LSPIV technology is an offshoot of classical flow visualization, laser speckle velocimetry, and conventional particle image velocimetry (PIV) (Adrian, 1991).

2.1 Background

PIV development has been rapid because of the advances in technology over the last 20 years. The development of PIV has been aided by parallel advances in optical measuring techniques, image processing, and flow visualization (Grant, 1997). Computer and digital video technology has eliminated many problems with processing time and digitizing photographic

images (Kruger, 2003). Charge-Coupled Device (CCD) cameras and new software have quickly moved the prototype stage of PIV into industrial and university laboratories (Usera, 1999). Currently, custom and commercial PIV systems are routinely used for aerodynamic and hydraulic research and in the automotive industry (Raffel et al., 1998). Adrian (1991) and Grant (1997) provide a concise history of PIV development and applications.

The development of LSPIV is more recent. LSPIV is the application of PIV to larger imaging areas for the purpose of measuring macro scale phenomena, such as open channel flow. LSPIV has simplifications over PIV, as well as unique problems. There have only been a limited number of studies on LSPIV applications to open channel discharge measurement (Appendix Appendix A: Comparison of Equipment and Image Processing Parameters Used). The main developers of LSPIV are at the Iowa Institute of Hydraulic Research (IIHR) and Gifu University in Japan. The most relevant research is reviewed in this chapter.

2.2 Steps in LSPIV Procedure

The LSPIV technique employs several steps to measure discharge in open-channels. Each step is a distinct set of routines often requiring specialized equipment. Figure 1 outlines the steps in LSPIV for measuring discharge in a low-order stream. Initially, site selection determines an optimum location for the measuring device. The images are recorded and saved during the image acquisition step. The images can be altered to improve results using image enhancement. Next, the images must be registered to the physical location and transformed to remove spatial distortion. In the image-evaluation step, the surface velocities are determined. If some velocities are incorrect, post-processing replaces the erroneous data. The corrected velocity values must be averaged spatially and temporally before a discharge can be estimated. The data can then be transferred to a remote location for further use. The steps from image acquisition to evaluation

will be referred to as 'pre-processing'. Additionally, steps after image evaluation are grouped together as 'post-processing'.

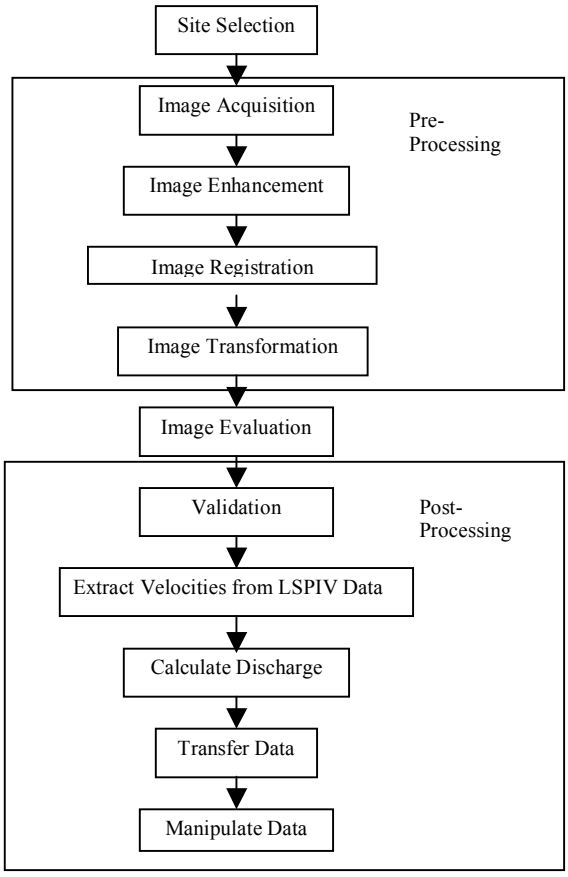

Figure 1. Flowchart showing the generalized steps involved in LSPIV. These steps are developed specifically for LSPIV application to low-order stream discharge measurement.

Although not every LSPIV application follows this exact method, the order of the steps presented in Figure 1 is consistent with the proposed work at Virginia Tech. It is also important to note that Figure 1 does not include the trial and error repetitions necessary to optimize various steps (Fujita et al., 1998). Bradley et al. (2002) noted that every measuring site would require the optimization of many image processing parameters. A brief description of various steps involved in LSPIV is included in the following sections.

2.2.1 Site Selection

The location of the LSPIV measuring equipment must maximize the accuracy and usefulness of the discharge data collected. International standards recommend locations that have long-term reach stability and ideal flow conditions. Additionally, site selection is based on criteria unique to LSPIV. The sampling location must be sufficiently illuminated, protected against equipment damage, and cannot have obstructions in the camera view. Important considerations in selecting appropriate site include the following (ISO 1997):

- Channel should be straight and uniform with a slope that minimizes abnormal velocity distributions,
- Flow direction should be parallel to the measurement section,
- The bed and margins of the channel should be stable and well-defined,
- The curves of the distribution of velocities should be consistent in the vertical and horizontal planes of measurement, and
- Vortices and dead water and confluences should be avoided.

The length of stream necessary for LSPIV measurements varies. Increased reach length improves the velocity averaging techniques, but is limited by camera lens and field-of-view.

2.2.2 Image Acquisition

Good image acquisition is crucial for obtaining accurate measurements with LSPIV. There are three key components to image acquisition using LSPIV. First, there must be adequate features on the stream surface to view. Second, the stream must be sufficiently illuminated to create contrast between the tracers and the surface. Finally, the camera must be able to capture the image field at the frame rate, field-of-view, and resolution required. Appropriate incorporation of all of these components is a prerequisite for the development of a functioning LSPIV device.

Researchers have not yet found an optimum tracer for large-scale outdoor LSPIV applications. A low-cost biodegradable material is necessary for LSPIV to be applied to monitoring stream and river discharges (Fujita et al., 1998). Several important characteristics constrain tracer particle selection:

- Particles must be biodegradable, environmentally safe, and low cost,
- Particles must be of sufficient size for image evaluation,
- Particles must sufficiently contrast with the background, and
- Particles must not agglomerate and must keep a uniform distribution over the image reach (although most evaluation methods can follow groups of particles).

Particles must also be applied with sufficient seeding density and distribution to capture velocity measurements across the image plane. The seeding density is defined as the number of tracer particles on the surface during image acquisition. Seeding density can be controlled (added by hand or with automated equipment) and is correlated to spatial resolution (York and Oberg, 2002). At larger seeding densities, the probability of predicting a valid displacement increases because more image pairs are present (Lee et al., 2002). However, excessive seeding densities can alter flow or make it difficult to illuminate all the particles (Gui and Merzkirch, 2000). Therefore, a homogeneous distribution of particles at a medium seeding density is optimum for image evaluation (Lee et al., 2002). Cruetin et al., (2003) found that seeding densities are not important near the river banks because of typical cross-correlation algorithms. The exact size and number of tracers depend on the evaluation algorithm used as discussed in section 2.2.5 Image Evaluation. The physical characteristics of the particles control their density and distribution.

The particles physical characteristics are important in numerous ways. For example, the particle diameter can affect the accuracy of LSPIV (Raffel et al., 1998). The diameter of the particles is a compromise between an adequate response to the fluid motion (small particles and a

density close to water) and a high signal-to-noise ratio (characteristic of large particles) (Melling, 1997). Small particles can also cause 'peak-locking effects', where displacements become biased to an integral pixel value. The optimum particle size for cross-correlation evaluation is 2.0 pixels (Raffel et al., 1998). However, the physical size of 2.0 pixels varies with field-of-view. Therefore, the size and type of the particles is a function of the field-of-view and resolution of the camera.

Cruetin et al. (2003) used natural tracers such as bubbles, foam, or ripple features. However, these particles may or may not be sufficient, and are rarely present in low-flow conditions. Another possibility is to add biodegradable tracers to the stream surface. Several tracers have been studied: straw, wood spheres, and biodegradable starch peanuts (Raffel et al., 1998 and Weitbrecht et al., 2002). Bradley et al. (2002) introduced leaves as tracers and had good results. However, the leaves were introduced manually to the stream.

Another important consideration is how tracers will be added to the water surface, especially in remote applications. Virtually no practical field research has been performed in this area. Weitbrecht et al. (2002) investigated a particle dispenser in a laboratory application. The dispenser used a roller brush driven by an AC motor to homogeneously seed 2-mm plastic beads. Ultimately, the design of a particle dispenser will be a function of the tracer selected. Therefore, it will be necessary to identify a low-cost and biodegradable tracer before the corresponding particle-dispenser can be designed. Additionally, adequate illumination is necessary for any particle selected.

Illumination is necessary to produce image resolution with a useable set of grey-levels (Etterma et al., 1997). A constant illumination is needed during image recording. PIV recording can use lights, lasers, or natural illumination. However, natural light is adequate for measuring stream flow in many outdoor conditions (Fujita et al., 1998, Bradley et al., 2002, Cruetin et al.,

2003). Unfortunately, it is sometimes difficult to achieve adequate illumination in field conditions. Cruetin et al. (2003) reported shadows and reflections introduce motionless patterns that caused significant analysis problems. Error caused by poor illumination can sometimes be solved by altering the image or using specialized camera lenses. If stream discharge measurements need to be collected in the dark, it will necessitate the use of artificial illumination.

The use of artificial illumination for LSPIV applied to stream discharge measurement is constrained by several factors. Safeguarding the equipment for rain, high water, and vandalism are serious concerns. The power required by lights is another problem in more remote locations. One way to conserve power is to only use light when recording images. Weitbrect et al. (2002) integrated a timing board that controlled illumination with the image capturing. However, Etterma et al. (1997) found that a constant illumination is needed to ensure accurate velocity measurement. Most laboratory LSPIV experiments have used halogen floodlights. Using a 'low-light' camera is an alternative to external lighting.

Selection of the proper camera is essential to the accuracy of LSPIV measurements. Cameras vary considerably in cost, resolution, and other specialized features. When selecting a camera, several considerations should be made including the size and coverage of the lens, the resolution of the camera, the image recording speed, and the cost and size of the camera. The low cost and availability of standard digital video equipment (and the associated computer hardware and software) makes their use for LSPIV very attractive (Raffel et al., 1998). The real strength of digital LSPIV recordings is that images can be captured in real-time, viewed, and processed with minimum delay. This allows for real-time modification of the seeding density, illumination, and other parameters (Willert and Gharib, 1991). However, trial and error is always necessary to optimize techniques at each measuring location (Fujita et al., 1998).

Different cameras are appropriate for laboratory versus outdoor use. LSPIV researchers have used small low-resolution video and digital cameras in flumes and models. Digital cameras are especially appealing for laboratory experiments because of their ease of use. Additionally, current research in LSPIV has used video recordings for large-scale open channel flow measurement. Cruetin et al. (2003) used a Sony DCR-TR V320 camera installed 14 m above the water surface to view 5000 m^2 area. Bradley et al. (2002) used a Panasonic Palmcorder PV IQ405 video camera for measurement on a river. Fujita et al., (1997) used a CCD camera to measure discharge on a river with an image area of 44,930 m^2 (512 X 512 pixels with 8-bit grey resolution). Field experiments at Virginia Tech will require a similar high resolution camera to adequately capture the image field. Camera lenses could also be used to reduce glare and shadows in the images (Creutin et al., 2003). Additionally, image enhancement tools will be used to remedy errors in image acquisition.

2.2.3 Image Enhancement

Several aspects of image acquisition process can introduce error, such as poor illumination, glare, and shadows. Image enhancement methods can remove some of these errors prior to image evaluation. Image enhancement is performed on a computer by altering the pixel values of the recorded image. Typical image enhancement methods used in LSPIV include increasing the signal-to-noise ratio, attenuating background noise, and improving the contrast and brightness of the image (Etterma et al., 1997). Care must be taken because poor image enhancement can increase noise and degrade processing results (Fujita et al., 1998).

It is important to reduce background noise for the purpose of tracking particles. Typical means of reducing background noise are filters and offset values. A low-pass filter is sometimes used to remove high-frequency noise components (Lloyd et al., 1995). Additionally, an offset value can be subtracted from the pixel values to account for background noise. Weitbrect et al.,

(2002) used 1 % of the maximum displacement value for an offset value. Another image enhancement technique is enhancing contrast between the particles and the background. One way to alter contrast is with a high-pass Laplacian filter, which can sharpen the particle image boundaries (Lloyd et al., 1995). Additionally, histogram equalization has been used in LSPIV applications to enhance contrast (Bradley et al., 2002 and Fujita et al., 1998). Image enhancement techniques are image specific and depend on the camera, lighting conditions, and image size. Many commercial image processing software packages can perform the most common image enhancement techniques. However, there is no method available for selecting the most appropriate image enhancement for LSPIV applications.

2.2.4 Image Registration and Transformation

In LSPIV field applications, the camera is usually at an oblique angle to the stream, which introduces spatial distortion (Bradley et al., 2002). The distortion is corrected through image transformation, which relates the pixels to their physical locations. The transformation can be corrected through implicit parameters of the camera. However, in LSPIV applications, the transformation is explicit, as ground reference points are used to numerically optimize the parameters (Cruetin et al., 2003). Several LSPIV studies have used an algorithm developed by Fujita et al. (1998) for image transformation. The equations to transform cathode-ray tube (CRT) (x, y) coordinates to physical coordinates (X, Y) are as follows.

$$X = \frac{b_1 x + b_2 y + b_3}{b_4 x + b_5 y + 1} \quad \textbf{(1)}$$

$$Y = \frac{b_6 x + b_7 y + b_8}{b_4 x + b_5 y + 1} \quad \textbf{(2)}$$

The symbol b_i (i = 1 - 8) is the transformation coefficient determined by the least square method using N pairs of known coordinates: $(x_1,y_1),(X_1,Y_1)\ldots(x_N,y_N),(X_N,Y_N)$. Transformation coefficients can be obtained by solving

$$TB = Z, \tag{3}$$

where:

$$T = \begin{bmatrix} x_1 & y_1 & 1 & -x_1X_1 & -y_1X_1 & 0 & 0 & 0 \\ . & . & . & . & . & . & . & . \\ . & . & . & . & . & . & . & . \\ . & . & . & . & . & . & . & . \\ x_N & y_N & 1 & -x_NX_N & -y_NX_N & 0 & 0 & 0 \\ 0 & 0 & 0 & -x_1Y_1 & -y_1Y_1 & x_1 & y_1 & 1 \\ . & . & . & . & . & . & . & . \\ . & . & . & . & . & . & . & . \\ . & . & . & . & . & . & . & . \\ 0 & 0 & 0 & -x_NX_N & -y_NY_N & x_N & y_N & 1 \end{bmatrix} \tag{4}$$

$$B = [b_1, b_2, ...b_8]^T \tag{5}$$

$$Z = [X_1, X_2, ...X_N, Y_1, Y_2, ...Y_N]^T. \tag{6}$$

The non-distorted image is obtained in three steps. First, using the ground reference points (GRP) a grid with step size ΔX and ΔY is generated. Second, the cathode ray-tube (CRT) coordinates (X, Y) using the inverse of Equations 1 and 2 are determined. Third, the intensity at (X, Y) is calculated by interpolation on the CRT plane. The algorithm requires a minimum of four physical reference points with additional points used to estimate uncertainty. It is important to note that the more distorted an image the more noise is caused by image transformation (Weitbrecht et al., 2002).

Several characteristics are unique to image transformation in LSPIV. Most stream images contain boundary areas that should be eliminated before image evaluation (Fujita et al., 1998). In order to work remotely, LSPIV systems will need ground reference points (GRP). Field LSPIV experiments have used GRP; however long-term studies have not used permanent GRP. Cruetin et al. (2003) used brightly painted tree stumps as a semi-permanent GRP. Installation of GRP is

expensive and permanent GRP could reduce cost and introduce less error. A total station can be used to measure both GRP and river bathymetry (Bradley et al., 2002). All image enhancement and transformation must be done prior to the evaluation.

2.2.5 Image Evaluation

Image evaluation techniques use image intensity fields to measure tracer displacements to estimate a surface velocity field. It is a critical step in LSPIV, requiring the most specialized techniques. Most LSPIV research has used correspondence techniques to determine particle displacement. Correspondence techniques, such as cross-correlation, search for the correlation of pixels between frames (Bradley et al., 2002). Although computationally intensive, correspondence techniques work well for the low image capture rates of LSPIV applications.

One correspondence technique, cross-correlation, compares an interrogation area (small area of the stream surface) in one image to many interrogations area in the corresponding image (Figure 2). The interrogation area is moved to every spot in the search area or region-of-interest (ROI) (Cruetin et al., 2003). The size of the interrogation window and ROI are user-controlled. The highest correlation coefficient in the ROI is taken as the probable particle location (Bradley et al., 2002). The low velocities in LSPIV applications make cross-correlation algorithms the most appropriate technique for tracking surface particles in open-channel flow. Additionally, cross-correlation algorithms work well for the velocities and the low seeding densities found in field applications (Fujita et al., 1998). Cross-correlation algorithms are often standard functions in image processing software (Raffel et al., 1998).

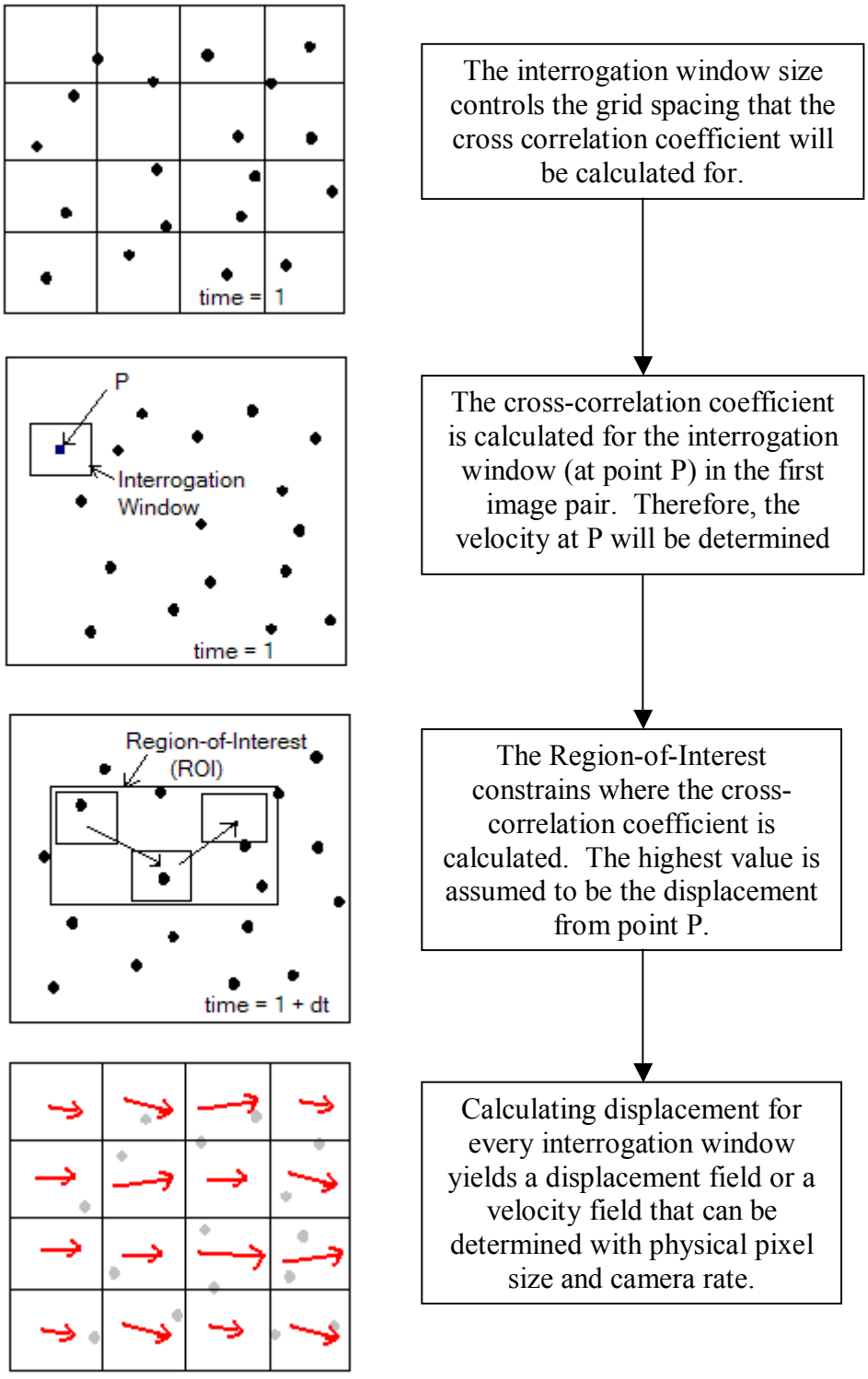

Figure 2. Flow chart for a typical cross-correlation algorithm. Although software programs use different algorithms, typically they follow this general flow chart.

Effective calculation of the cross-correlation coefficients is imperative for accurate velocity measurements. Several successful LSPIV research projects (Bradley et al., 2002 and Cruetin et al., 2003) have used a correlation coefficient given by Fujita et al. (1998):

$$R_{ab} = \frac{\sum_{i=1}^{MX}\sum_{j=1}^{MY}\{(a_{ij} - \overline{a}_{ij})(b_{ij} - \overline{b}_{ij})\}}{\left\{\sum_{i=1}^{MX}\sum_{j=1}^{MY}(a_{ij} - \overline{a}_{ij})^2 \sum_{i=1}^{MX}\sum_{j=1}^{MY}(b_{ij} - \overline{b}_{ij})\right\}^{1/2}} \quad \textbf{(7)}$$

Where R is the cross-correlation coefficient and MX and MY are the sizes of the interrogation area in each image. The variables a_{ij} and b_{ij} are the distributions of the gray-level values in the two interrogation areas separated by time interval dt. The over-bar indicates the mean value of the intensity for the interrogation area. Solving the cross-correlation coefficients directly is too computationally intensive for near real-time processing. Therefore an alternative is necessary.

Typical PIV applications use Fourier transforms to improve the computational efficiency. This is implemented by using the correlation theorem which states that the correlation of two functions is equivalent to a complex conjugate multiplication of their Fourier transforms (Raffel et al., 1998). Using Fast Fourier Transforms (FFT) to calculate correlation coefficients can significantly increase computational efficiency (Adrian, 1991 and Willert and Gharib, 1991). The method, shown in Figure 3, outlines the steps for calculating cross-correlation coefficients using FFTs. Various software packages (e.g. Matlab or Mathmatica) have pre-defined commands that perform two-dimensional FFT's.

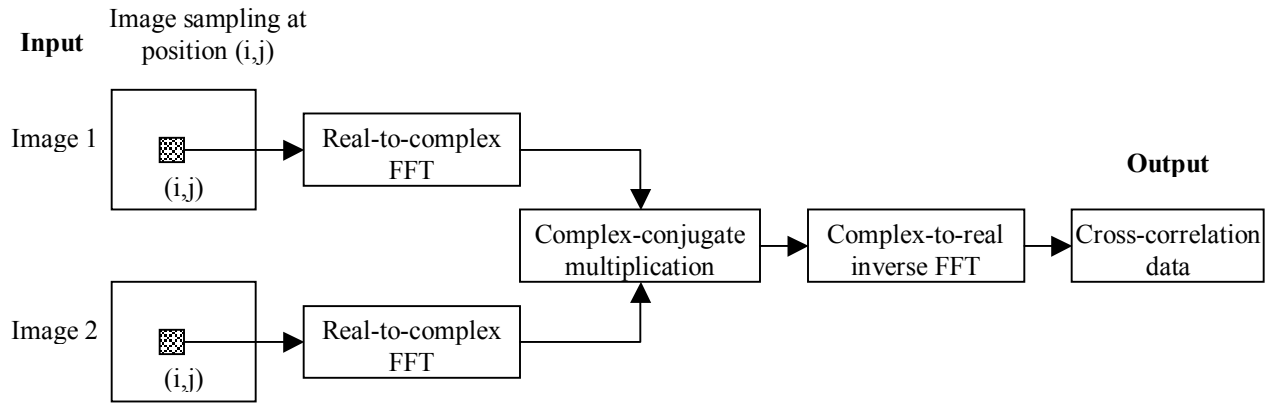

Figure 3. Implementation of cross-correlation using fast Fourier transforms (Raffel et al., 1998).

A potentially challenging aspect of image evaluation is selecting the proper processing parameters such as size of the ROI and interrogation window sizes, time-step between images, and vector pitch (to a lesser extent) (Raffel et al., 1998). The time step should be small enough for sufficient accuracy, but large enough to avoid long computation times. As an additional constraint, the duration of the image capture must be long enough to provide an accurate average velocity (see 2.2.7 Obtaining Stream Velocities from LSPIV Data). Fujita et al. (1998) asserted their discharge measurements were independent of interrogation area size, for a very large image plane (40,000 m^2). However, in most applications, an optimum interrogation area size is considered a necessary component to cross-correlation accuracy.

Optimization of the interrogation window size is a principal means of acquiring accurate velocity measurements using cross-correlation. The interrogation window size is a tradeoff between different aspects. The window size must be small enough to preserve the spatial scale of interest (any scale smaller than the window size is lost). Stevens and Coates (1994) noted that the interrogation window must not be larger than 1/5 of the smallest length scale to resolve that scale. However, most applications of LSPIV use relatively large spatial scales. Additionally, small sizes avoid second-order effects (e.g. displacement gradients) (Raffel et al., 1998). However, the

interrogation area size must be large enough to recognize larger groups of patterns (Raffel et al., 1998). The cross-correlation algorithms require a certain number of matched pairs, typically four, before the detection rate will decrease rapidly (Raffel et al., 1998). Tests by Weitbrecht et al. (2002), using changing particle concentrations, showed that there should be at least five particles per interrogation area. The same researchers showed that maximum particle displacement between two frames should be one-half of the interrogation area.

The interrogation window size must also be selected to avoid long computation times. The computation time increases proportionally to the interrogation area size (Raffel et al., 1998). Bradley et al. (2002) found computation time is linearly dependent on number of images and quadratically dependent on the desired accuracy. The improvement in computer processing speeds has allowed for a great advancement in image processing once the limiting factor in LSPIV. Research has shown image processing speeds of 133 – 200 MHz are adequate for real-time flow analysis (Bradley et al., 2002 and Etterma et al., 1997). Besides optimizing the interrogation window, there are additional tools available for improving the accuracy of cross-correlation.

To improve accuracy, the ROI can be automatically displaced between images or 'offset'. Offset windows increase the likelihood of finding corresponding particles between images by approximating their location. Several off-set methods exist including first-order, second-order, and adaptive methods. First-order direct window offsets (DWO) use the first pass to estimate the location of the window in the second image pair for any subsequent passes (Figure 4). In second-order offset the window is shifted in both images of the pair. Typically the interrogation window size is decreased with subsequent passes to increase displacement resolution. Additional, methods exist for increasing accuracy using cross-correlation techniques.

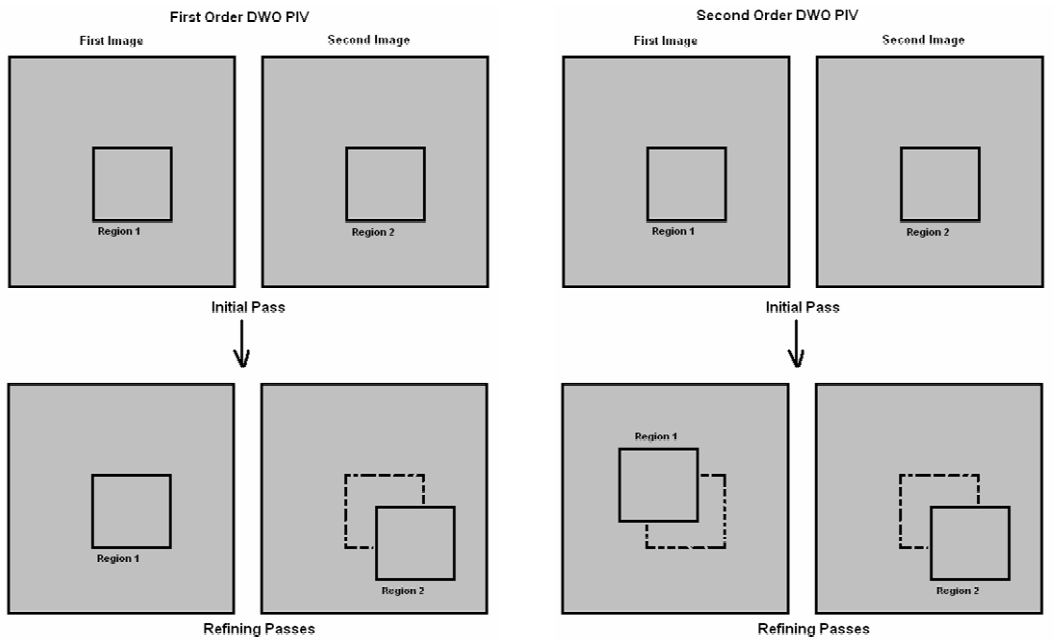

(a) (b)

Figure 4. (a) Method for first-order direct window offset (DWO). (b) Method for second-order DWO. Window offsets can increase accuracy in image evaluation. (Courtesy of Personal Communication with Jason Carneal)

Several more recently developed offset methods make use of adaptive measures and shortcuts. For example, the computational efficiency can be increased by comparing the new window offset value to the previous value and skipping unnecessary correction calculations (Raffel et al., 1998). Additionally, a dynamically adaptive local cross-correlation method (Figure 5) was developed by Abvien and Vlachos (2002). This method can capture multiple length scales, often present in open channel flow. The method uses the first pass to estimate velocity to refine the window size and estimate window offsets for subsequent passes. Offset interrogation areas are also used for sub-pixel interpolation (Westerweel et al., 1997).

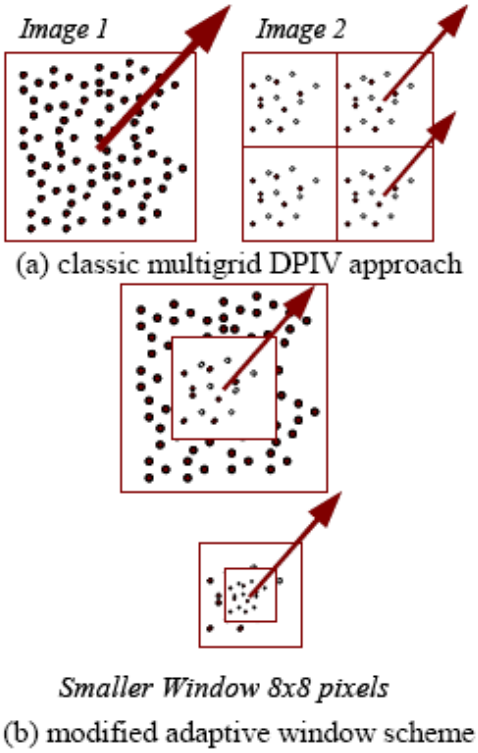

Figure 5. Comparison of classic multigrid approach and adaptive scheme of Abiven and Vlachos (2002). (a) Classic PIV interrogation method (b) Adaptive method that uses multiple passes to refine the interrogation window size and ROI offset.

The exactness to which the particles are located determines the accuracy of the velocity measurements. Displacement estimation is used to track particles to necessary sub-pixel accuracy. For example, the most common estimation technique in PIV is a three-point estimator. Three-point estimators find the maximum correlation value and use three points in each direction to apply a three-point estimator, typically a Gaussian curve (Raffel et al., 1998). Westerweel et al. (1997) used offset interrogation windows to estimate sub-pixel accuracy to 0.04 pixels. Advanced sub-pixel estimation methods were developed for industrial design at high velocities. For this reason, sub-pixel displacement estimation algorithms may be overly complicated for open-channels where flow is principally in one dimension. Therefore, less complicated methods would reduce computation time and simplify image processing. Regardless of the evaluation technique, there will be some error in measured velocity vectors.

2.2.6 Image Post-Processing

Image post-processing is used to reduce incorrect velocity data before a discharge estimate is made. The errors typically result from a lack of flow tracers, poor image quality, or correlation anomalies resulting from unmatched image pairs (Cruetin et al., 2003). Image post-processing is most necessary in complex flows such as vortices, rarely present in stream reaches selected for discharge monitoring (Lloyd et al., 1995). However, stream flow near the banks will often show incorrect velocity vectors that will require post-processing. LSPIV output data requires several post-processing steps (Raffel et al., 1998):

- Validation of the raw data,
- Replacement of incorrect data,
- Data reduction, and
- Analysis of the information.

Initially, the velocity data must be validated by inspecting for potential errors. Error-detection algorithms label vectors that do not satisfy the continuity of flow as erroneous (Lloyd et al., 1995). More commonly, algorithms look for the typical features of incorrect vectors (Raffel et al., 1998):

- Vectors magnitude and direction differ considerably from their surrounding neighbors,
- Vectors often appear at the edges or drop out areas of the data field, and
- Usually appear as a single incorrect vector.

An accepted technique for identifying erroneous vectors is by comparing a vector to its neighbors (Cruetin et al., 2003). Too many vectors exist for visual inspection, thus computer processing is necessary (Raffel et al., 1998). This is commonly done with a global histogram operator, which compares neighboring velocity vectors to a given threshold (Raffel et al., 1998). The vector comparison can be made with either bilinear interpolation from nearby cells or through

weighted averaging of neighboring cells. Additionally, the absolute divergence values from the continuity of flow can be used to search for erroneous vectors (Raffel et al., 1998). Once erroneous vectors are identified, they are typically replaced with a value interpolated from nearby cells. All field sites require an optimization period to find the most appropriate post-processing methods. Following post-processing the stream's surface velocity field can be estimated.

2.2.7 Obtaining Stream Velocities from LSPIV Data

Conventional discharge methods require calculation of average velocities across the width of the channel. However, velocity measurements from LSPIV are instantaneous point velocities. The velocity at any point in a stream is continually fluctuating with time and varies in space. Therefore, the instantaneous velocity values must be averaged temporally and spatially (including both with depth and across the cross-section). The mean velocity in time is determined by averaging velocities over a set number of images (with known time intervals). Several researchers have proposed time periods for velocity collection. A review by Pelletier (1988) found recommended time periods from 40 - 60 seconds. The USGS recommends a time period of 40 - 70 seconds (Rantz et al., 1982). Research results, shown in Figure 6, illustrates that uncertainty increases exponentially at below 60 seconds time intervals. Velocities slower than 0.4 m/s require increased exposure times, as shown in Figure 7. Therefore, it is important to correlate the time of exposure of the measuring device to the stream velocity. Fujita et al. (1998) used a one-second frame rate and 100 images (100 seconds), each with 960 velocity vectors. Etterma et al. (1997) also used one-second frame rate and 100 images. Fujita et al., (1997) used 60 consecutive images and a one-second frame rate, for measuring a flooded river. One-hundred instantaneous point velocities provides an accurate average but avoids long computation times. Additionally, a one-second frame rate is long enough to increase velocity accuracy. However, too large of a frame rate would increase noise and cause a loss of image pairs (Raffel et al., 1998). The time-averaged

point velocities are only at the stream surface and do not represent the average stream velocity (with depth) at that point.

Velocity varies with depth because of the frictional forces of the bed-water and air-water interfaces. Therefore, several techniques have been proposed to estimate the average velocity within the stream profile. Bradley et al. (2002) assumed a logarithmic profile in a kinematic flow analysis of a stream. Cruetin et al. (2002) assumed a parabolic velocity profile where a 0.85 multiplier was used to convert surface velocity to mean velocity. The 1/7 power law has been used by multiple researchers (Fujita et al., 1998 and Weitbrect et al., 2002). Weitbrect et al. (2002) multiplied surface velocities by a theoretical factor of 0.82. The ISO (ISO 748, 1997) recommends correlating the surface velocity with the velocity at 0.6 of the total water depth. Correction coefficients should vary between 0.84 and 0.90, with the higher ranges used for smooth beds. The use of a correction coefficient will introduce error, but modifies the velocity data into the necessary form for calculating discharge.

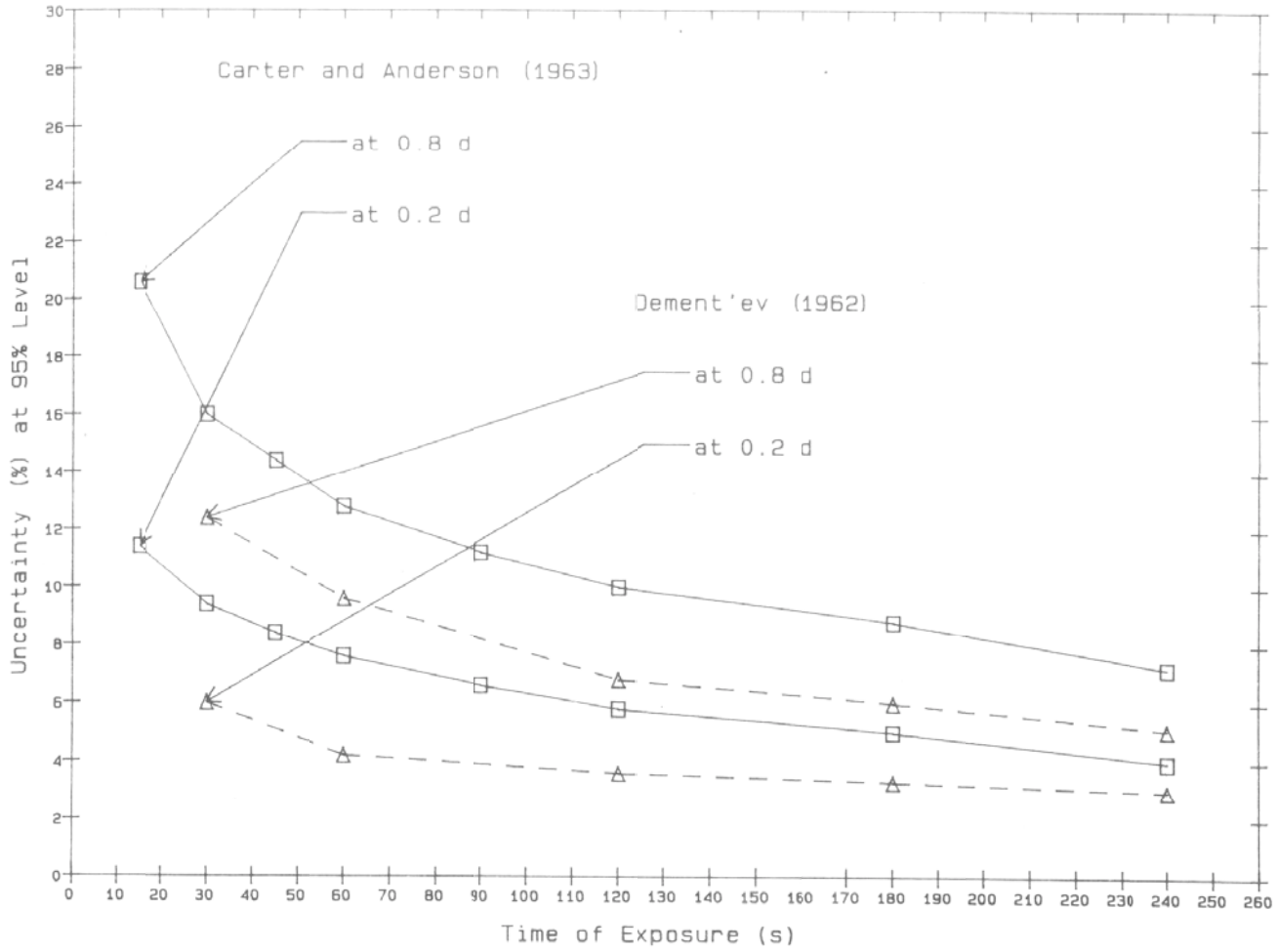

Figure 6. Uncertainty versus time of exposure of the measuring device (Pelletier, 1988). Notice the exponential increase in uncertainty when the time of exposure is less than 60 seconds.

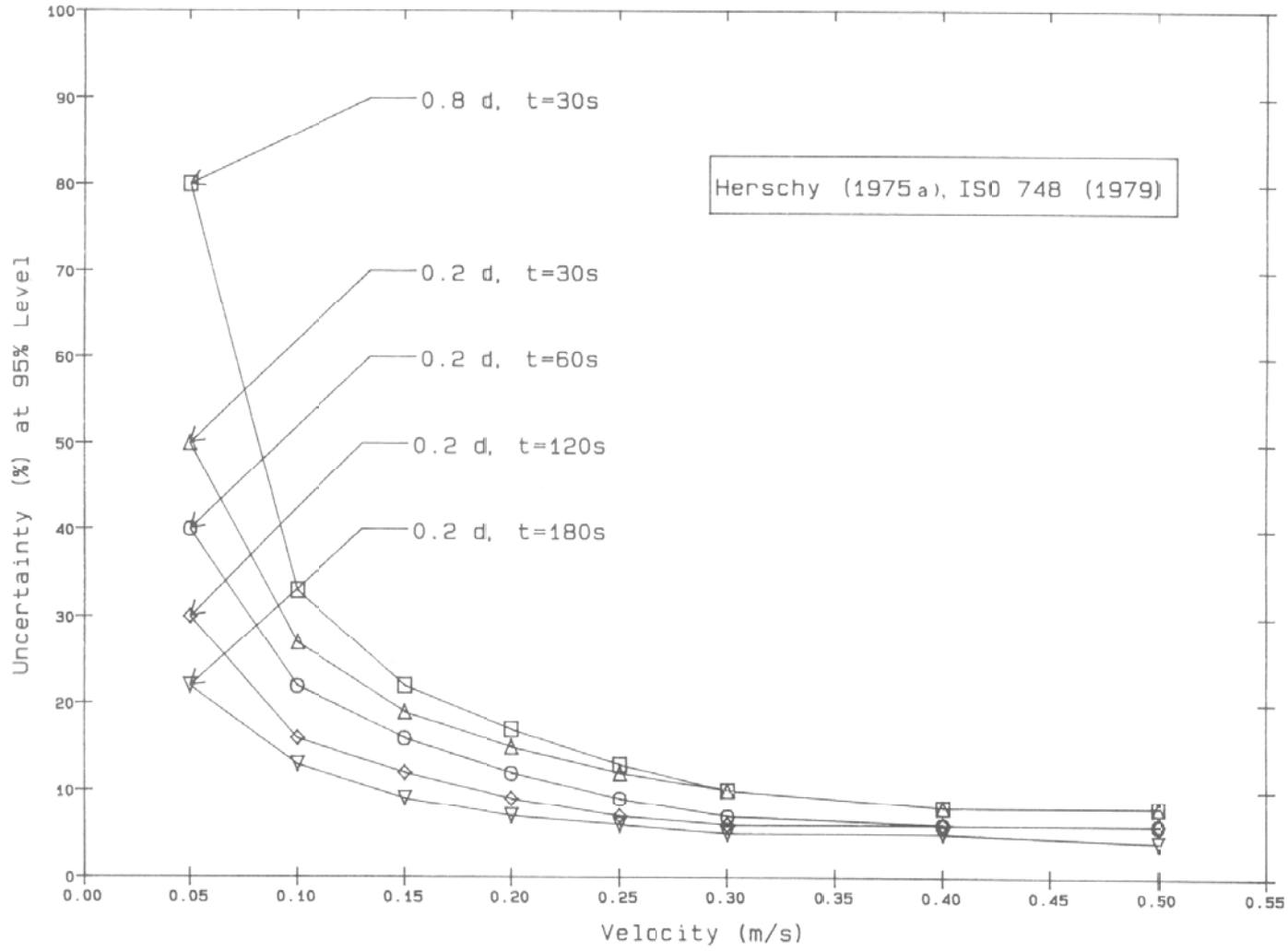

Figure 7. Uncertainty versus velocity for differing time of exposures of the measuring device (Pelletier, 1988). Notice that uncertainty is relatively constant when velocity is more than 0.30 m/s.

2.2.8 Calculating Discharge

The LSPIV velocity measurements are used to calculate discharge using the same area-velocity procedures as other devices (e.g. current meter). The discharge calculations follow the U.S. and international standard procedures. The standards have evolved to minimize deviance from the theoretical river discharge (Pelletier, 1988),

$$Q = \iint_A v(x, y)dxdy \quad \textbf{(8)}$$

Where A is the cross-sectional area and v(x, y) is the velocity field over width x and depth y.

In standard discharge measurement, the depth and the velocity are assumed to vary linearly between verticals across the cross-section. The most common method for measuring discharge is to divide the measuring cross-section into several smaller sections or segments and measure velocity at each vertical. The total discharge through the cross-section is the sum of the products velocity, width, and depth of each segment, generally termed area-velocity methods (Pelletier, 1988):

$$Q_c = \sum_{i=1}^{n} b_i d_i v_i \quad (9)$$

Where b_i is the width of cross-section i; d_i is the depth of vertical i; v_i is the mean velocity in the vertical i; and n is the total number of verticals. The LSPIV data must be averaged across the finite widths of the stream for use in Equation 9. Figure 8 illustrates that uncertainty increases exponentially with decreasing verticals in the cross-section, however the uncertainty does not decrease when the number of verticals exceeds 35. Additional error is present in measuring of stage at each vertical.

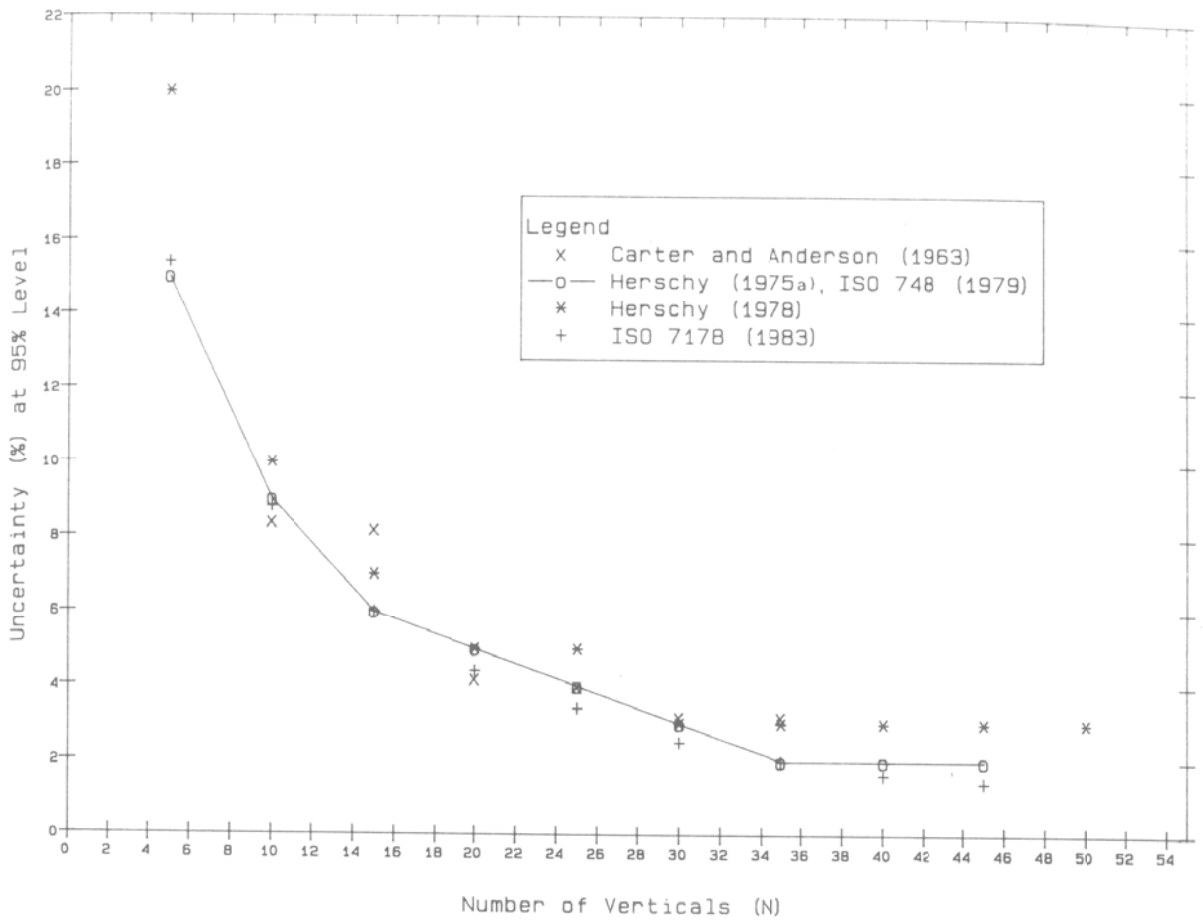

Figure 8. Uncertainty of discharge measurements versus number of verticals used to calculate discharge (Pelletier, 1988). Notice that uncertainty does not increase when the number of verticals exceeds 35.

The stream cross-section area is needed to estimate discharge. Depth measurements, at each vertical, approximate the cross-section in Equation 9. Standardized methods for measuring cross-section area (depth) reduce error. Measuring with sounding rods, wet-lines, or laser measuring equipment are common methods. Standard methods are available from the USGS (Rantz et al., 1982) and the ISO (ISO 748, 1997). The need to measure GRP makes laser measuring equipment (e.g. total stations) particularly attractive for measuring

both GRP and cross-section. Once depth has been measured, discharge is typically calculated using the mid-section or mean-section method (ISO-748, 1997).

The midsection method has been shown to be slightly more accurate than the mean section method for calculating discharge in open-channels (Rantz et al., 1982). The midpoint method assumes the depth and velocity measured at a given vertical is representative of the partial area centered on that vertical (Figure 9). This method defines the partial area as a rectangle, centered at the measurement vertical, with a depth equal to the measured depth at the section vertical. The width of the partial area extends to the halfway point between the section vertical and the adjacent section vertical on either side. The stream measurement section is defined by *n* observation verticals in each discharge measurement, similar to Equation 9. The average flow velocity of an observation vertical is determined by measuring the velocity at each section. This velocity is assumed to represent the average velocity in the entire partial area (Rantz et al., 1982).

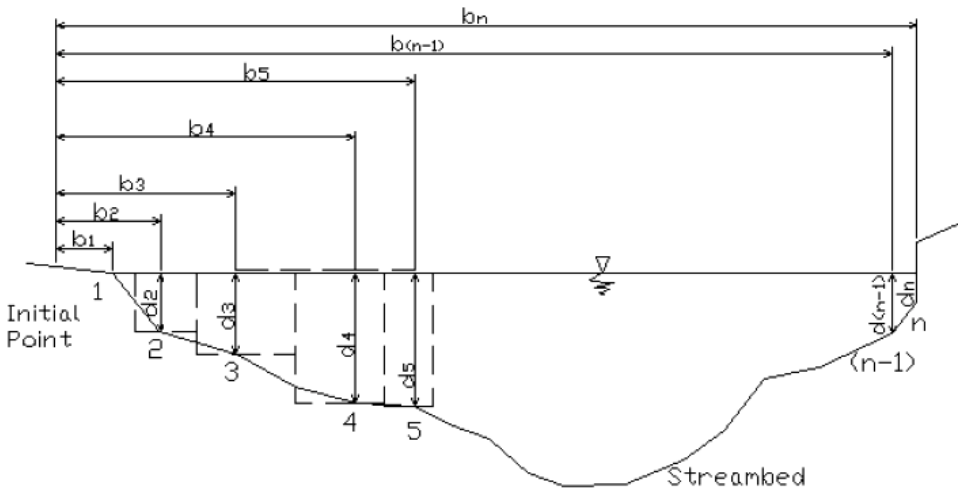

LEGEND

1, 2, 3, …n	Observation verticals
b1, b2, b3, . . . bn	Distance from the initial point to the observation vertical, feet
d1, d2, d3, . . . dn	Depth of water at the observation vertical, feet
Dashed lines (---)	Partial section boundaries

Figure 9. Schematic for determining discharge using the mid-section area velocity method. The midsection method has been shown to be more accurate than the mean section method (Rantz et al., 1982).

The mid-section method can be further simplified into equations, capable of estimating discharge. The discharge in the partial area (q_i) is calculated using the equation (Buchanan and Somers, 1984):

$$q_i = v_i \left[\frac{b_{(i+1)} - b_{(i-1)}}{2} \right] d_i \quad \textbf{(10).}$$

Where v_i is the mean velocity at vertical i, b_i is the distance from the initial point to vertical i, $b_{(i-1)}$ and $b_{(i+1)}$ are the distance from the initial point to vertical (i-1) and (i+1) respectively,

and d_i is the depth of the water at vertical i. Using this equation, a boundary depth of zero will produce zero discharge in the boundary area. However, the boundary (sidewall) may be a vertical line and would therefore have a depth. To remedy this problem the velocity at sidewall can be estimated (Table 1) from the depth at the sidewall and mean velocity (Rantz et al., 1987):

Table 1 Relationships necessary to estimate discharge for boundary areas using the midsection method. The velocity at a vertical located very near the sidewall can be related to the mean velocity in a vertical at a distance equal to the depth (Rantz et al., 1982).

Distance from sidewall (as a ratio of depth at sidewall)	Mean vertical velocity as related to the mean vertical in that section (V_d)
0.00	$0.65(V_d)$
0.25	$0.90(V_d)$
0.50	$0.95(V_d)$
1.00	$1.00(V_d)$

2.2.9 Transferring Discharge Data

After the discharge is calculated, the data must be stored or transferred to a remote location. Data transfer allows for 'real-time' monitoring, reducing field technician support, improving data dissemination, and monitoring the operation of the equipment. Also, data transfer is required for automated measurements. The technology for wireless data transfer is available and is currently being implemented by the USGS to reduce monitoring costs (Charles Merk, personal communication, 10 February 2004).

There are many techniques available for remote data transfer. The technique must be chosen based on reception, data transfer rate, and cost of each data transfer system. A study by Grady et al. (1999) found that telephone modems were most economic, followed by radio and cellular systems. Data transfer using a telephone modem is inexpensive, but requires a physical connection. Cellular technology is a wireless alternative. An improving coverage area is making cellular technology sufficient for data transfer from most small Virginia

watersheds (Jeff Wynn, personal communication, February 2004). A cellular system can use a data-logger to store the data prior to transmission. Conveniently, several commercial data-loggers can integrate a cellular modem for remote data transfer. Additionally, instead of retrieving new data, field technicians could collect data from the data logger for verification and backup. The new communication technology could calculate and transfer discharge measurements in near real-time.

Real-time measuring is a valuable tool for water quality monitoring and hydrologic research. Real-time monitoring using LSPIV will not transmit data continuously. However, a continuous system may be possible in the future by decreasing the computation time. Instead of continuous real-time data transmission, the measurements would be made at distinct times and transmitted individually or in set time increments. Wireless technology and improving computer processing speeds is making real-time LSPIV monitoring possible (Willert and Gharib, 1991). Kruger et al. (1999) developed a real-time image velocimeter for laboratory use. The hardware is a 900 MHz clock speed Intel-compatible PC and 30 GB hard drive. With such a system, LSPIV could be extended to real-time or near real-time monitoring of a river reach (Fujita et al., 1997). Additionally, with the appropriate data processing methods and equipment, LSPIV would be applicable to remote measurement (Bradley et al., 2002). For real-time monitoring to be practical, there needs to be easy access to the data.

The internet provides an excellent way to disseminate real-time data. The internet systems require specialized software and a fast internet connection. Toràn et al. (2001) proposed a system for distribution of monitoring data across the internet. They suggest using a measurement station, a control center, and remote stations. The data are transmitted to a

control center, which is a PC designed to communicate with the field modem. The control center uses its hard drive to store data and run an internet server. This allows any computer with internet service to remotely access the data. Therefore, discharge data can be manipulated by any internet user.

2.2.10 Manipulating Discharge Data

The discharge data can be used in the raw form or transferred to a more meaningful format. A surface-water modeling program may use the raw data. However, typically the stream flow data are used to construct a stage-discharge relationship. Numerous standards and methods exist for constructing a stage-discharge relation. The ISO 1100-2: Measurement of liquid flow in open channels - Part 2: Determination of the stage discharge relationship (ISO, 1998) illustrates several methods. The USGS has also outlined methods in Measurement and Computation of Streamflow: Volume 2 Computation of Discharge (USGS, 1983). The ability to construct accurate stage-discharge relationships would make LSPIV a very useful tool for measuring discharge.

2.3 Evaluation of A LSPIV Prototype

2.3.1 Error and Accuracy

LSPIV must measure discharge at an adequate accuracy to be adopted for widespread monitoring use. To accomplish this, error and accuracy analysis should be conducted to quantify the difference between actual and measured stream discharge. Identification of uncertainty at various steps involved in LSPIV is critical to reducing error (Pelletier, 1988). Error comes from three general sources:

- Velocity measurements from image processing,
- Averaging velocity in time and space, and/or

- Measuring cross-sectional area.

Velocity-area measuring techniques, typically used with current-meters and stage recorders, estimate discharge with cross-sectional area and velocity. Therefore, there has been considerable research into estimating error for measuring depth and averaging velocity data. Of principal concern in LSPIV, is estimating error resulting from image processing; because this error is more difficult to quantify and has dramatic effects on accuracy. All of the steps involved in image processing can contribute to error in LSPIV velocity measurements.

Currently there is no single acceptable method for evaluating the uncertainties of image processing (Bradley et al., 2002). One method is to create artificial images using Monte Carlo simulation where the displacement data is known (Raffel et al., 1998). These images can be used in image processing to estimate error. However, these images do not permit evaluation of how specific parameters (e.g. particle diameter, evaluation parameters, and background noise) influence error. Image processing techniques can also be evaluated in a laboratory flume, with known discharge. However, in outdoor conditions there are limited means to estimate image processing error. The lack of ability to specifically identify the sources of error makes error reduction more difficult. Unfortunately, in most LSPIV research, an inclusive error has been estimated that encompasses image processing error.

To be competitive with other devices, LSPIV must have low measurement error. Importantly, to outperform measurements made with critical depth methods (e.g. weirs and flumes), velocity-area methods must measure average velocity with a 2 – 3 % error (Yorke et al., 2002). A robust means of estimating uncertainty for a single discharge measurement was proposed in ISO: 5168 (1998). This standard proposes estimating random and systematic

uncertainty and combining them using either a root-sum-square model (U_{RSS}) or additive model (U_{ADD}):

$$U'_{Q_{RSS}} = \sqrt{\left(2s'_Q\right)^2 + \left(B'_Q\right)^2} \quad \textbf{Equation (11),}$$

$$U'_{Q_{ADD}} = B'_Q + 2s'_Q \quad \textbf{Equation (12).}$$

Where s'_Q is the overall percentage experimental standard deviation:

$$s'_Q = \sqrt{s'^{\,2}_{F_m} + \frac{1}{m}\left(s'^{\,2}_b + s'^{\,2}_d + s'^{\,2}_{\bar{v}}\right)} \quad \textbf{Equation (13)}$$

where s'_{F_m} is the percentage experimental standard deviation (subsequently referred to as deviation) due to the limited number of verticals (Table 2), $s'^{\,2}_b$ is the deviation due measuring the width of segments, $s'^{\,2}_d$ is the deviation due to measuring the depth of the segments, m is the number of verticals, and $s'^{\,2}_{\bar{v}}$ is the deviation in estimating the average velocity in each vertical.

$$s'_{\bar{v}} = \sqrt{s'^{\,2}_p + s'^{\,2}_c + s'^{\,2}_e} \quad \textbf{Equation (14)}$$

Where s'_p is the is the deviation due to the limited number of points taken in the vertical (Table 3), s'_c is the deviation of the velocity measuring equipment, s'_e is the deviation due to pulsations in the flow (Table 4 and Figure 8). Additionally, the overall systematic uncertainty (B'_Q) is estimated using the equation,

$$B_Q^{'} = \sqrt{B_b^{'2} + B_d^{'2} + B_c^{'2}} \qquad \textbf{Equation (15)}$$

where $B_b^{'}$ is the percentage systematic uncertainty (referred to as uncertainty) if the instrument measuring width, $B_d^{'}$ is the uncertainty in the instrument measuring depth, and $B_c^{'}$ is the uncertainty in the calibration of the instrument measuring velocity (zero in the case of LSPIV).

Studies by Adrian (1991) and Buchave (1992) found 3% image processing error is possible. However, Bradley et al. (2002) conservatively estimated errors in the LSPIV velocity measurements to be about 20%. Pelletier (1988) investigated errors in measuring cross-sectional area. Pelletier found random uncertainty of ±1 % and ±3 % for measuring depth, depending on depth, and less than ±1% for the systematic uncertainty. Higher accuracy is possible for measuring width; Pelletier found random and systematic uncertainties did not exceed ±1%. Despite the need to quantify individual sources of error, most LSPIV researchers have not made such an attempt. Instead, LSPIV accuracy is typically estimated based on measurements from other conventional measuring equipment.

Table 2. Uncertainty in the measurement of mean velocity versus number of verticals (ISO 748). Notice that uncertainty does not increase appreciably when over 35 verticals are used.

Number of verticals	Uncertainties (95 % confidence level)
5	± 15
10	± 9
15	± 6
20	± 5
25	± 4
30	± 3
35	± 2
40	± 2
45	± 2

Table 3. Uncertainty versus number of points in a vertical (ISO, 1997). LSPIV applications find only a surface velocity corresponding to an uncertainty of 15% because of the assumptions necessary to estimate average velocity.

Method of measurement	Percent uncertainty (95 % confidence level)
Velocity distribution	± 1
5 points	± 5
2 points	± 7
1 point	± 15

LSPIV must be as accurate as conventional discharge monitoring techniques to be a viable alternative. Unfortunately, large ranges in open channel flow velocities can cause LSPIV accuracy to vary widely (Weitbrecht et al., 2002). Several large-scale field studies have measured LSPIV accuracy with current meters and/or gauging stations for comparison. Two studies (Bradley et al., 2002 and Cruetin et al., 2003) found discharges estimated with LSPIV to be within the estimated error of current meter measurements. Fujita et al. (1997) found LSPIV discharge measurements within 3% of the stage-discharge relation. The discharge estimates using LSPIV by Cruetin et al. (2003) also compared well (4% difference) with traditional USGS gauging stations. However, the USGS found that under 'good' conditions, a stage-discharge relation is accurate only to ± 10% (Novak, 1985). Comparing

LSPIV to current meters may be more apt because they are the instrument best replaced by LSPIV.

It is imperative that current meters are accurate when they are used for comparison against LSPIV. The operation of a current meter is standardized to minimize error. One method, ISO 748: Measurement of liquid flow in open channels - Velocity area methods (ISO, 1997) outlines standard procedures for current meter operation in a variety of conditions. Additionally, the work by the USGS (Rantz et al., 1983) recommends standard procedures for current meter use. Figure 10 shows the uncertainty of a current meter versus velocity. It is important to note, that at low velocities the current meter has the highest uncertainty. Conversely, LSPIV would likely have its lowest error at low velocities, because the depth profiles would be the most uniform.

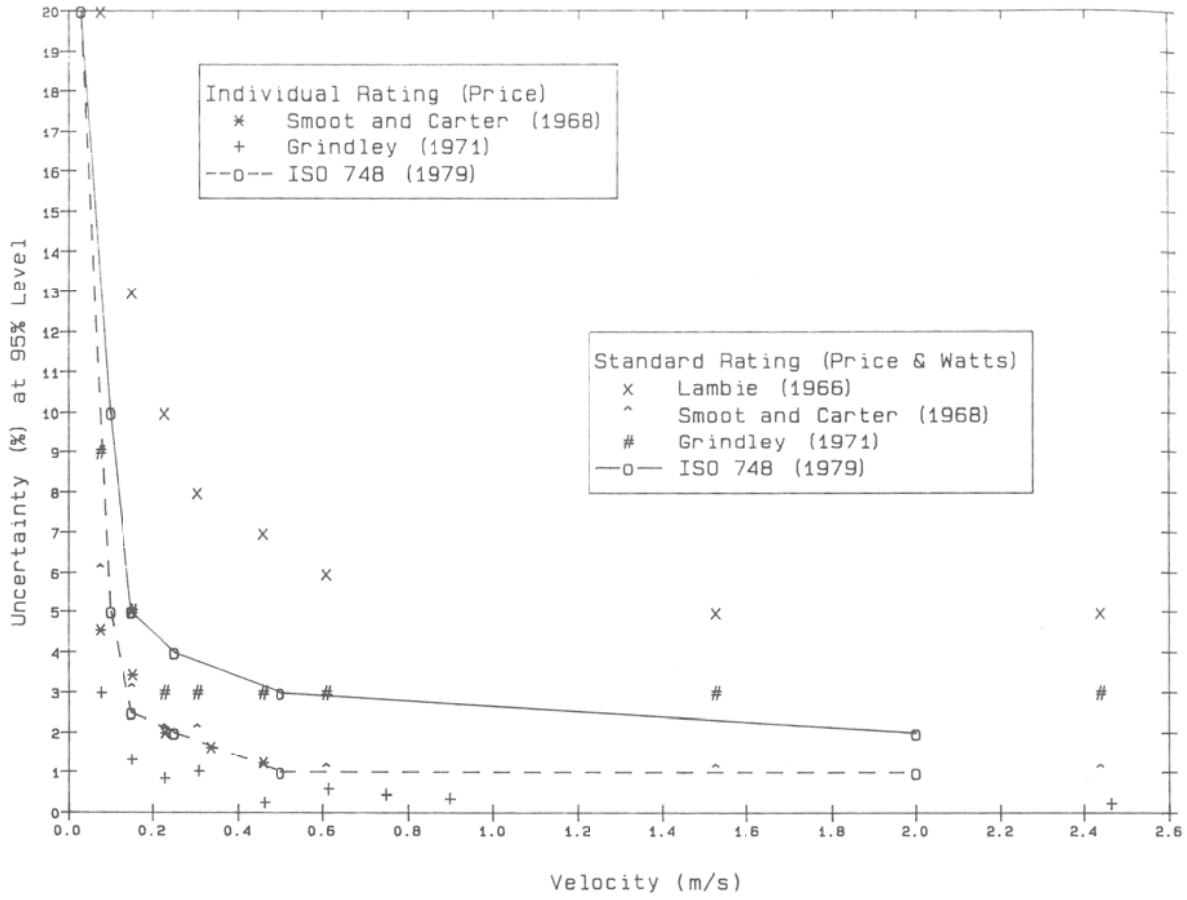

Figure 10. Uncertainty of the current meter at a 95 % confidence level (Pelletier, 1988). The accuracy of the current meter measurements is important because these meters will be used as a means of comparison for LSPIV.

2.3.2 Methods of Prototype Design

Many methods are available for designing and testing a prototype. In LSPIV design, attention must be paid to these general methods, as well as specific considerations for selecting LSPIV equipment and methods. The USGS Hydro 21 committee developed a three-step program to evaluate technologies that may be used to more cost-effectively and safely measure open-channel flow (Melcher et al., 1999):

1. Determine the optimum conditions for each parameter by reviewing test results for various flow and channel conditions. Preliminary information should be provided on

depth limits and the effects of electrical conductivity and sediment concentration on flow measurements,

2. Controlled laboratory tests to determine actual performance. This step should provide accuracy information under various conditions,
3. Testing and development of field equipment. The equipment should be developed in a modular form to permit modifications. The field tests should be done at a USGS gauging station to allow comparison to accurate baseline data. The initial test should be performed under typical river conditions of geometry, velocity, stability, and water chemistry. Further tests at different conditions will need to be performed only after satisfactory performance under typical conditions.

These guidelines from USGS demonstrate a scientifically-based method of testing new discharge measuring technology. However, the selection of LSPIV methods and equipment is project and product specific. Raffel et al. (1998) suggest several criteria for LSPIV method and parameter selection:

- Evaluate the spatial and/or temporal resolution of the flow field under investigation,
- Determine the required resolution of the velocity fluctuations,
- Determine an optimum time interval between the individual PIV measurements, and.
- Locate necessary equipment within budget constraints.

The USGS guidelines are an established methodology of testing and developing a prototype. The guidance by Raffel et al. (1998) was used in developing the image processing component in LSPIV for this study.

CHAPTER 3: METHODOLOGY

The goal of this study was to evaluate the accuracy and feasibility of using large-scale particle image velocimetry (LSPIV) to measure discharge in Virginia's low-order streams. To accomplish this goal, three objectives were identified to develop and test the LSPIV technology according to a USGS three-step procedure for evaluating emerging open-channel discharge measuring technologies (Melcher et al., 1999): First, optimum operating parameters for various conditions were determined. Second, the prototype was tested under controlled laboratory conditions. Finally, the field equipment was developed and tested for a variety of stream flow conditions. Therefore, as a first-step, a laboratory prototype was developed to identify optimum operating parameters, based on information from the literature review and available resources.

3.1 Laboratory Methods

The objective of the laboratory experiments was to construct a laboratory-scale LSPIV prototype for measuring water surface velocities and, thus discharge, in a hydraulic flume. Additionally, the prototype was tested under various conditions to identify optimum parameters. To assess accuracy, the prototype measurements were compared to discharge measurements from two other treatments: the flume manometers and a Marsh-McBirney Flo-Mate 2000 current meter (ELD, 1987 and Marsh-McBirney, 1987). Overall, the collection of LSPIV data in the laboratory follows the standard LSPIV methodology outlined in Figure 1. The laboratory flume provides a controlled setting where the discharge measurement methods can be compared with minimal error. Additionally, the conditions within the flume can be controlled to test the effect of experimental factors on the accuracy of the prototype.

The effects of three factors on discharge accuracy were investigated. The number of particles on the water surface (seeding density) was varied to examine the effect of low seeding densities. This is important in field applications, where seeding at high densities may be difficult. Additionally, the effect of an oblique camera angle on LSPIV accuracy was investigated. In field applications the camera is typically at an oblique angle, and an operating range of minimal error is needed for field applications. The final factor investigated in the laboratory was the Froude number of the flow. The Froude number, Fr, is a dimensionless number that is proportional to the inertial forces divided by the gravitational forces:

$$Fr = \frac{V}{\sqrt{gL}} \qquad \textbf{(16)}$$

Where V is the velocity, g is the gravitational forces, and L is the characteristic length. The Froude number is typically used in open-channel wave and surface behavior calculations. In this experiment, Froude number was selected because it identifies the flow regime (Fr < 1 = subcritical, Fr >1 = supercritical) and is a measure of the flow magnitude. Additionally, the Froude number provides an estimate of wave effects and possible out-of-plane losses (three-dimensionality). The LSPIV prototype measured discharge at different levels of the three factors, which were compared to measurements from a current meter and the flume manometers in the accuracy analysis.

The Statistical Consulting Center at Virginia Tech provided assistance in the development of the statistical experiment as is explained in more detail in section 3.1.5 Laboratory Statistical Design. A split-plot design was selected to minimize the time necessary to test each factor and maintain independent replications. Two replications were

used in the first experiment to gather 40 data points. The first experiment tested the effect of five levels of seeding density (1, 2, 3, 4, and 5 particles per interrogation window). The second experiment used five replications to collect 80 data points and tested the overall accuracy of LSPIV discharge measurements. Additionally, this experiment identified the effects of four levels of camera angle (0, 15, 30, and 45 degrees) and Froude number (0.05, 0.15, 0.25, and 0.35). Intrinsic in performing a split-plot statistical experiment was the design of an effective experimental setup within the flume and the development of an operating procedure for collecting the data.

3.1.1 Experimental Setup and Hardware

Flume Setup

The laboratory experiments were conducted in the Biological Systems Engineering's Soil and Water Resources Laboratory at Virginia Tech. All experiments were performed in a one foot-wide re-circulating flume (B-16 Hydraulic Demonstration Channel Series Model# 6201). The unit consists of a channel, a headtank with gate, movable tailgate, reservoir, and two circulating pumps. The channel slope can vary from 0 to 14 percent, with a 1% slope used in these experiments. The two high-volume low-heard pumps are each capable of producing a total flow of 95 gallons per minute. The discharge was measured using orifice meters fitted on the two pumps. The discharge was calculated using calibrated equations for the orifice meters (ELD, 1987):

$$Q = K \cdot \frac{\pi d^2}{4} \cdot \sqrt{2g\Delta h} \qquad (17)$$

Where K is the flow coefficient calculated by the flume manufacturer (0.8139), d is the diameter of the orifice (0.1979 ft), and h is the manometer deflection in feet. The

manometers were calibrated to atmospheric pressure before each measurement. No error information was given by the manufacturer for the orifice meters. However, preliminary investigation using a V-notch weir measured discharges within 5% of those estimated by the manometer equation. Additionally, only two significant digits could be estimated from the flume's manometers, which could cause errors of 5% to 15% for the flow range evaluated.

The experimental setup was designed to minimize the time required between tests and minimize error in the measuring devices. First, the discharge was set to achieve the desired Froude number and was given sufficient time to stabilize in the channel. Subsequently, discharge measurements were made using all treatments. The setup allowed simultaneous measurement of all three treatments, as shown in **Figure 11**. The camera had an unobstructed field-of-view. A screen was placed at the end of the flume to keep particles from entering the flume reservoir. A constant lighting source was provided with two 65-W fluorescent lights. The lights were positioned to minimize surface glare, but provide adequate illumination to the field-of-view. Additionally, the current meter was located behind the camera to minimize surface disturbance. The current meter was operated using procedures outlined by the manufacturer.

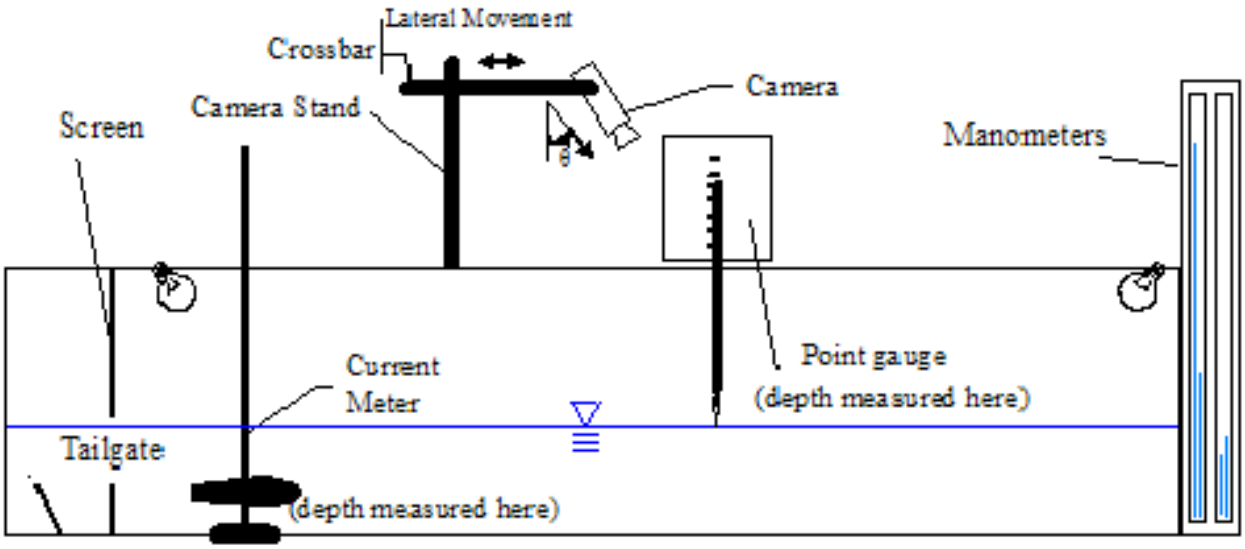

Figure 11. Laboratory setup for testing the LSPIV prototype. The setup layout maximized accuracy of the measuring devices and eased in adjusting the measurement conditions.

Use of Current Meter

A current meter was selected as a comparison to LSPIV measurements because of its accuracy and common use by field technicians. The current meter selected was the Marsh-McBirney Flo-Mate 2000 and it was operated under the guidelines given in the Installation and Operations Manual (Marsh-McBirney, 1994). The Flo-Mate 2000 estimates velocity by measuring electromagnetic induction and using Faraday's law to estimate velocity. The sensor includes an electromagnetic coil that produces a magnetic field, and a pair of carbon electrodes to measure the voltage induced by the moving conductor, in this case water (Marsh McBirney, 1994).

The data were collected in the operating range of the current meter. The velocity operating conditions for the Flow-Mate 2000 are from -0.5 fps to 19.99 fps and the temperature can vary from 32 °F to 160 °F. The Flo-Mate 2000 has a specified accuracy of

±2% of the measured velocity plus the zero stability (Marsh McBirney, 1994). The zero stability is the variability of the velocity reading in still water, and is estimated at ±0.05 fps. Prior to data collection the current meter zero-stability was checked using a bucket of water. During the laboratory experiments the zero stability was always below ±0.05 fps.

The velocities were collected at 0.6 water depth using a USGS top-setting wading rod. The stage was measured at the wading rod to ± 0.01 foot accuracy. Velocity measurements were collected at 1.5, 3, 5, 7, 9 and 11 inches from the channel boundary. Operating depths ranged from 0.3 to 1.3 ft, depending on the Froude number tested. Fixed point averaging (FPA) was used to minimize any noise in the data over time. The FPA method averaged velocities over a period of time by mimicking an RC circuit. The time period was specified as 20 seconds in the laboratory experiment. The discharge was calculated using the mid-section method, outlined in Section 2.2.8 Calculating Discharge. Additional equipment and materials were necessary for the LSPIV prototype, such as a camera and particle tracers.

Use of LSPIV Prototype

The laboratory LSPIV prototype was developed after an extensive review of literature regarding previous LSPIV research. The camera used in the study was a Pelco monochrome CCD camera (Model # MC3651H-2). This camera was selected because of its high resolution (480 X 640 pixels), low-light capabilities (Sony EXview HAD CCD technology), 8-bit per pixel output (optimum for the evaluation software used), and its robustness for outdoor use. Additionally, an extra-wide lens (f# 1.4) was selected for a large field-of-view. The lens was a Pelco C748M varifocal lens with direct-drive auto-iris. The auto-iris was automatically adjusted by the camera, depending on light conditions. Using a f# in the range

of 1-3 increases the signal to noise ratio (Abiven and Vlachos, 2002). The camera produced an analog output that was digitized via an ImagingSource® Video to FireWire Converter (Model # DFG/1394-1). This information was accessed as 8-bit black and white images using the image acquisition toolbox (Version 1.2) within Matlab (Release 14). A custom-written Matlab program was used to collect 25 images at 25 Hz. The high image capture rate was necessary to capture reasonable pixel displacements for high velocities versus a small field-of-view. A DELL Inspiron 5100 with 256 MB RAM, Pentium 4 CPU, and 2.40 GHz operating speed was used to collect and analyze the data. A data collection procedure was also developed to minimize error.

The LSPIV prototype used wood beads as the tracer particles. They were painted white to enhance contrast. The seeding density was determined before each replication. The beads were added to the surface by hand to minimize agglomeration. However, significant agglomeration occurred, especially at lower velocities. To change the camera angle a custom-made stand was attached to the flume. The stand allowed for multiple angles and an adjusting cross-bar kept a constant field-of-view. Marks on the stand allowed for good repeatability in every configuration. The data were collected and recorded by a team of three people using a data collection sheet (Appendix B Data Collection Sheets). After the data were collected, the LSPIV images were processed to estimate discharge.

3.1.2 Image Pre-Processing

Pre-processing is necessary to prepare the images for evaluation and was comprised of image enhancement, registration, and transformation (Figure 13). Image enhancement is necessary to improve the contrast of the particles and the background. Matlab provided several filters for improving contrast and increasing sharpness (Mathworks, 2004).

Preliminary work selected the best filter or combination of filters. The Matlab filter **imadjust** was used to adjust the intensity values closer to a bell-shaped curve increasing the contrast. The command stretches the low and high values such that 1% of the data are at the extreme ends of the pixel intensity spectrum (Figure 12). The average low pixel intensity values reflect the black background and white particles. The controlled lighting conditions reduced the need for advanced image enhancement techniques.

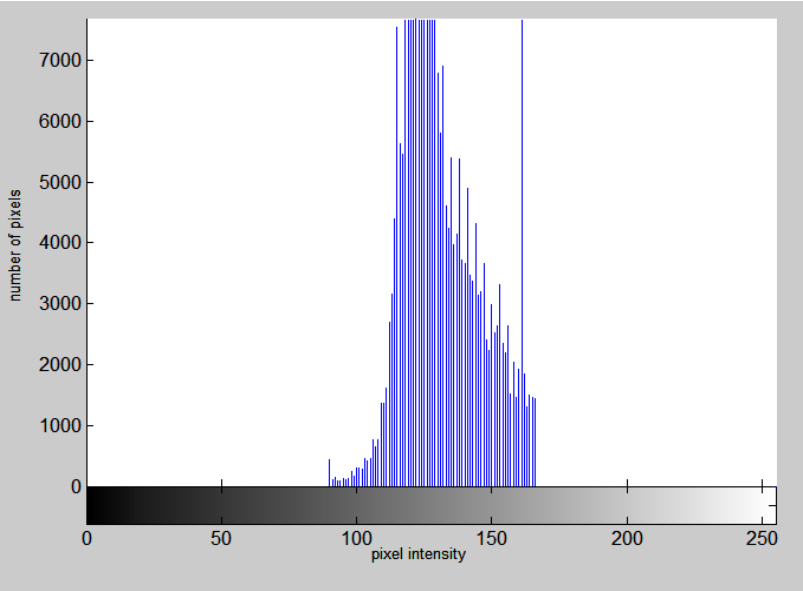

(a)

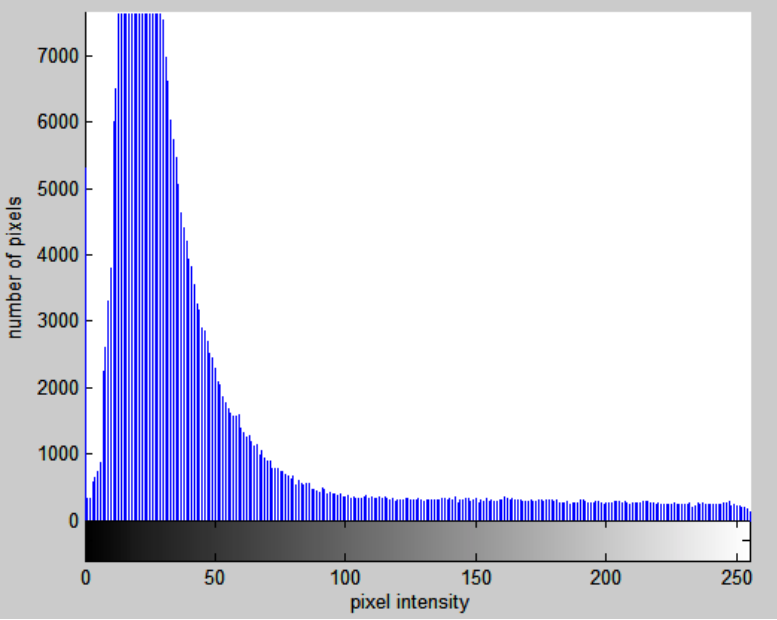

(b)

Figure 12. (a) Pixel histograms for the original image and (b) pixel histogram for the enhanced image. The enhanced histogram is spread across all pixel intensity values and grouped at opposite ends of the spectrum to enhance contrast.

Image registration is the process of identifying points of known location on an image with an unknown coordinate system. This process is necessary to transform an image and

remove spatial distortion. In the laboratory experiments, points were identified using a template placed in the flume prior to data collection. The template had a 1 by 1-inch grid pattern. Prior to the experiment, the pixel and physical locations of twelve reference points were found for all four camera angles.

The reference points were used to create transformation equations. A preliminary investigation used the 1 by 1-inch grid to estimate the effectiveness of different transformation techniques, including that proposed by Fujita et al. (1998). More effective techniques showed the parallel and perpendicular lines in the transformed image. It was found that the Matlab 'local-weighted mean' (**lwm**) function was the most accurate of the methods investigated. The **lwm** function infers a second-order polynomial transformation function based on the six closest control points:

$$(u, v) = [\, x \cdot y \cdot xy \cdot x^2 \cdot y^2 \,] \cdot T^{-1} \qquad \textbf{(18)}$$

Where u and v are the horizontal and vertical pixel location of the corrected point, x and y are the physical location of up to six control points, and T^{-1} is the transformation matrix (transformation coefficients). The **lwm** function creates a separate transformation function for every reference point. The procedure worked well (Figure 13) and images were cropped prior to image evaluation. The average dimensions of the pre-processed images were approximately 400 by 700 pixels. The large size of the images increased the computation time to approximately 40 seconds per image.

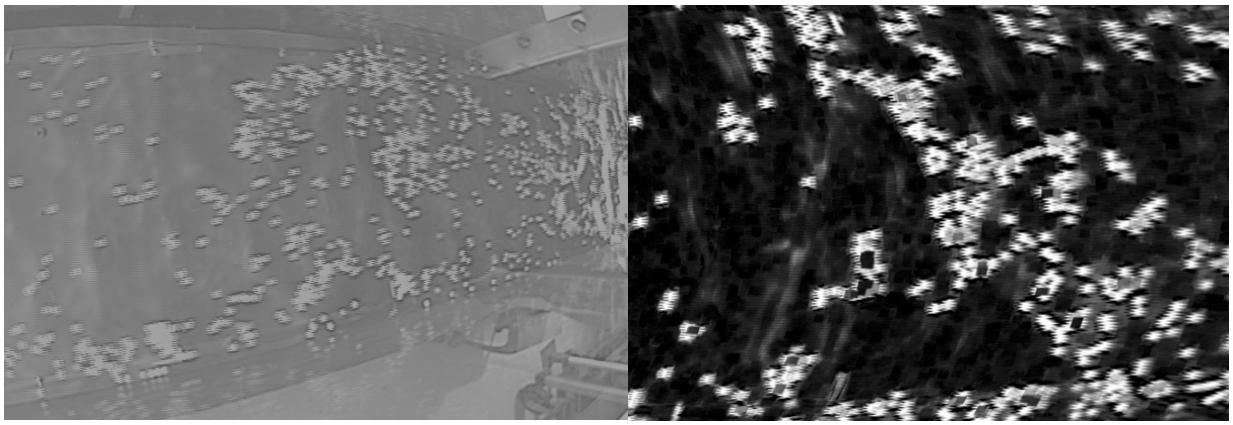

(a) (b)

Figure 13 (a) original image and (b) the preprocessed image. A filter was used within Matlab to alter the pixel intensity values to enhance contrast. Additionally, 12 control points were used to register and transform the image. The image was also cropped. Image enhancement was minimal due to the controlled illumination in the laboratory.

3.1.3 Image Evaluation

Image evaluation is a critical component to LSPIV measurement accuracy. Therefore, we collaborated with Dr. Pavlos Vlachos in the Mechanical Engineering Department at Virginia Tech. The software developed by Dr. Vlachos and his partners (DPIV Version 1.0) is as robust as any used in LSPIV applications. This program uses cross-correlation algorithms, window off-set schemes, and a novel adaptive window interrogation method (Abiven and Vlachos, 2002).

The displacement vectors were calculated by estimating cross-correlation coefficients using Fast Fourier Transforms (section 2.2.5 Image Evaluation). The region-of-interest (ROI) was selected to be four times the maximum displacement of interest. Additionally, a single-order direct window offset was used (section 2.2.5 Image Evaluation). Therefore, the laboratory procedure used (256, 64) ROI window size as a first pass, and then a (128, 64) offset window as a second pass. The second pass increased the range of spatial scales that could be measured. The cross-correlation coefficients, and corresponding displacement vectors, were calculated at the user-

specified grid spacing (Figure 14). The grid spacing was specified at 32 pixels as an optimum combination of resolution and computation requirements. This produced a 12 by 20 vector surface velocity field. The method evaluated sub-pixel accuracy using the three-point Gaussian estimation method. The image evaluation procedures were slow, requiring approximately 80 seconds per image pair. Therefore, two computers were networked together to perform the image evaluation and post-processing simultaneously.

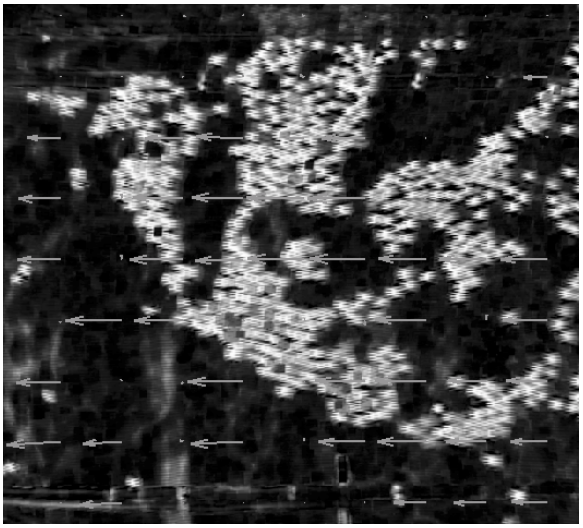

Figure 14. Surface velocity field produced by one image pair from laboratory experiments. The grid spacing interrogation window sizes were chosen to provide adequate resolution without being too computationally intensive.

3.1.4 Image Post-Processing

Image post-processing uses the displacement fields calculated during image evaluation to estimate discharge. First, velocities are calculated from the displacement fields and physical pixel size. Next, these velocity fields are averaged spatially and temporally. Finally, the velocity data are used to estimate discharge with area-velocity methods. Custom-written Matlab programs were used to complete these steps (Appendix C Matlab Image Processing Programs. Image validation was not efficient using a 3 X 3 filter because of blurring the velocities at the edges.

The physical size of a pixel must be estimated to calculate velocities from pixel displacements:

$$\vec{v}_{xy} = d_{xy} \cdot L \cdot F \quad \textbf{(19)}$$

Where $\vec{v}_{xy}$ is the x and y components of a velocity vector (ft/s), d_{xy} is the displacement in pixels, L is the physical pixel size (ft/pixel), and F is the frame rate (Hz). The flume setup presented difficulties in estimating the physical pixel size. Increasing the depth in the flume only by a few inches greatly changed the field-of view and corresponding physical pixel size. Therefore, preliminary measurements were made at several depths to estimate a linear relationship between stage and physical pixel size. The velocity fields could then be estimated using the frame rate of 25 Hz.

The velocity fields must be converted to average velocities for one cross-section of the channel. The flume dimensions could then be used to estimate discharge. First, a surface correction factor of 0.95 was used to estimate average velocity from surface velocity. This value was determined from preliminary testing indicating a parabolic vertical velocity profile. The plexi-glass flume provided minimal resistance necessitating smaller correction coefficient. However, at shallower depths the velocity profile may have changed and that was not reflected in the surface correction coefficient. Additionally, the velocity data were averaged parallel to the flow into 12 velocity vectors (varied slightly depending on field-of-view). Subsequently, the velocity was averaged temporally across all 24 image pairs. Lastly, the discharge was calculated using the mid-section method with the average velocities and channel dimensions (Section 2.2.8 Calculating Discharge). The stage used for LSPIV calculations was an average of the

point-gauge and the current meter depth, roughly capturing any water slope. Discharge results are described in 4.1 Laboratory Results and Discussion.

3.1.5 Laboratory Statistical Design

The laboratory data were collected in a split-plot statistical design. Split-plot data are collected in clusters to ease collection procedures and reduce error. This type of data collection requires specialized analysis procedures to account for covariance, explained in this section. At the guidance of the Statistical Consulting Center, two experiments were used to increase the degrees of freedom testing each factor (Dr. Golde Holstein, personal communication, March 2004). The first experiment focused on the effects of seeding density and the second on the effects of camera angle and Froude number.

The first experiment was used to evaluate the effect of seeding density, collecting 40 data points in two replications with the three treatments. The experiment measured discharge under five levels of seeding density corresponding to 1, 2, 3, 4, and 5 particles per interrogation window. Additionally, two levels of Froude number (0.05, 0.35) and two camera angles (0 and 30 degrees) were evaluated for interaction with seeding density. Froude numbers greater than 0.35 would have been desirable, but were not practical due to current meter operating conditions (not recommended for depths below 0.3 ft). The data were collected in two blocks with 20 repetitions each (Figure 15). The effect of seeding density on LSPIV accuracy was tested using all four different combinations of camera angle and Froude number.

Block 1			
Trial	Camera Angle	Froude Number	Seeding Density
1	Level 1	Level 1	Level 1
2	Level 1	Level 1	Level 2
3	Level 1	Level 1	Level 3
4	Level 1	Level 1	Level 4
5	Level 1	Level 1	Level 5
6	Level 1	Level 2	Level 1
7	Level 1	Level 2	Level 2
8	Level 1	Level 2	Level 3
9	Level 1	Level 2	Level 4
10	Level 1	Level 2	Level 5
11	Level 2	Level 1	Level 1
…	…	…	…
20	Level 2	Level 2	Level 5

Block 2			
Trial	Camera Angle	Froude Number	Seeding Density
21	Level 1	Level 1	Level 1
22	Level 1	Level 1	Level 2
23	Level 1	Level 1	Level 3
24	Level 1	Level 1	Level 4
25	Level 1	Level 1	Level 5
26	Level 1	Level 2	Level 1
27	Level 1	Level 2	Level 2
28	Level 1	Level 2	Level 3
29	Level 1	Level 2	Level 4
30	Level 1	Level 2	Level 5
31	Level 2	Level 1	Level 1
…	…	…	…
40	Level 2	Level 2	Level 5

Figure 15. Depiction of data collection procedure for the first laboratory experiment. Each block tests all treatments at all combinations of factors (two replications are referred to as block 1 and 2).

The second experiment was used to evaluate the effect of the camera angle and Froude number, as well as to test the overall accuracy. This experiment fixed the seeding density at its most accurate level (five particles per interrogation window), and collected discharge measurements over four levels of Froude number (0.05, 0.15, 0.25, 0.35) and camera angles (0, 15, 30, 45 degrees). The data were collected in a manner explained in Figure 15, however in four blocks of 20 repetitions each, for a total of 80 repetitions. Several methods were used to evaluate the influence of the experimental factors on the accuracy of the data.

An error analysis was used to investigate the differences in LSPIV discharge measurements from the other treatments. The relative error was calculated using both the manometer and current meter as the control:

$$\%\,\mathrm{Re}\,lativeError = \frac{[LSPIV(cfs) - control(cfs)]}{control(cfs)} \times 100 \qquad \textbf{(20)}$$

Additionally, a confidence interval was estimated for the treatments using equation 17:

$$\overline{Y} = z_{\alpha/2}\sigma_{\overline{Y}} \qquad \textbf{(21)}$$

where $z_{\alpha/2}$ is the value of the z-statistic with tail area of α/2 (equal to 1.96 with α=0.05) and $\sigma_{\overline{Y}}$ is the sample mean standard error (equal to $\sigma \div \sqrt{n}$). The combination of small discharges (on the order of 10^{-1} cfs), only two significant digits, and high variability reduced accuracies in the error analysis. Therefore, statistical inferences may prove more useful.

Statistical analysis techniques were developed in consultation with the Statistical Consulting Center. The Statistical Analysis Software (SAS) Version 6.03 was used to analyze the data. The split-plot data were collected in clusters, and therefore showed covariance. Therefore, an analysis of covariance (ANACOVA) was necessary to interpret the data. ANACOVA uses both regression and an analysis of variance. However, in ANACOVA the error terms in the regression models are changed to account for a covariate, in this case discharge.

The SAS **Proc Mixed** command was used to evaluate the split-plot design (Appendix D Statistical Analysis Programs). The **Mixed** command uses linear regression; however it allows the data to exhibit correlation and non-constant variability. A mixed model is similar to a linear regression, except it allows for both correlation and heterogeneous variances (SAS Version 6.03 User's Manual):

$$y = X\beta + Z\gamma + \varepsilon \qquad \textbf{Equation (22)}$$

where X and Z are the known matrixes, β is error due to fixed effects, γ is error due to random effects, and ε is independent random error. The command assumes both γ and

ε are normally distributed. The degrees of freedom were found using the Satterwaithe method (SAS, 2004). Ultimately, a mixed model can be used to estimate Type III fixed effects for the factors of interest. The model estimates an F-statistic and subsequently a p-value based on the F-distribution. The significance levels were used to determine the factors that had a significant effect on accuracy.

Further investigation was made after the variables showed significance in the split-plot analysis. Comparison between different levels of the factors was possible using multiple comparisons. The SAS **Contrast** command tests an F-statistic using an identical method as the mixed model. The **Contrast** command uses a pairwise comparison and estimates both fixed and random effects. It was used to evaluate differences between factor levels (e.g. accuracy at 15 versus 30 degrees). Other techniques were used to measure overall treatment accuracy.

When the mixed model showed significance, a one-way ANOVA was used to test equality under identical conditions. The ANOVA was used to test LSPIV accuracy against the other treatments. A t-test was most appropriate for testing differences between samples (Walpole et al., 2002). The **Proc ttest** and **paired** commands were used to test paired samples by calculating a t-statistic:

$$t = \frac{\bar{x} - m}{s_d - \sqrt{n}} \qquad \textbf{Equation (23)}$$

where $\bar{x}$ is the sample mean of the paired differences, s_d^2 is the sample variance of the paired differences, and n is the number of paired samples. A p-value can be estimated using a t-test statistic based on the t-distribution. The t-test procedure assumes that the samples are randomly drawn from normally distributed populations an unknown mean

and standard deviation. This assumption should be valid for hydrologic events. Additionally, the samples were gathered on various days and from multiple sites to reduce covariance. This study also has greater than 15 samples and should therefore produce little error according the central limit theorem (SAS, 2004). Specific statistical commands used are given in Appendix D Statistical Programs.

A significance level (alpha value) was set prior to data collection. Additionally, ranges of significance levels aided in analyzing and discussing the results (Table 4). The statistical analysis did not produce numerous factors of a high level of significance. However, a combination of the error and statistical analysis methods was used to best evaluate the LSPIV prototype.

Table 4. Levels of significance (alpha values) and corresponding statistical importance used in the analysis of the laboratory data.

Level of significance (α)	Interpretation
0.95-0.99	Moderately significant
0.99-0.9999	Highly significant
<0.9999	Very highly significant

3.2 Field Methodology

The objective of the field component of this study was to develop a LSPIV field prototype and operating procedure and perform an accuracy analysis using the prototype. The prototype was developed based on the equipment and methodology used in the laboratory. Additionally, a comprehensive operating procedure was developed to minimize error. The operating procedure was used to collect discharge measurements from two field sites. A total of twenty discharge measurements were collected from September to November 2004. Discharge measurements were made with a Marsh-McBirney Flo-Mate 2000 and permanent control structure as a means of comparison. The LSPIV prototype measurements were subsequently analyzed for their accuracy.

3.2.1 Field Sites

Field sites were selected based on USGS standards and site requirements specific to the LSPIV prototype (Rantz et al., 1985). The USGS recommends straight reaches with parallel flow lines, a uniform bed, and minimal vegetation in the channel. Additionally, the prototype requires a confined channel or a small floodplain to capture high-flow events. Sites were also selected to minimize glare and shadows on the water surface. A total of four sites were investigated, however two sites with permanent control structures (e.g. weirs) were chosen.

The prototype was tested on two low-order streams in the Blacksburg, Virginia area. The sites did have bed disturbances and could show complex flows in some situations. However, adverse conditions are typical in low-order streams and provided an opportunity for a more robust test of LSPIV. Additionally, the prototype was tested at

the outlet of both an urban and an agricultural watershed. The two locations allowed for testing under different flow and physical conditions.

Stroubles Creek

Discharge measurements were first collected for Stroubles Creek on the Virginia Tech campus. Stroubles Creek is a second-order stream at the Duck Pond and drains a 1,767-acre watershed. The water level in the creek ranged from 0.31 to 1.85 ft with stream widths of 8 to 14 ft during the measurement period. The watershed has a variety of land uses (Stroubles Creek TMDL, 2004):

Table 5. Land use classifications for the Stroubles Creek watershed above the Duck Pond, The watershed contains the town of Blacksburg with a high (50%) level of impervious area.

Land Use	Percentage of Watershed Area
Forested	4.2%
Commercial and Transportation	21.7%
Open Urban Green Space	14.8%
Low Density Residential	3.7%
Medium-Density Residential	36.5%
High-Density Residential	11.9%
Improved Pasture	6.5%

The watershed is dominated by urban and suburban land uses (Figure 16). Therefore, the watershed has considerable impervious surface area. As a result, Stroubles Creek watershed is 'flashy' with a fairly small time of concentration and increased peak flow (measured up to 40 cfs). These flow characteristics necessitated a short data collection period to reduce the effects of changing stage on discharge measurement accuracy.

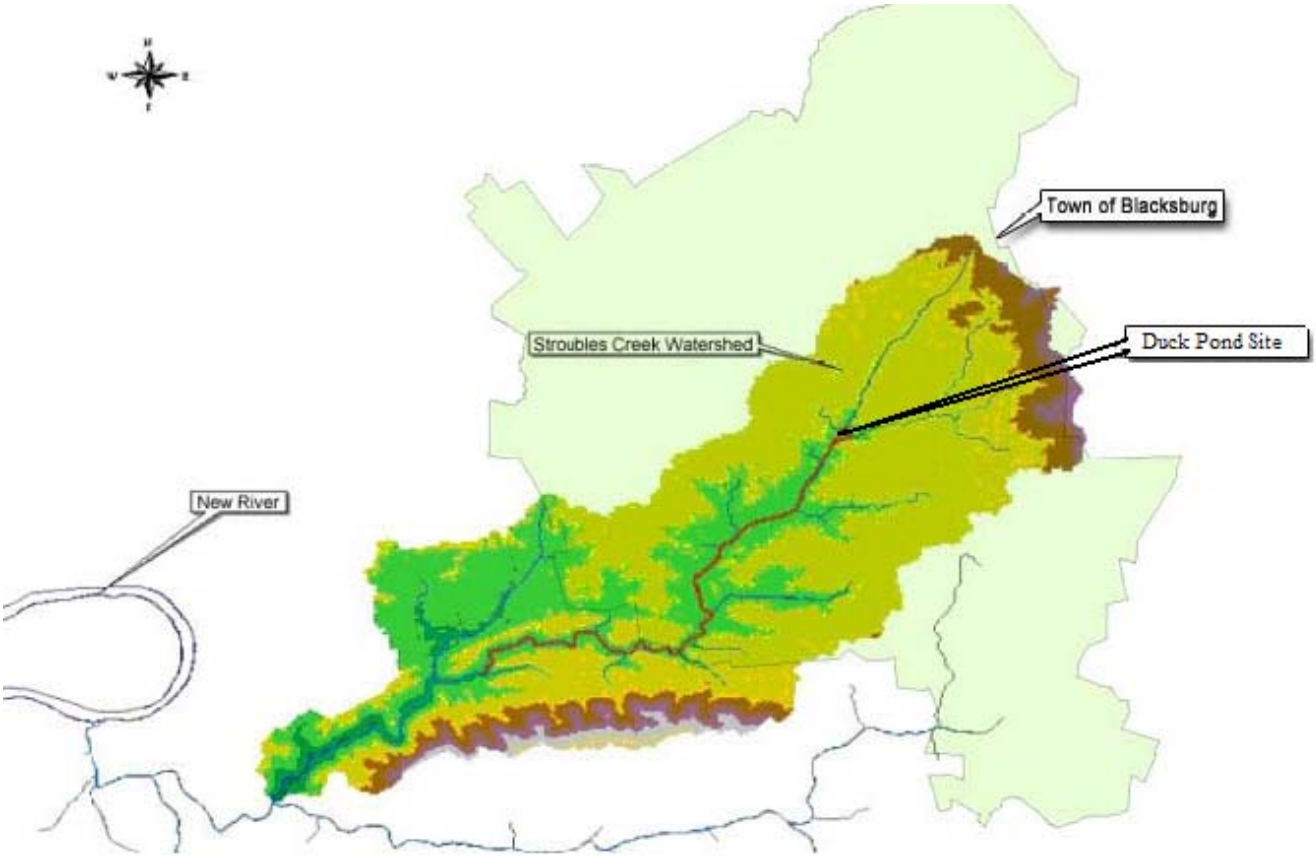

Figure 16. Stroubles Creek watershed. The testing location was at the Duck Pond and included only the portion of the watershed upstream (Zhou, 2004). The watershed is dominated by urban land uses.

The measurement site was located upstream of the Duck Pond on the Virginia Tech campus (Figure 17). The weir at the site has a rectangular low-flow opening and a 150 degree V-notch. It was designed and constructed by the Civil Engineering Department (Thye, 2003). The rating curve was developed in the laboratory and adapted for the field using similitude procedures by Brian Thye for his Master's project. The weir and rating curve seem best suited for measuring high-flows. Stage during baseflow conditions was approximately six inches and provided reasonable conditions for the current meter measurements. There was relatively no tree-cover and associated problems from shade. The camera pointed roughly east causing some surface glare early in the day. The camera angle was approximately 30 degrees from vertical.

The Duck Pond site had a confined channel with minimal bed disturbances. However, construction work on the weir and stream banks near the measurement site necessitated the relocation of the prototype and re-surveying of the channel bathymetry. Work on the weir was performed to reduce leakage problems. Therefore, measurements for low-flow conditions, collected prior to the construction work, had to be discarded. Additionally, a large storm with high winds knocked down the prototype. Subsequently, the prototype was moved to Crab Creek and was secured more properly. Eventually, the prototype was moved back to the Duck Pond site and was re-calibrated using a larger field-of-view.

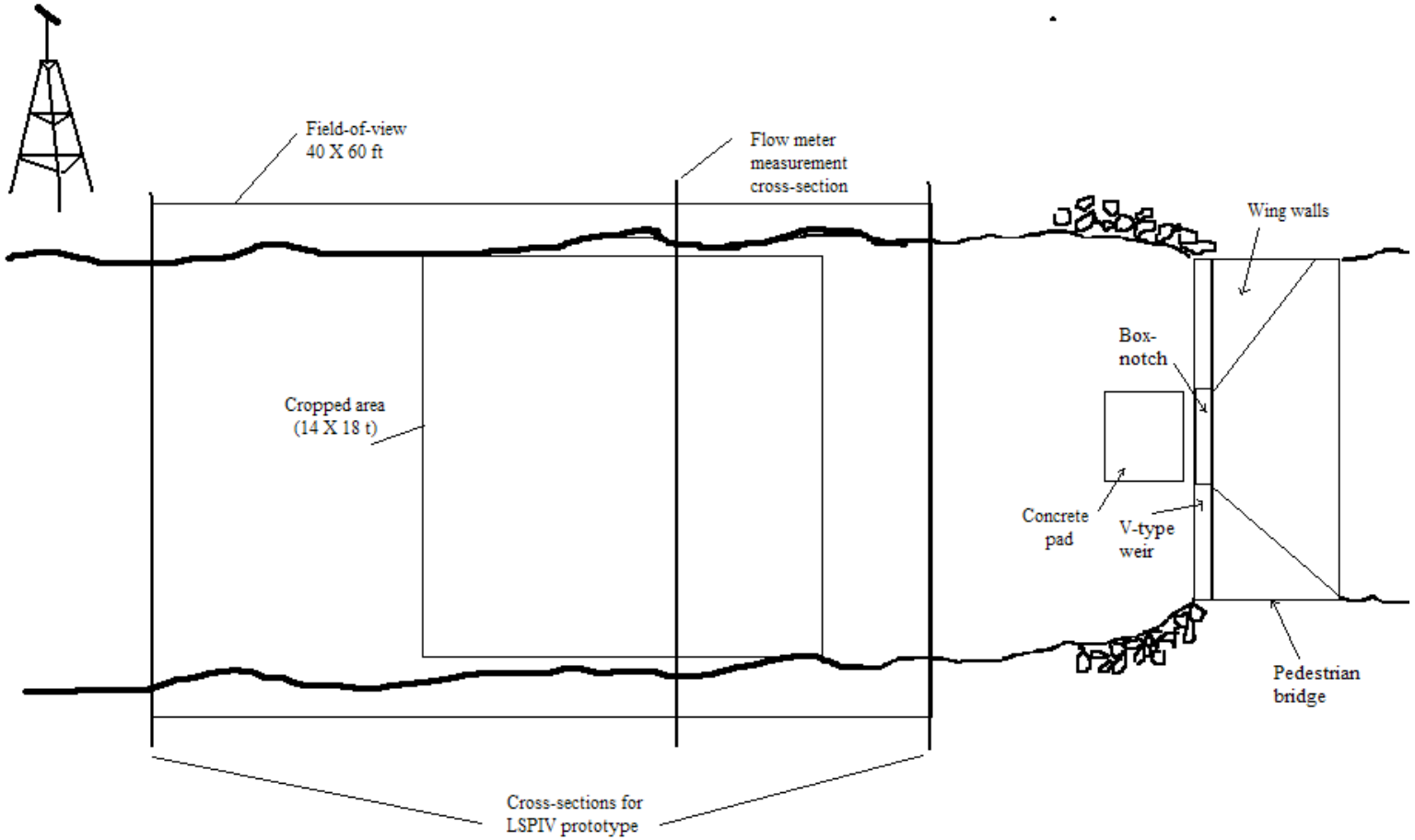

Figure 17. Schematic depicting the experimental setup on Stroubles Creek at the Duck Pond (drawing is not to scale). The setup was designed to maximize the accuracy of the LSPIV prototype and Flo-Mate 2000 for comparison to the site weir.

Crab Creek

The second field site was Crab Creek located on US Route 11 between Christiansburg and Radford, Virginia. The measurement site was at the outlet of a 786-acre agricultural watershed (Figure 18). Crab Creek is a third-order stream at the measurement location. The water level in the stream ranged from 0.68 to 1.84 ft during the measurement period and discharges as high as 63 cfs (roughly a two year return period) was measured. The watershed landuse has not significantly changed since 1967 (Mitchem, 1997):

Table 6. Land use fractions for Crab Creek watershed as reported in 1967 (Carr and Buford, 1967).

Land Use Type	Percentage of total watershed area
Cultivated	40 %
Pasture	42 %
Wooded	13 %
Idle	4 %
Roads	1 %

The watershed has an average slope of 12 % (Carr and Buford, 1967) with a moderate time of concentration. The US Department of Agriculture (USDA) installed discharge monitoring equipment at this site in 1957.

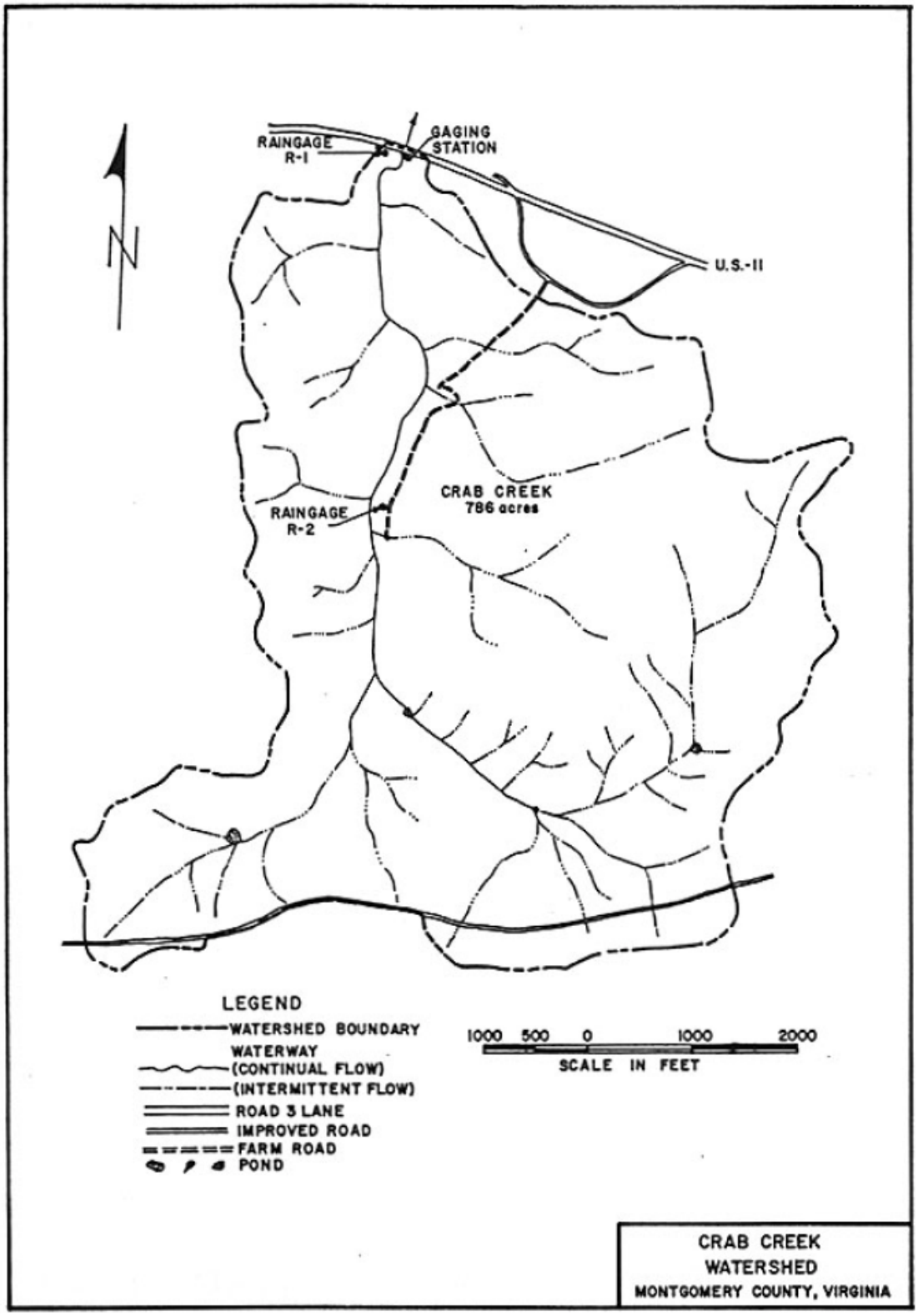

Figure 18. Crab Creek watershed located between Radford and Christiansburg, Virginia (Carr and Buford, 1967). The 786 acre watershed is dominated by row crops and pasture.

The reach on Crab Creek was selected because it included a calibrated USDA gauging station (Figure 19). The gauging station uses double 6 X 6 ft culverts modified with twin Virginia V-notch weirs. Discharge measurements were collected by the USDA from 1957 to 1979. Significant sediment had accumulated behind the weir. The site was prepared by removing enough sediment to allow measurements using the staff gauge. However, the researchers noted that the removal of all sediment was impractical and would not likely improve the rating curve significantly (Mitchem, 1997).

The LSPIV prototype used a measurement reach located roughly 100 ft upstream of the gauging station. This section provided a well-defined parabolic-shaped channel with a bedrock bottom. However, this measurement reach also produced some difficulties. The reach was located downstream of a bend. The flow was accelerating outside of the bend and there were eddy effects on the inside. Additionally, riffles upstream of the measuring area produced some surface disturbances. However, this was the best reach upstream of the weir. Lastly, the prototype encountered glare problems during midday. This is surprising because the area was well-shaded by large trees. Difficulties with the camera may have exacerbated the glare problems. The camera was operated at an angle of 35 degrees from vertical.

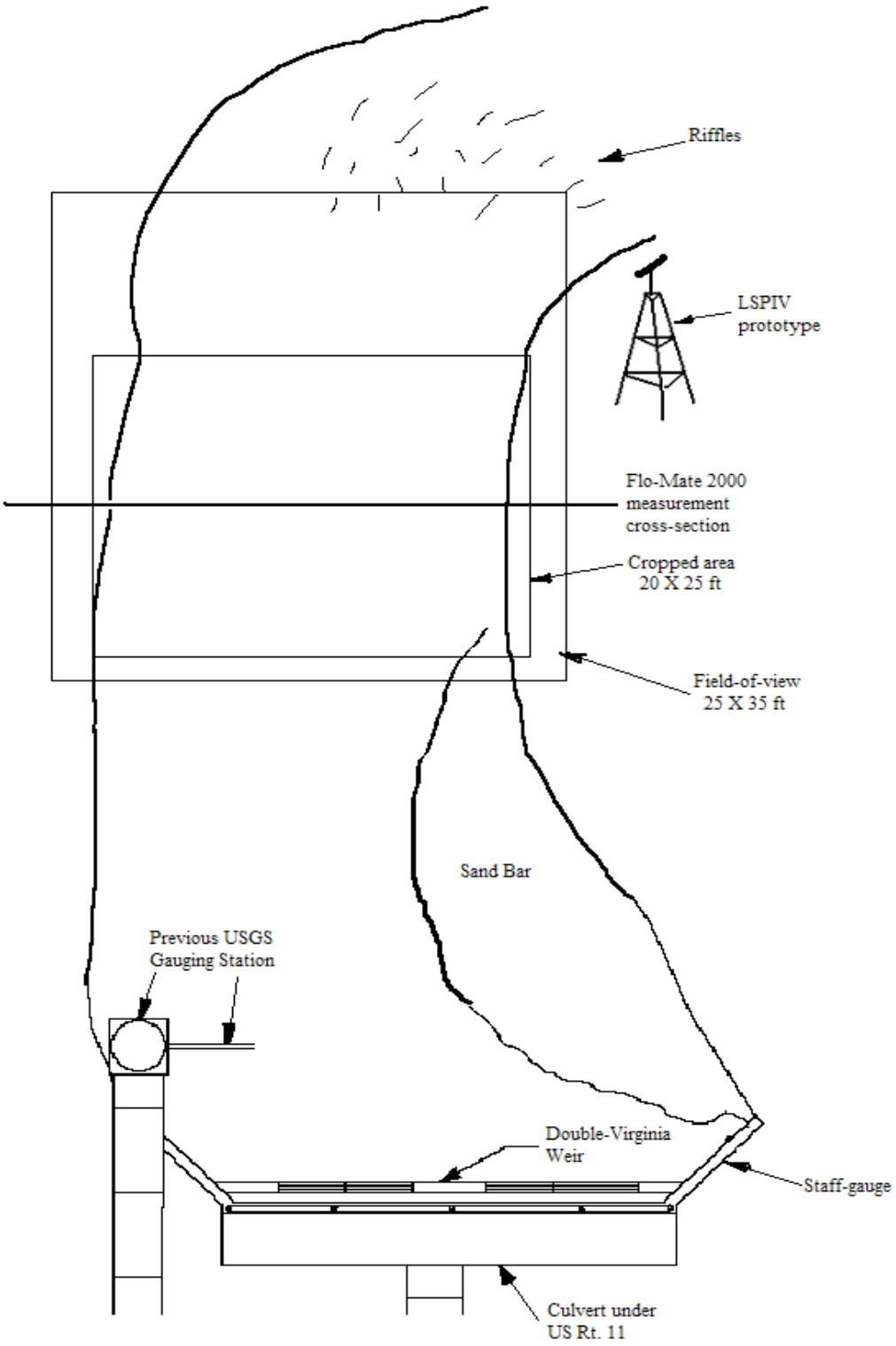

Figure 19. Schematic depicting the experimental setup at Crab Creek. The setup was designed to maximize the accuracy of the LSPIV prototype and Flo-Mate 2000 for comparison to the site weir.

Site Preparation

The ground reference points (GRP) and channel cross-section were surveyed prior to the collection of images. The GRPs are necessary to register and transform the image. The cross-section information is required for estimating discharge. The survey information was collected using a Leica Model TC407 (Leica, 2003). The station uses a laser level and prism to estimate distance and angles to within 1.5 inches and 1º 30', respectively. Data points were saved onto internal memory using the station and acquired and manipulated by a spreadsheet.

Temporary GRP were collected at each site and anytime the camera position was adjusted. Temporary GRP were identified by acquiring a single image of the measurement area and identifying features at the water surface (Figure 20). The features identified were rocks, exposed bedrock, trees, and roots. The features were marked on the image, within ± 1 pixel, using an image editing program. Subsequently, the point was surveyed with the Leica survey equipment. A total of 10 to 12 GRP were taken at each site depending on the identifiable features. The registration process using these points is explained in section 3.2.5 Image Pre-Processing.

Figure 20. Twelve temporary GRP shown for the Stroubles Creek field site (picture enhanced for clarity). The points were necessary to register and transform the image to remove spatial distortion.

Two channel cross-sections were surveyed for use with the LSPIV prototype. The channel cross-section was surveyed at the bottom and top of the field-of-view (Figure 17). The average of the two cross-sections was used to estimate discharge with the LSPIV velocity measurements. A minimum of 20 points were used to estimate each cross-section. Points were collected at approximately one foot intervals across the channel, with closer points during changes in slope. A Microsoft Excel spreadsheet was used to spatially average the two cross-sections. Additional cross-section measurements were taken during the operation of the current meter.

3.2.2 Use of Current meter

A current meter was used as a reference for the LSPIV measurements because of its accuracy and common use by field technicians. The current meter selected was the Marsh-McBirney Flo-Mate 2000 (Marsh-McBirney, 1994). The Flo-Mate 2000 estimates velocity by measuring electromagnetic induction and using Faraday's law to estimate velocity. The sensor includes an electromagnetic coil that produces a magnetic field, and a pair of carbon electrodes to measure the voltage induced by the moving conductor, in this case water (Marsh McBirney, 1994).

Depth and velocity measurements were taken at fixed lengths across the width of the stream. A tape measure was fixed across the stream and a minimum of ten depth, velocity, and distance measurements were taken (Figure 21). Therefore, a wetted cross-section measurement was made with each operation of the Flo-Mate. The velocities were collected at 0.6 water depth using a USGS top-setting wading rod. The stage was measured at the wading rod to ± 0.01 foot accuracy. Operating depths ranged from 0.3 to 3.5 ft and velocities from -0.11 to 1.93 fps. Measurement collection was performed with one or two technicians and data were recorded on the sheet shown in Appendix B. The discharge was calculated using the mid-section method, outlined in Section 2.2.8 Calculating Discharge.

Figure 21. A photo showing technician gathering velocity measurements using the Marsh-McBirney Flo-Mate 2000, at Crab Creek. The Flo-Mate was operated in accoradance with the manufacturer's operating procedures (Marsh-McBirney, 1994).

3.2.3 Use of Weir

In the field component of this study, discharge measurements made with LSPIV were compared to those obtained form weirs already existing in the stream. Weirs measure discharge by suppressing the flow into a nappe. The main reason that weirs have been in widespread use is because a unique relationship between stage and discharge can be developed. However, variability in the stage discharge relationship can come from several sources (Ackers et al., 1978):

1. Channel roughness can influence flow conditions and is subject to seasonal changes.
2. Stream bed level can affect the stage measurements by removal and deposition of sediment.

3. Temporary change in flow can result in a hysteresis effect depending on the rate of rise or fall of the flow.
4. Influence of downstream conditions.

If a standard type of weir is used and constructed according to established guidelines, no field calibration is necessary (Ackers et al., 1978). It is because of these established standards that weirs are commonly used as the statistical control for field investigations.

3.2.4 Use of LSPIV Prototype

The LSPIV field prototype used equipment and methods that had been developed in the laboratory. However, the field prototype equipment necessitated several improvements over the laboratory prototype: resistance to weather and vandalism, adjustability for use at multiple locations, and adoption to sunlight illumination. Additionally, software and data processing methods were improved for poor illumination, complicated channel geometries, correcting spatial distortion in the field, and spatially averaging velocity data. In addition to these requirements, the prototype was designed to be easy-to-operate, inexpensive, and accurate. Construction of the prototype was completed in the summer of 2004. Operating instructions for assembling and operating the prototype are included in Appendix G Prototype Operating Instructions.

Prototype Equipment and Materials

The field prototype is capable of measuring discharge in a variety of flow conditions and stream sizes. The prototype's hardware is mounted on a custom-made steel stand, shown in (Figure 22). The stand is a tripod that can be disassembled into three legs and a telescoping camera mount. The tripod legs have rungs for strength and also to allow access to the camera. The tripod was mounted to the ground using two-foot rebar stakes hammered into holes through each foot. Additional ground stakes were attached with steel cable to reduce any 'top-heavy'

effects from the camera enclosure. The camera was mounted such that its height could be adjusted with a telescoping mount. The height could be changed from 6½ to 15 ft; a feature that allowed adjustment of the camera's field of view. Additionally, the angle of the camera mount can be adjusted to change the field-of-view and decrease distortion. Both the telescoping sections and angle adjustment were adjusted via tension screws mounted on the steel tubing.

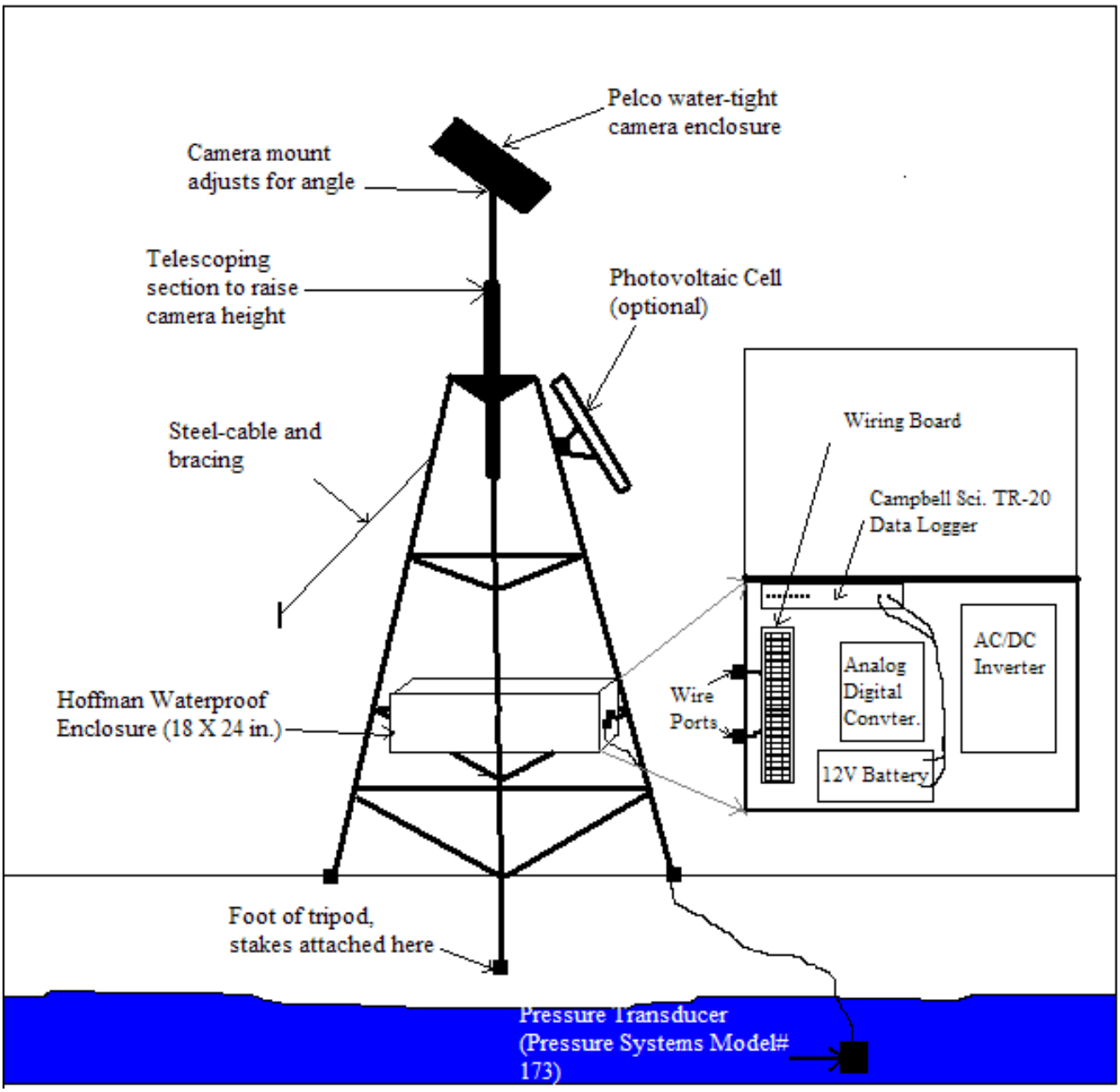

Figure 22. LSPIV field prototype schematic, showing the stand, waterproof box and contents, and pressure transducer (wires were omitted for clarity). The prototype was capable of acquiring images and measuring stage with the assistance of a field technician.

The field prototype used the same camera and lens as the laboratory experiments (Pelco monochrome CCD camera (Model # MC3651H-2)). This camera was selected because of its high resolution (480 X 640 pixels), low-light capabilities (Sony EXview HAD CCD technology), 8-bit

per pixel output (optimum for the evaluation software used), and its robustness for outdoor use. Additionally, an extra-wide lens (f# 1.4) was selected for a large field-of-view. The lens' large field-of-view and focal length proved useful; however, other lenses may be more suitable depending on the channel dimensions. Preliminary work was necessary to adjust the camera to provide high-quality images.

The camera parameters were optimized at each field site. The parameters of interest are the macro and micro focus, gain, contrast, and backlight illumination. After the field-of-view was established at the site, the camera was focused to the water surface. Additionally, the back focus was adjusted for resolution. The automatic gain setting was used to adjust the gain for low-levels of illumination. Also, the electronic shutter control and flickerless camera options were used to compensate for excessive light levels. Finally, the DC lens level adjustment was changed to provide maximum contrast. It should be noted that contrast levels should be adjusted for bright sunlight conditions or glare problems can be exacerbated. The camera was operated from a waterproof enclosure.

A waterproof camera enclosure was necessary to mount and weatherproof the camera. The enclosure was is a Pelco EH2500 Series dust-tight enclosure (Model# EH2512-1). The enclosure was selected because it adequately fit the camera and offered water-resistant features. Additionally, the enclosure is equipped with a 120 V AC heating element to defrost the enclosure window. A sun-shield was also employed to reduced glare on the window. Additional desiccant was placed in the enclosure to reduce moisture. The back of the enclosure was further waterproofed by applying lithium grease to the O-ring and exposed screws. The wire outlet ports on the back of the enclosure were closed with caulk after they had been wired to the equipment enclosure.

The hardware in the field was stored in a Hoffman waterproof enclosure mounted on the stand (Series 12). The enclosure had a dimension of 18 X 24 in. and was sealed using a rubber gasket and screw fasteners. Desiccant packs were used to minimize moisture. The enclosure was attached via U-clamps to the stand and secured using a padlock. The enclosure contained the wiring board that was used to run all the equipment with one 12 V DC battery or photovoltaic cell. An AC/DC inverter (Radio Shack Model# 22-146) was used to provide power to the camera enclosure defroster and/or a laptop computer if necessary. The camera produced an analog output that was digitized via an ImagingSource® Video to FireWire Converter (Model # DFG/1394-1). Also, the enclosure contained a Campbell Scientific datalogger and 12-V battery to record measurements from a pressure transducer.

The pressure transducer and datalogger system was used to make continuous stage measurements. The pressure transducer allowed accurate measurement of stage simultaneous to image acquisition by the prototype. A pressure transducer was mounted with an anchor to the stream bottom. The pressure transducer (Model 173) was manufactured by Pressure Systems and can be operated from 0 – 16,000 psi (Pressure Systems, 2003). The transducer was calibrated by measuring voltage over a variety of stages and fitting a linear equation to the data. The calibration showed errors of ± 0.05 ft of the actual stage. A 10 mV excitation was provided by the Campbell Scientific CR500 datalogger (Campbell Scientific, 2001). The pressure transducer was wired to the datalogger following instructions given in the user manual to produce mV output (Pressure Systems, 2003). The datalogger was set to excite the transducer and take a measurement every ten minutes. However during prototype operation, the stage was read with a Campbell Scientific CR10KD keyboard display attached to the datalogger. The pressure transducer and data logger system improved the usability of the LSPIV prototype.

Starch packing peanuts were used as the tracer particles. The starch peanuts are good tracers because they are environmentally friendly, contrast with the background, do not agglomerate, are very inexpensive, and have an adjustable size. Starch peanuts are made by exploding starch fibers (from corn, potatoes, etc) using heat. Therefore, the starch particles are 100 % organic and dissolve in water. The partial dissolution of the particles made them less vulnerable to wind effects. The particles were applied to the water surface by hand (Figure 23).

Figure 23. A photo showing starch packing material being applied to the water surface in low-flow conditions. Starch packing material served as the tracer particles for the LSPIV prototype.

Prototype Operation and Image Acquisition

The LSPIV prototype collected measurements following a simple procedure. First, the camera image was checked with a live preview. Next, the water surface was seeded with starch material. Subsequently, the images were acquired as the tracers passed through the field-of-view. Last, the stage from the pressure transducer was measured and recorded. This procedure is best

performed by two technicians; however, it is possible for one technician to do it. Image acquisition parameters were optimized for flow conditions prior to acquiring the images.

A custom-written Matlab program was used to change the acquisition parameters and acquire and save the images (Appendix C Matlab Image Processing Programs). The camera was accessed using a Hewlitt-Packard (Pavilion ZV5000 model) laptop connected via a Firewire cable to an analog to digital converter. The images were stored in individual folders on the hard-drive. The user specified the frame rate, delay time, and total number of images in the image acquisition program prior to image collection. Forty images were collected because they provided a good temporal average and reasonable computation times. The delay time could be specified, therefore a single technician could run the program and seed the stream. A 50-second delay was sufficient to seed the stream and allow the tracers to move into the field-of-view before images were acquired. The frame-rate was selected based on flow conditions.

The frame-rate determines the tracers' average pixel displacement between images. Therefore, frame-rates were selected to provide displacements that were optimum for the image evaluation algorithms used. In this case, large pixel displacements necessitated using large region-of-interests (ROI), which could reduce accuracy. The frame rate was therefore increased at high flows (velocities) to maintain pixel displacements between 5 to 15 pixels. This was achieved, in most cases, by using frame rates from 2 to 5 Hz. However, displacements were not always optimum because of a large range of spatial scales. Selecting a frame rate is site-specific and depends on the maximum velocity and physical pixel size. Appropriate selection of the frame rate for unknown channel velocities can be difficult. A rough calculation for maximum velocity can be made using Manning's equation for bankfull conditions. However, a better method would be to acquire images at faster frame rate (6-8 Hz) and discard images, as needed, to increase the average

displacement. After the range of displacements is known the frame rate can be more precisely specified.

Figure 24. A photo of the LSPIV prototype in use at Crab Creek. The prototype was transportable and could be used for a variety of site conditions.

3.2.5 Image Pre-Processing

Pre-processing is necessary to prepare the images for evaluation and was comprised of image enhancement, registration, and transformation. Image enhancement is necessary to improve the contrast of the particles and the background. Shadows, surface glare, and uneven illumination reduce quality of the images. Matlab provided several filters for improving contrast and increasing sharpness (Matlab 7.0 Help, 2004). Preliminary work selected the best filter or combination of filters for sunlight illumination. The enhancement scheme used subtracts the image background and subsequently improves contrast with a filter.

Non-uniform illumination can be corrected by subtracting the constant background from the foreground feature of interest. Morphological opening operations are used to estimate the image background by performing an erosion followed by a dilation operation (Matlab 7.0 Help, 2004). The operations have the effect of removing objects that cannot completely contain the structuring element. The structuring element used was a disk with a 15 pixel diameter. The element diameter was determined from preliminary investigations. The morphological operations enhanced contrast, but also improved the illumination for further contrast enhancement.

The Matlab filter **imadjust** was used to adjust the intensity values to increase contrast. The command stretches the low and high values such that 1% of the data is at the extreme ends of the pixel intensity spectrum (**Error! Reference source not found.**). The low pixel intensity values reflect the black background and white particles. The enhancement scheme proved effective in enhancing contrast; however, problems from glare and shadows were encountered. The images was registered and transformed after the image enhancement was completed.

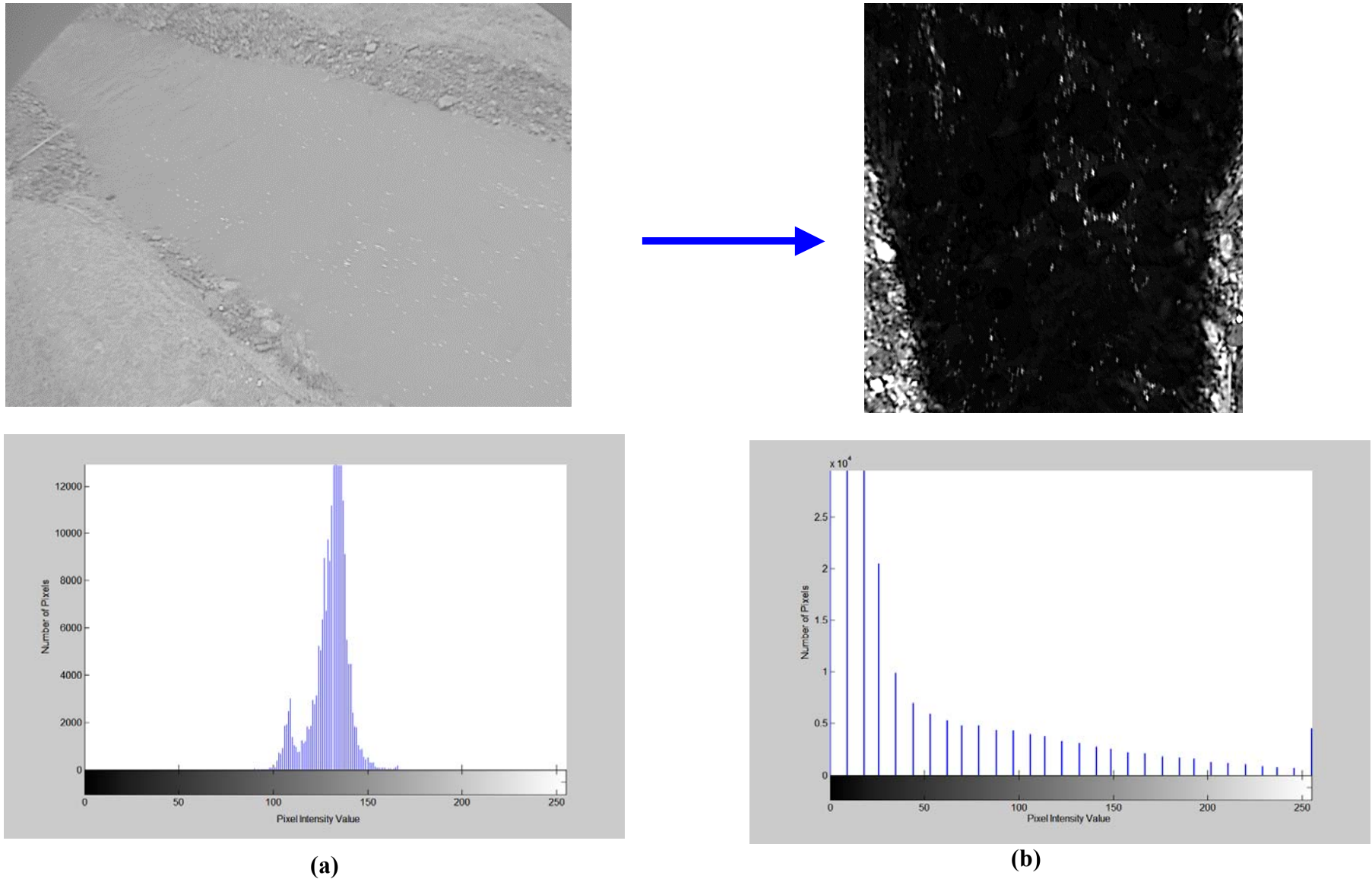

Figure 25. Results from image preprocessing that included enhancement, registration and transformation, and cropping. (a) The original image from the Duck Pond site (picture enhanced for clarity) and the pixel intensity histogram. (b) The preprocessed image corresponding to the original image. The histogram for the preprocessed image shows improved contrast.

Image registration and transformation is used to remove spatial distortion. Image registration is the process of identifying points of known location on an image with an unknown coordinate system. Points were identified across an image and surveyed for physical location, as explained in 3.1.1 under heading Use of LSPIV Prototype. Ten to twelve points were collected for each prototype location. Image transformation equations were developed using these data points.

Transformation algorithms develop mathematical relationships between the distorted image and physical space using the registration points. A preliminary investigation used several different Matlab functions to develop the transformation equations. It was found that the Matlab '**affine'** function was the most accurate of the methods investigated. The **affine** transformation can include translation, rotation, scaling, stretching, and shearing. The transformation can shear the x and y dimensions independently, which is most appropriate for the oblique camera angle. Additionally, the control points were rotated such that the principal direction of flow was in the y-axis. Three pairs of control points are required to solve for the transformation matrix:

$$(u, v) = [x \cdot y \cdot 1] \cdot T^{-1} \quad \textbf{(24)}$$

Where u and v are the horizontal and vertical pixel location of the corrected point, x and y are the physical location at of up to six control points, and T^{-1} is the 3 X 2 transformation matrix (six transformation coefficients). The images were cropped after the transformation was performed (**Error! Reference source not found.**). The cropped area was specific to each site, but the area was large enough to contain the floodplain. Additionally, the location was chosen to maximize parallel flow lines and minimize glare and shadows. The average dimensions of the pre-processed images were approximately 550 by 650 pixels. The large size of the images increased the computation time to approximately 30 seconds per image. The cropped images were analyzed to determine tracer displacements using cross-correlation algorithms.

3.2.6 Image Evaluation

Image evaluation is a critical component to LSPIV measurement accuracy. In this study, image evaluation used an updated version of the DPIV program (Abiven and Vlachos, 2002) that was used in the laboratory experiments. This program uses cross-correlation algorithms, window off-set schemes, and a novel adaptive window interrogation method (Abiven and Vlachos, 2002). The displacement vectors were calculated by estimating cross-correlation coefficients using Fast Fourier Transforms (as explained in section 2.2.5 Image Evaluation). The software has been shown to be accurate to 0.1 pixel using three-point Gaussian sub-pixel estimation (Abiven and Vlachos, 2002). The DPIV software is user-friendly, but requires several user-defined evaluation parameters.

Several parameters must be specified prior to image evaluation, including the region-of-interest (ROI), window-offset scheme, and grid spacing. The ROI was selected to be four times the maximum displacement of interest. Additionally, a single-order direct window offset was used (section 2.2.5 Image Evaluation). The ROI sizes varied depending on the size of the image and the average tracer displacement. For a larger field-of-view, such as the Duck Pond site, a ROI of (256, 128) was used as a first pass, a (256, 64) window as a second pass, and a (32, 32) window as a final pass. For the smaller field-of-view at the Crab Creek site the ROI window sizes were decreased. A first pass with a (128, 64) window was performed, followed by a second pass using a (128, 32) window, and a final pass using a (16, 16) window. Multiple ROI passes increase the range of spatial scales that could be measured. The multiple pass scheme used in this study reduces the need to specify numerous ROI sizes for many different flow conditions.

The cross-correlation coefficients, and corresponding displacement vectors, were calculated at the user-specified grid spacing (Figure 26). A 32-pixel grid spacing provided an optimum combination of resolution and computation requirements. The 32-pixel grid spacing

produced a 14 X 18 vector surface velocity field. The method evaluated sub-pixel accuracy using the three-point Gaussian estimation method. The image evaluation procedures were markedly faster than in the laboratory experiment, requiring approximately four seconds per image pair. The reduced computation time is a function of the updated evaluation software (Jason Carneal, personal communication, 2004). Smaller grid-spacing was investigated (4 and 8 pixels in the x-axis), but did not provide significantly improved results (Appendix H Region-of-Interest and Grid Spacing Sensitivity Analysis). The velocity fields were averaged to compute discharge in the post-processing steps.

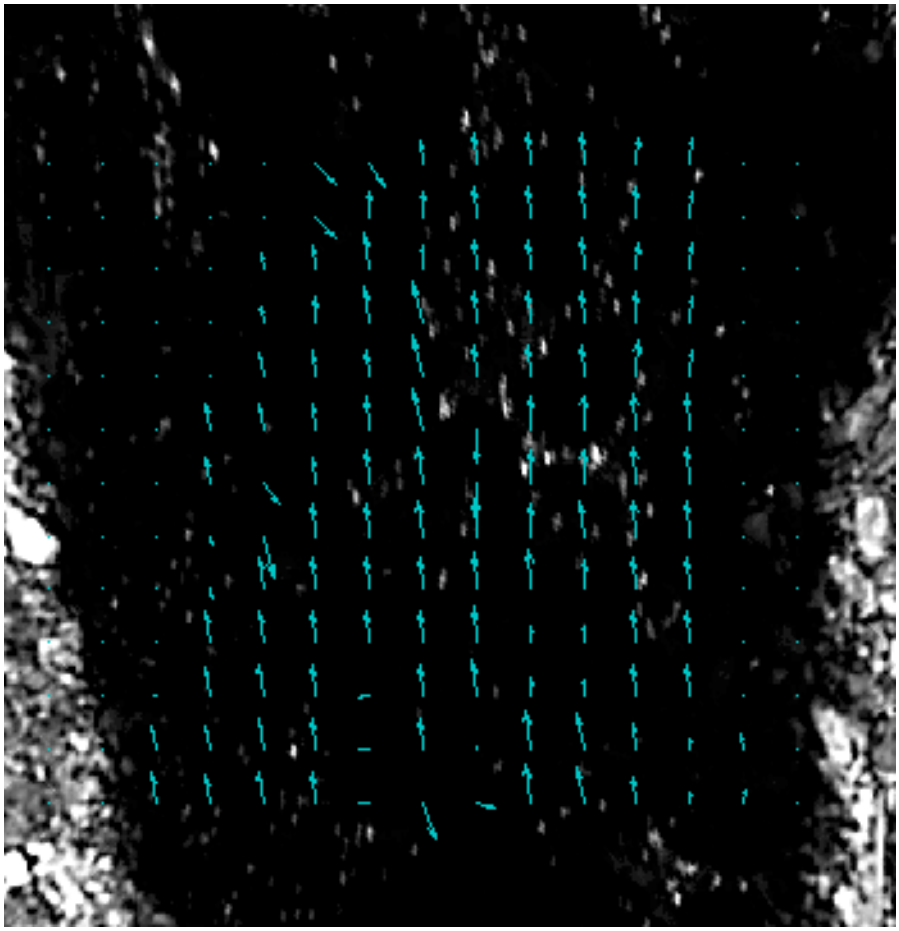

Figure 26. Typical velocity field calculated using DPIV version 1.0 for Stroubles Creek at the Duck Pond. After the velocity fields vectors were generated and spatially and temporally averaged to estimate discharge.

3.2.7 Image Post-Processing

Image post-processing calculates discharge using the displacement fields found in image evaluation. First, velocities are determined from the displacement fields. Next, these velocity fields are spatially and temporally averaged. Finally, the velocity data are used to estimate discharge with area-velocity methods. Custom-written Matlab programs were used to complete these steps (Appendix C Matlab Image Processing Programs). Image validation was not efficient using a 3 X 3 filter because of blurring the velocities along the streambanks.

Velocities must first be determined from the displacement fields. The physical size of a pixel must be estimated to calculate velocities from pixel displacements:

$$\vec{v}_{xy} = d_{xy} \cdot L \cdot F \qquad \textbf{(25)}$$

Where $\vec{v}_{xy}$ is the x and y components of a velocity vector (ft/s), d_{xy} is the displacement in pixels, L is the physical pixel size (ft/pixel), and F is the frame rate (Hz). The displacements are known from the evaluation and the frame rate was defined during image acquisition, as explained in the section Prototype Operation and Image Acquisition. However, the physical pixel size is unknown and must be estimated. Therefore, a method was developed to estimate physical pixel size for any field-of-view. The method estimates physical pixel size based on the stream width and number of LSPIV vectors:

$$L = \frac{W}{V \cdot G} \qquad \textbf{(26)}$$

Where W is the width of the stream in feet, V is the number of velocity vectors used to calculate discharge, and G is the grid spacing in pixel (in this case, 32 pixels). The stream width is back-calculated from the channel cross-section using the stage measured with the pressure transducer. The number of velocity vectors (V) depends on stage and is user-specified. However, a

relationship between the stage and number of vectors could be developed to help automate the procedure. Change in stage did not significantly change the physical pixel size (Table 7). The relatively constant physical pixel size resulted because the differences in stage (up to 1.5 ft) were small compared to the focal length (from 20 - 40 ft). After the velocity fields were determined a scheme was used to estimate the average velocities for area-velocity methods.

Table 7. Post-processing parameters used at all measurement locations and times. The physical pixel size stayed relatively constant with stage. The surface correction coefficient was estimated using a linear relationship between stage and velocity profile correction.

	Date & Time	Stage (ft)	Physical Pixel Size (ft/pixel)	Surface Correction Coefficient
Stroubles Creek Site 1	9/7/2004 11:00	0.49	0.019	0.88
	9/9/2004 9:00	0.62	0.019	0.88
	9/8/2004 13:00	0.81	0.02	0.9
	9/8/2004 12:00	1.06	0.02	0.91
	9/8/2004 10:00	1.68	0.021	0.93
Stroubles Creek Site 2	10/31/2004 16:00	0.33	0.05	0.85
	10/23/2004 12:30	0.39	0.04	0.86
	10/19/2004 8:30	0.42	0.04	0.86
	10/20/2004 17:00	0.45	0.04	0.86
	10/22/2004 9:00	0.46	0.04	0.86
	10/13/2004 10:00	0.6	0.04	0.88
	10/28/2004 9:00	0.58	0.04	0.88
Crab Creek	10/5/2004 8:30	0.68	0.018	0.88
	9/29/2004 9:30	0.85	0.019	0.9
	9/30/2004 8:30	0.86	0.021	0.88
	9/30/2004 18:30	0.86	0.02	0.88
	9/29/2004 17:30	0.98	0.021	0.9
	9/29/2004 8:00	1.02	0.021	0.91
	9/28/2004 11:00	1.84	0.021	0.93

To calculate discharge, the velocity fields must be converted to average velocities across one cross-section of the channel (Figure 27). To calculate average velocities, the surface velocities were changed to depth-averaged velocities, the velocity fields were spatially averaged to

a single cross-section, and the cross-sections were temporally averaged across all image pairs. Velocity varies with depth because of the frictional forces at the bed-water interface. Therefore, a surface correction coefficient is used to estimate an average velocity over the vertical profile based on the surface velocity. The ISO (ISO 748, 1997) recommends correlating the surface velocity with the velocity at 0.6 of the total water depth using correction coefficients that vary between 0.84 and 0.92. Additionally, Creutin et al. (2003) show a trend of increasing correction factor is necessary for higher stages. Therefore, a method was developed to determine correction coefficients as a function of stage. The method assumes that at baseflow condition the correction coefficient is 0.85 and at high-flow conditions (known from debris or floodplain) the correction is reduced to 0.93 (following a range of guidance proposed in ISO 748). A linear relationship can easily be drawn, where 0.85 is the y-intercept. This method was used at both field sites. Additionally, the velocity data were averaged parallel to the flow into between 6-15 velocity vectors, depending on stage. Subsequently, the cross-section velocities were averaged temporally across all 39 image pairs. These velocity vectors were used in area-velocity methods to calculate discharge.

The channel bathymetry information is necessary in area-velocity methods. The cross-section was determined using laser-level equipment, as specified in the section on Site Preparation. The stage was measured using a pressure transducer mounted in the deepest portion of the stream. The stage and cross-section were used to estimate channel area. Lastly, the discharge was calculated using the mid-section method with the average velocities and channel dimensions (Section 2.2.8 Calculating Discharge). Boundary walls were vertical, at either site, and therefore bank correction coefficients were not necessary. The prototype's discharge

measurements were compared to those made using a Flo-Mate 2000 current meter and permanent weir.

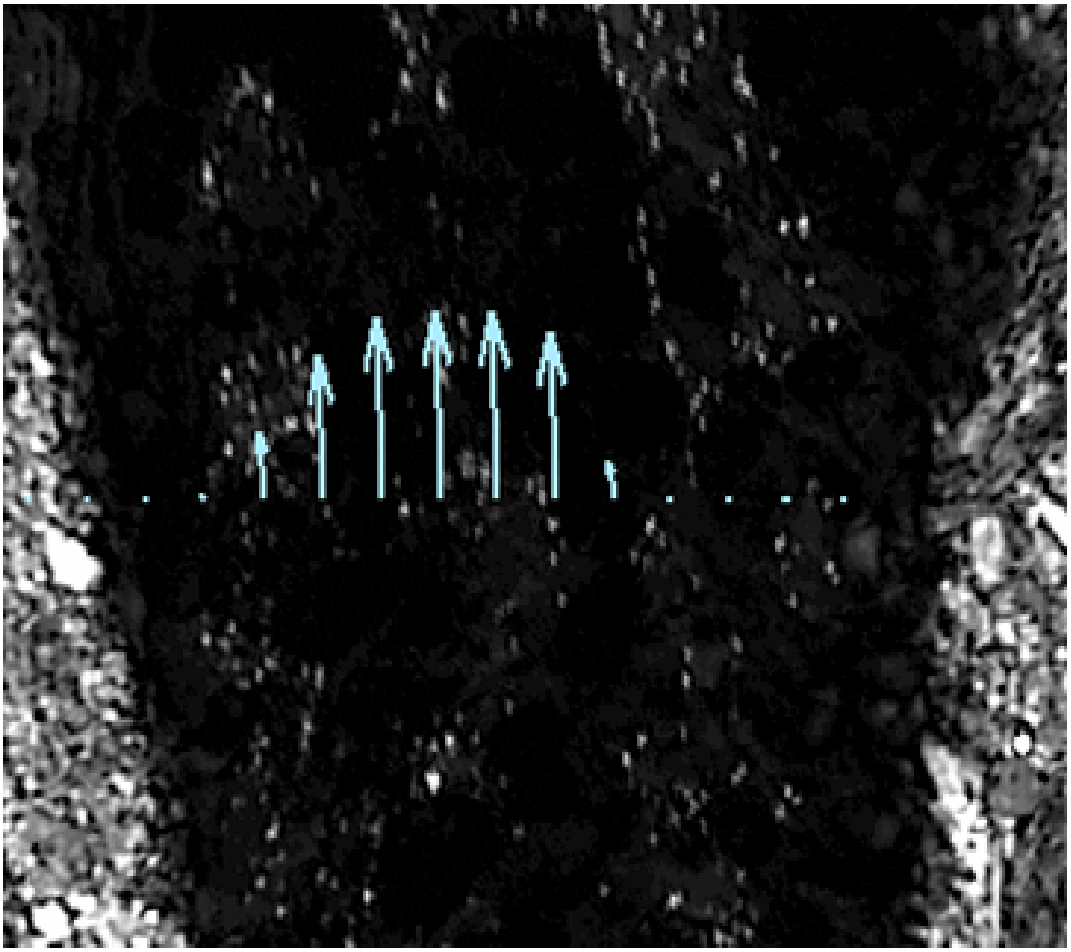

Figure 27. Cross-section LSPIV velocity vectors overlaid on enhanced image from the Duck Pond site. The discharge was calculated using these velocity vectors and the channel bathymetry.

3.2.8 Accuracy Analysis

An accuracy analysis of the LSPIV prototype discharge measurements was completed using error estimation and statistical comparisons. The prototype was compared against a Flo-Mate 2000 and two separate weirs. A total of twenty measurements were taken with each device from two locations. An error analysis was used to investigate the differences in LSPIV discharge measurements and the other control devices. The relative error was calculated using both the weir and current meter as the control using Equation 20. Additionally, a confidence interval was

estimated for the treatments using Equation 21. Subsequently, a statistical analysis was performed to detect differences among the measurement techniques.

Statistical analysis techniques were developed in consultation with the Statistical Consulting Center at Virginia Tech. An ANOVA was used to test the prototype accuracy against the other treatments. A t-test was most appropriate for testing differences between samples (Walpole et al., 2002). The **Proc ttest** and **paired** commands were used to test paired samples by calculating a t-statistic:

$$t = \frac{\bar{x} - m}{s_d - \sqrt{n}} \qquad \textbf{Equation (27)}$$

where $\bar{x}$ is the sample mean of the paired differences, s_d^2 is the sample variance of the paired differences, and n is the number of paired samples. The t-test procedure tested the null hypothesis:

$$H_o : \mu_1 - \mu_2 = \mu_d = 0 \qquad \textbf{Equation (28)}$$

where μ_1 and μ_2 are the paired means from two treatments and μ_d is the difference, in this case assumed to be zero. A p-value can be estimated based on the studentized t-test. The t-test procedure assumes that the samples are randomly drawn from normally distributed populations with unknown means and standard deviations. This assumption should be valid for hydrologic events. Additionally, the samples were gathered at random time intervals and from multiple sites to reduce covariance. This analysis also used has greater than 15 data points and should therefore produce little error according the central limit theorem (SAS, 2004).

CHAPTER 4 RESULTS AND DISCUSSION

This study was a proof-of-concept experiment investigating LSPIV as a means of measuring open-channel discharge. A laboratory experiment investigated the effects of several factors on LSPIV accuracy. Additionally, field experiments were performed to test accuracy compared to conventional methods. The methodology is explained in Chapter 3 and results are presented here.

4.1 Laboratory Results and Discussion

The objective of the laboratory research was to construct a laboratory-scale LSPIV prototype for measuring water surface velocities in a laboratory flume and test the accuracy of the prototype under various conditions. Three factors affecting the conditions in a 1-ft wide re-circulating flume were tested. The prototype accuracy was tested at five levels of seeding density, corresponding to 1, 2, 3, 4, and 5 particles per interrogation window. The camera angle was also varied to test accuracy using a 0, 15, 30, and 45 degree oblique angle. The flume was used to maintain the Froude number at four levels, 0.5, 0.15, 0.25, and 0.35. The effects of Froude number were investigated on all three treatments.

The experiment tested the prototype against a Marsh-McBirney Flo-Mate 2000 and a calibrated manometer discharge equation, given by the flume manufacturer (ELD, 1987). The prototype and the current meters tended to under-predict the discharge compared with the control. The high error and variability using the current meter is consistent with results from Mitchem (1997), which found median relative error of -27.5 % in the same flume used in this study. However, the overall accuracy of the prototype in this study was strongly influenced by testing various levels of the factors, some expected to have reduced accuracy. Statistical analysis was

performed to test the effect of the factors on the accuracy of the prototype. This analysis provided optimum parameter ranges for future laboratory and field applications.

4.1.1 Effects of Seeding Density

The tracer seeding density determines the number of velocity vectors calculated with LSPIV. As a result, poor seeding densities will produce poor velocity fields and inaccurate discharge measurements. For this reason, the first set of experiments investigated the effect of seeding density on LSPIV accuracy. Seeding densities were specified using an average particle count of 1, 2, 3, 4, and 5 per interrogation window. In this case, the window size was 1024 pixels and there were roughly 250 interrogation windows per image. Therefore, one particle per interrogation window corresponded to roughly 250 particles in the field-of-view. Additionally, to test for interactions, the data were collected for various combinations of Froude numbers and camera angles (Table 8).

Table 8. Discharge measurements made during for the first experiment in three treatments with two replications. This experiment tested five levels of seeding density using four combinations of Froude number and camera angle. Values in parenthesis represent flume manometer discharge measurements.

	LSPIV Discharge Measurements and (Control) (cfs)				
				Range	
	Mean	Median	Standard Deviation	Minimum	Maximum
Low Froude number (0.05) and 0 degree camera angle	0.09 (0.11)	0.09 (0.11)	0.02	0.07	0.11
High Froude number (0.25) and 0 degree camera angle	0.08 (0.15)	0.08 (0.15)	0.01	0.07	0.10
Low Froude number (0.15) and 30 degree camera angle	0.10 (0.11)	0.11 (0.11)	0.04	0.03	0.14
High Froude number (0.25) and 30 degree camera angle	0.13 (0.16)	0.13 (0.16)	0.01	0.11	0.15

The prototype under-predicted the discharge rate compared with the control at all seeding density levels. Under-predictions were exacerbated at the higher Froude number (Figure 28). The low Froude number (0.05) produced less error, but showed more variance than the higher Froude number (0.25). Agglomeration was present at the lower Froude number and corresponding slow velocities, especially during low seeding densities. The agglomeration likely caused high variance in the discharge values at the low Froude number. The 95% confidence interval encompassed the control discharge values for the low Froude number, but not at the higher Froude number. Several outlier values may have been caused by poor seeding distribution due to agglomeration. However, a consistent application method made seeding densities random. Therefore, all results were included in the analysis.

The results indicated that seeding density has a significant effect on the LSPIV discharge accuracy. The results showed improved accuracy relative to the flume and Flo-mate 2000 measurements when seeding density is above 3 particles per interrogation window (Figure 29). Error is significantly greater for the 1 and 2 particle per interrogation window levels because the lack of image pairs creates zero vectors and thus under-predicts discharge. Relative error confidence intervals include zero for the 3, 4, and 5 particle levels. Therefore, these seeding densities do not show significant error compared to the control, at a 95% confidence limit. However, the data show high variance partly due to agglomeration at low velocities. The variance can be reduced by increasing seeding density, which should compensate for particle agglomeration. Overall, the trend of increasing accuracy with increasing seeding density is in agreement with findings of other researchers (Raffel et al., 1998). A statistical analysis was performed to examine the differences between different levels of seeding density.

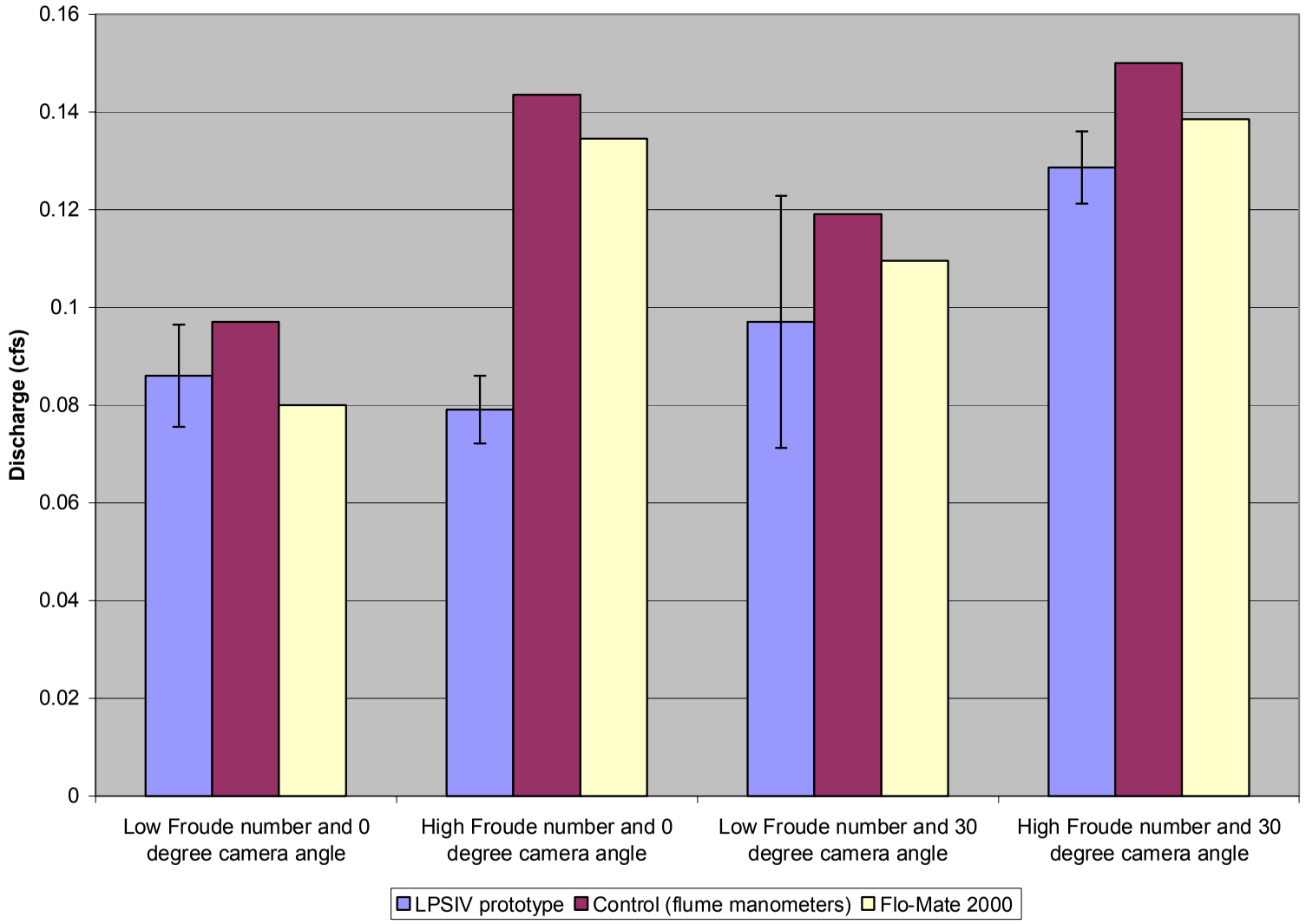

Figure 28 The laboratory experiment tested LSPIV accuracy under varying seeding densities. The median LSPIV discharge measurement, over all seeding densities, is shown for several configurations. The 95% confidence interval is included for each prototype measurement. The mean Flo-Mate 2000 and manometer discharge measurements are also shown.

Investigations into prototype accuracy were made using analysis of covariance (ANACOVA) and pairwise comparisons (contrasts). Fixed-effects are the bias caused by one or more factor(s) and were determined using ANACOVA. This analysis showed that seeding density had a significant effect on accuracy in the first experiment (with α=0.95) (Table 9). Pairwise contrasts tested custom hypotheses using an F-statistic. The contrasts estimated any differences between levels, while accounting for random effects. The comparisons showed an improvement in accuracy with seeding density greater than 3 particles per interrogation window (Table 9). Higher seeding densities should cause improved velocity estimation (Raffel et al., 1998, Weitbrecht et al., 2002). The results of this study are also in agreement with the work of Weitbrecht et al. (2002), who found maximum accuracy in velocity measurements at 5 particles per interrogation window. In future field work, seeding density should be maximized to increase accuracy. However, seeding at high densities is a limitation in field applications; therefore, a minimum of 3 particles per interrogation window is advised to produce accurate results. The most accurate seeding density (5 particles) was used to test the effect of Froude number and camera angle on LSPIV discharge accuracy. The next experiment also provided a better estimate of overall prototype accuracy.

Table 9. Results from the first laboratory experiment testing the effect of seeding density on the discharge accuracy of the prototype. Statistical analysis used SAS (Version 6.03). The fixed effects were tested using an ANACOVA using a mixed model. The contrasts were made in a similar fashion using pairwise comparisons.

Fixed Effects		
Effect	F Value	p-value
Interaction of Froude number Vs. seeding density	0.96	.4742[0]
Interaction of camera angle Vs. seeding density	0.63	0.7460[0]
Interaction of camera angle, Froude number Vs. seeding density	0.62	0.7542[0]
Froude number	19.66	<0.0001[3]
Camera angle	6.09	0.0032[2]
Seeding Density	2.67	0.0108[1]

Contrasts		
Effect	F Value	p-value
Froude number 0.05 vs. 0.25	7.85	0.0061[2]
Camera angle 0 vs. 30 degrees	38.01	<0.0001[3]
Seeding density 1 vs. 2 particles per interrogation window	5.31	0.0234[0]
Seeding density 2 vs. 3 particles per interrogation window	3.80	0.0541[1]
Seeding density 3 vs. 4 particles per interrogation window	0.13	0.7238[0]
Seeding density 4 vs. 5 particles per interrogation window	0.5	0.4801[0]

Superscripts refer to level of significance of the results: 0 – not significant, 1 – moderately significant, 2 – highly significiant, 3 – very highly significant.

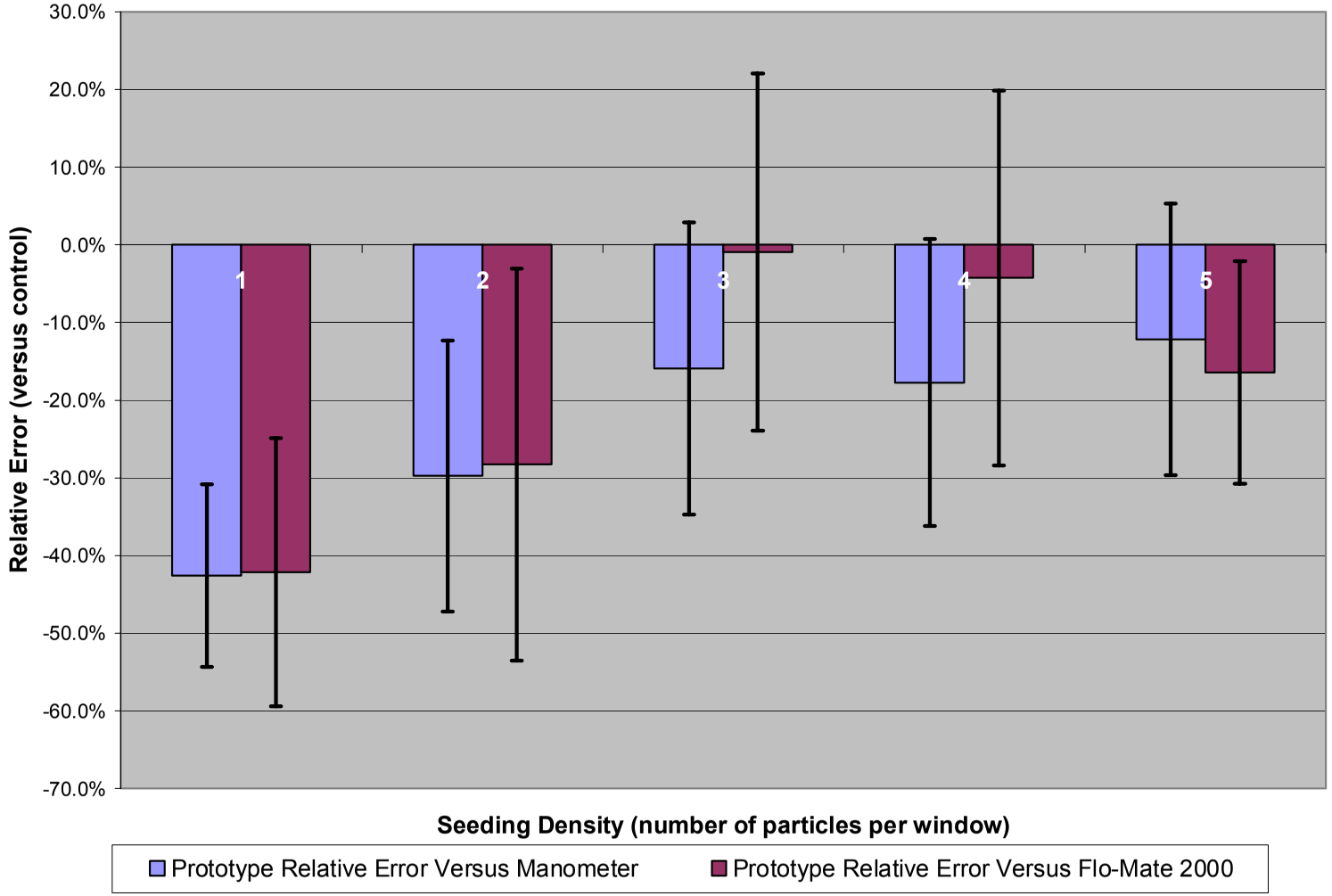

Figure 29. Relative error in flow measurements by the LSPIV compared to the Flo-Mate 2000 and flume manometers. The prototype was measured under five levels of seeding density. Error bars reflect 95% confidence interval

4.1.2 Effects of Froude Number

The Froude number is a proxy for surface disturbances (e.g. waves) and flow regime (laminar versus turbulent). In this study, LSPIV was tested for a range of Froude numbers (0.05 to 0.35) to estimate any effects from different hydraulic conditions. The LSPIV prototype underestimated the manometer discharges over the range of Froude numbers in both experiments (Figure 28 and Figure 30). Several additional trends are also evident: under-predictions are more dramatic at higher Froude numbers while certain camera angles performed better at high Froude numbers. These effects are illustrated in Figure 30, the camera angles produce different results because they have slightly different field-of-views. As a result, specific camera angles may be more appropriate for high Froude numbers. Additionally, Figure 31 shows LSPIV has decreased discharge measurements with increased Froude number. At the lower values of Froude number (0.05 and 0.15) the 95% confidence interval includes the control measurement. Conversely, the greatest variance is present at these same low Froude numbers because of sporadic tracer agglomeration at low velocities. The Flo-mate 2000 discharge measurements were roughly 10% lower than the control measurements for all Froude numbers (Figure 30).

Statistical analysis showed that Froude number significantly affected both LSPIV and current meter accuracy (Table 11). The bias caused by different Froude numbers (fixed-effects) was found to be a very significant factor on LSPIV accuracy. Despite the trends in accuracy noted before, pairwise comparisons did not show differences in accuracy between successive levels of Froude number. This suggests that the range of Froude numbers did alter LSPIV accuracy, but the increments between levels did not produce statistically different results. The under-predictions of the LSPIV discharge measurements at high Froude numbers could have been caused by out-of-plane losses. Out-of-plane losses are displacements that are not captured

by LSPIV measurements because the motion is perpendicular to the water surface (Raffel et al., 1998). This three-dimensional movement is caused by surface disturbances, such as waves. Additionally, some displacements may have occurred outside of the ROI at the highest Froude numbers (and velocities). Both of these problems could have caused the under-prediction of the discharge values found at most Froude numbers tested. Losses from three-dimensionality could also explain why certain camera angles showed improved results. Camera angles with moderate oblique angles (e.g. 15 degrees) may reduce out-of-plane losses because less tracer movement is perpendicular to the field-of-view. These results are important in interpreting how LSPIV will behave in field conditions.

Table 10. Discharge measurements collected for the three treatments using five replications. This experiment tested four levels of Froude number and camera angle with a fixed seeding density. Overall, the prototype tends to under-predict the discharge measured by the control.

	Discharge (cfs)				
	Mean	Median	Standard Deviation	Minimum	Maximum
0 degree camera angle and Froude number = 0.05	0.12	0.12	0.01	0.11	0.13
0 degree camera angle and Froude number = 0.15	0.15	0.15	0.01	0.14	0.15
0 degree camera angle and Froude number = 0.25	0.18	0.17	0.01	0.17	0.20
0 degree camera angle and Froude number = 0.35	0.16	0.17	0.03	0.12	0.19
15 degree camera angle and Froude number = 0.05	0.12	0.13	0.02	0.09	0.13
15 degree camera angle and Froude number = 0.15	0.16	0.16	0.01	0.14	0.18
15 degree camera angle and Froude number = 0.25	0.19	0.19	0.01	0.18	0.20
15 degree camera angle and Froude number = 0.35	0.21	0.21	0.01	0.20	0.22
30 degree camera angle and Froude number = 0.05	0.10	0.09	0.01	0.09	0.12
30 degree camera angle and Froude number = 0.15	0.13	0.13	0.02	0.11	0.15
30 degree camera angle and Froude number = 0.25	0.15	0.15	0.03	0.12	0.19
30 degree camera angle and Froude number = 0.35	0.17	0.18	0.02	0.15	0.19
45 degree camera angle and Froude number = 0.05	0.09	0.09	0.01	0.08	0.11
45 degree camera angle and Froude number = 0.15	0.12	0.12	0.01	0.11	0.13
45 degree camera angle and Froude number = 0.25	0.15	0.15	0.01	0.15	0.16
45 degree camera angle and Froude number = 0.35	0.18	0.18	0.01	0.18	0.19

Although the Froude number cannot be controlled in the field, its effect on discharge accuracy is important in site selection. Areas that have surface disturbances from turbulence or upstream structures should be avoided. Additionally, bias should be considered from surface effects for a variety of stages. A decrease in accuracy can be expected due to out-of-plane losses at higher Froude numbers, especially using a zero degree camera angle. The under-prediction problem could be solved by changing the camera angle to capture three-dimensionality, switching to a two camera stereoscopic view, or by using a bias correction factor. The results of this study may be sufficient for developing a correction factor for out-of-plane losses in the field. However, the field experiments have a much larger focal length, which could reduce the error caused by surface disturbances. Additionally, a correction factor would only be viable for the small range of Froude numbers tested. For these reasons, a correction factor will be investigated if LSPIV discharge accuracy in the field follows similar trends with respect to Froude number.

Table 11. Results from the second laboratory experiment testing the effect of camera angle and Froude number on the discharge accuracy of the prototype. Statistical analysis used SAS (Version 6.03). The fixed effects were tested using an ANACOVA using a mixed model. The contrasts were made in a similar fashion using pairwise comparisons.

Fixed Effects*		
Effect	F Value	p-value
Froude number	631.91	$<0.0001^{3}$
Froude number (on LSPIV only)	16.79	$<0.0001^{3}$
Camera angle (on LSPIV only)	6.15	$<0.0001^{3}$
Interaction of Froude number vs. camera angle	1.5	0.0609^{0}

Contrasts*		
Effect	F Value	p-value
Froude number 0.05 vs. 0.15	35.52	$<0.0001^{3}$
Froude number 0.15 vs. 0.25	42.54	$<0.0001^{3}$
Froude number 0.25 vs. 0.35	9.91	0.0019^{2}
Camera angle 0 vs. 15 degrees	21.26	$<0.0001^{3}$
Camera angle 15 vs. 30º	35.52	$<0.0001^{3}$
Camera angle 30 vs. 45º	2.48	0.1171^{0}

*Superscripts refer to level of significance of the results: 0 – not significant, 1 – moderately significant, 2 – highly significant, 3 – very highly significant.

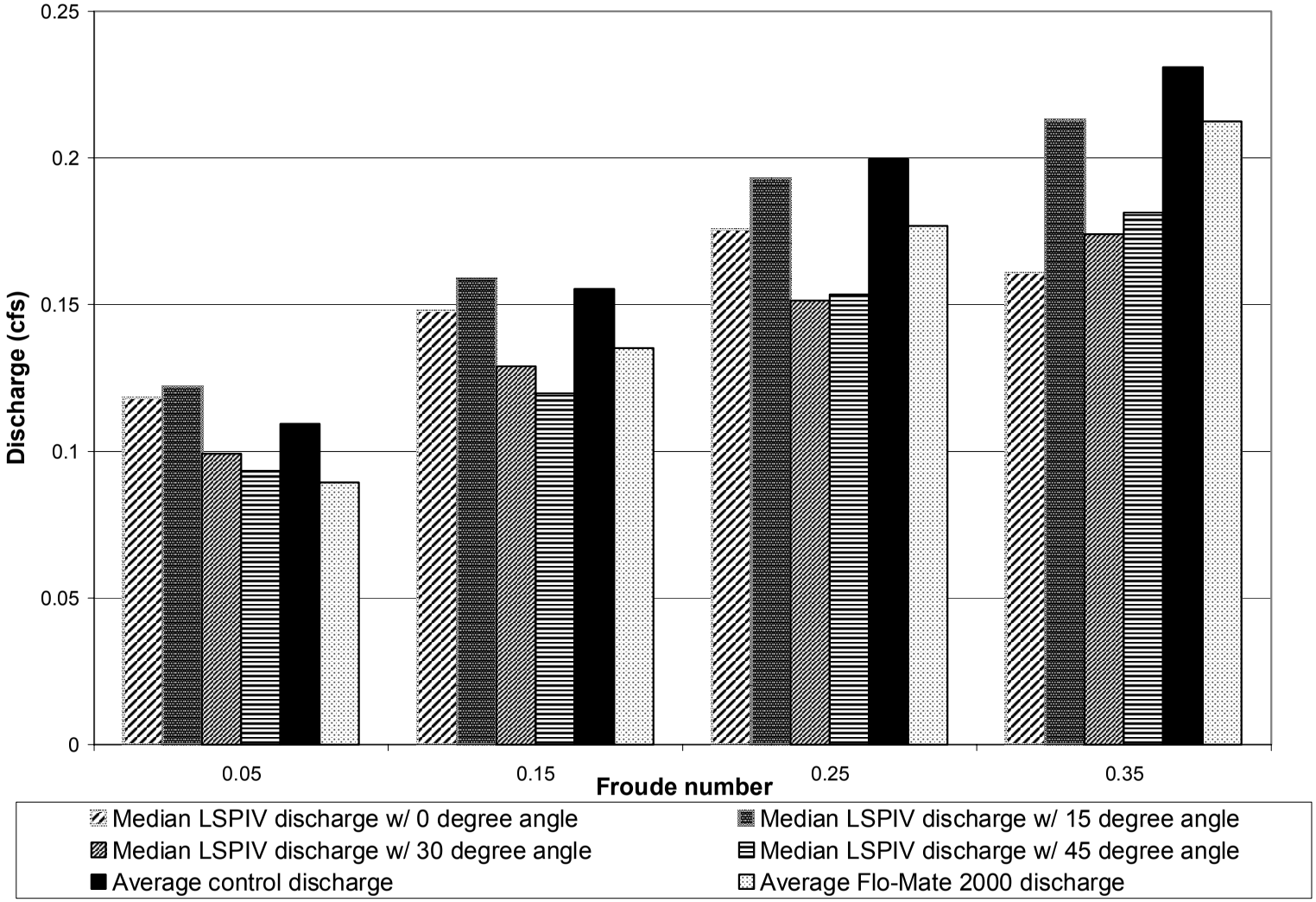

Figure 30 The median LSPIV discharge measurement from 5 replications, using four levels of camera angle and Froude number . The mean Flo-Mate 2000 and manometer discharges are also shown.

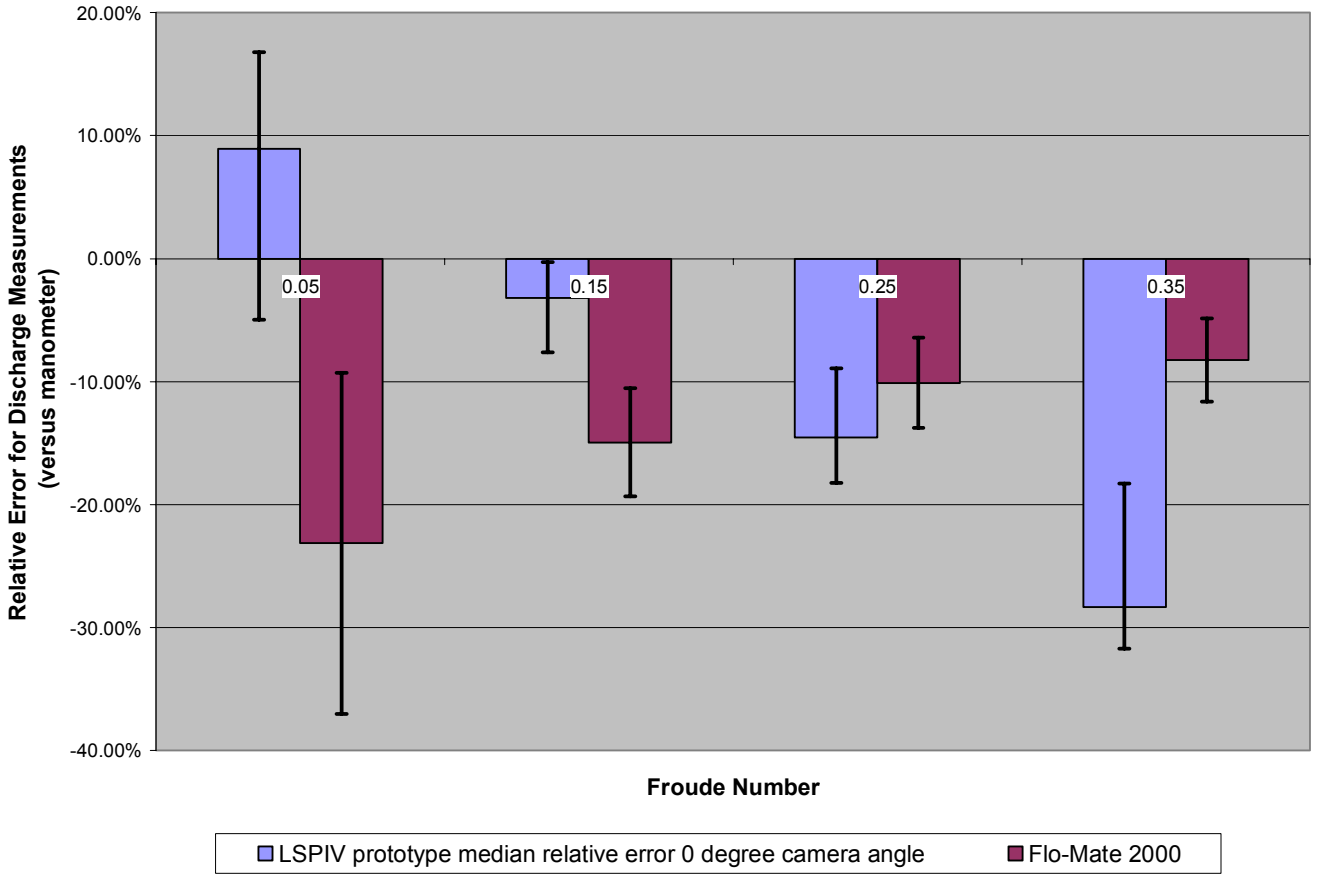

Figure 31. Relative error in LSPIV prototype and Flo-Mate 2000 discharge measurements compared to the control. Error is significantly higher at large Froude numbers (error bars reflect 95 % confidence interval).

4.1.3 Effects of Camera Angle

Determining the effects of the camera angle on LSPIV discharge measurement accuracy will aid in developing an operating range for field applications. The more oblique the camera is to the stream surface the more error is produced in image registration and transformation. Conversely, it has been shown that zero degree camera angles may produce bias at high Froude numbers from out-of-plane losses. These experiments tested a range of viable camera angles from 0 to 45 degrees in four increments. The results indicate that camera angle does influence the accuracy of LSPIV discharge measurements (Figure 30). The mean and median LSPIV

measurements underpredicted discharge at all camera angles, compared with the control. The accuracy of 0 and 15 degree camera angles was adequate with errors ranging from 0.0% to -48.1% and the 95% confidence intervals encompassing the control measurements. However, the measurements using a zero degree camera angle show high variance. This can be attributed to out-of-plane losses, which could cause the under estimations observed. Statistical methods were used to identify differences between the camera angles tested.

The ANACOVA results indicated that the camera angle significantly affected the accuracy of the LSPIV measurements (p-value =0.0001). Additionally, pairwise comparisons showed that a camera angle of 45 degrees produced statistically different discharges from 0, 15, and 30 degree angles (Table 11). The results suggest that accuracy can be markedly reduced when a camera angle above 30 degrees is used. Additionally, under-prediction due to out-of-plane losses is possible with a zero degree camera angle. Therefore, a camera angle operating range of 5 to 25 degrees was determined to be optimum for this setup. This operating range will be used while optimizing the field-of-view, to determine the position of the camera in field applications.

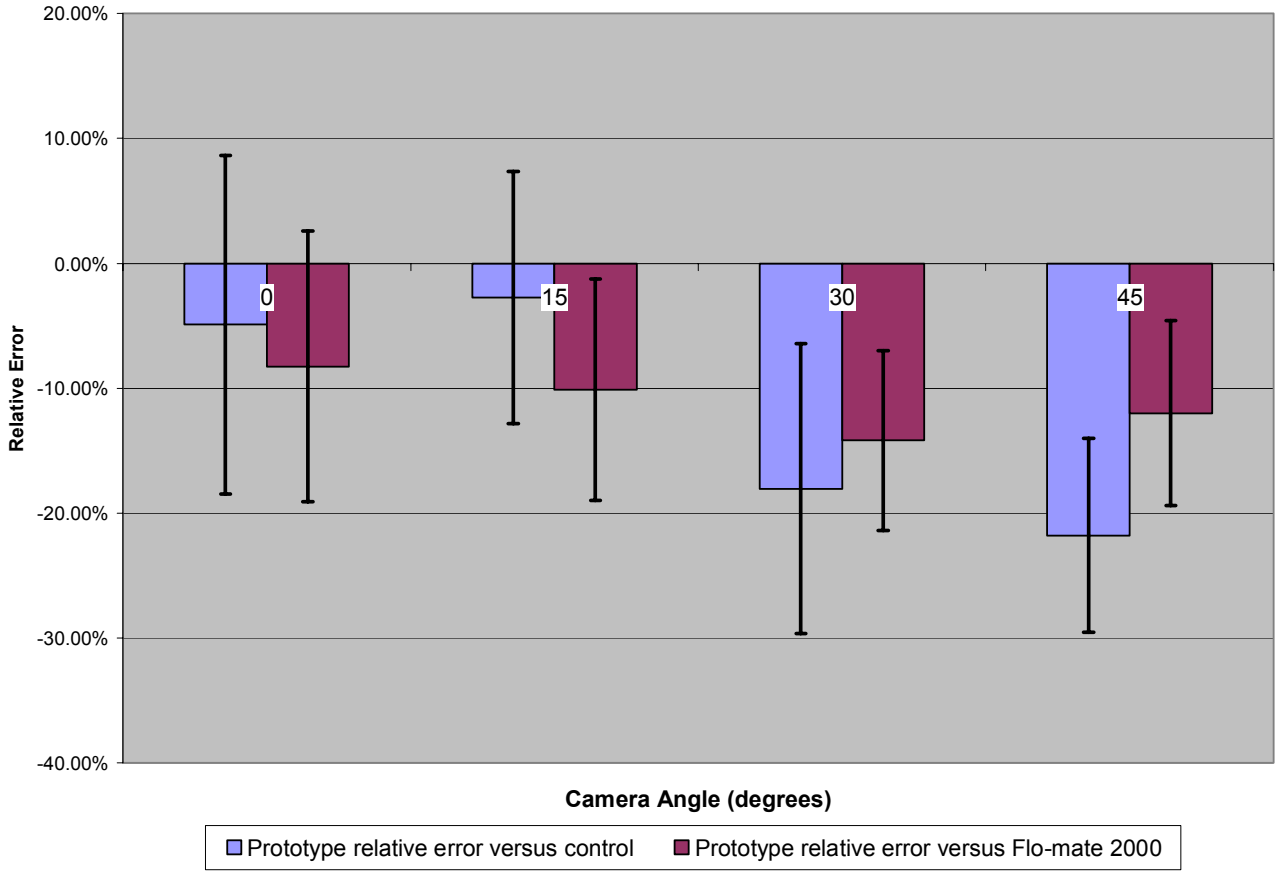

Figure 32. Relative error of LSPIV discharge measurements versus Flo-Mate 2000 and flume measurements over four camera angles. The LSPIV shows the least error with a 15 degree camera angle and significantly more error with a 45 degree camera angle (error bars reflect 95 % confidence interval).

4.1.4 Interaction Between Factors

Possible interactions between the factors were also investigated in the statistical analysis. The results show that the interaction between camera angle and seeding density does not influence accuracy (Table 9). Additionally, interaction between Froude number and seeding density was not shown to significantly affect LSPIV accuracy. However, it was observed that agglomeration occurred more prevalently at slower velocities (low Froude numbers). Therefore, low velocities may require high seeding densities to help remediate this problem. The Froude number and camera angle did not interact to significantly affect LSPIV discharge measurements (Table 11). It was noted that higher Froude numbers produced error using a zero degree camera

angle. These errors were attributed to out-of-plane losses. The culmination of these errors determined the overall LSPIV accuracy.

4.1.5 Overall Accuracy

Overall, the prototype measured similar discharges to the current meter and flume for the conditions investigated in the laboratory. Pairwise comparisons showed that the current meter and LSPIV showed no statistical differences in discharge measurements (p-value = 1.53). Additionally, one-way ANOVA (t-test) was used to test paired data under different camera angles and Froude numbers. These results indicate that the LSPIV and flume measurements were not statistically different at the lowest Froude number of 0.05 (t-value = 1.50). The ANOVA also shows that LSPIV produced discharge measurements with no statistical difference from the flume measurements using a 15 degree camera angle (t-value = 0.79). Therefore, the 15 degree camera angle was most appropriate for the range Froude numbers tested.

4.1.6 Summary and Implications for Further Work

The results from the laboratory work indicated that all the three factors investigated significantly affected LSPIV discharge accuracy. Discharge measurements were improved with seeding densities above 3 particles per interrogation window. Additionally, low seeding densities showed particle agglomeration at slow velocities. An increased Froude number likely caused surface disturbances that resulted in an under-estimation of discharge because of out-of-plane losses. The reduced accuracy due to surface disturbances may be corrected by using an oblique camera angle. Using a camera angle of 15 degrees produced discharge measurements that were not significantly different from the flume measurements. This camera angle was likely oblique enough to reduce out-of-plane losses, but was small enough not to overly distort the

image. The response of LSPIV to the factors tested will be used to enhance accuracy in further work.

The laboratory conditions provided an excellent environment to develop and test an LSPIV prototype. Although errors were significant, insight into prototype operation was gained from preliminary development and use. It was learned that seeding densities should be maximized and the camera angle must be kept within the operating range specified. Also, a bias correction factor based on Froude number may be necessary in field application. Finally, the laboratory 'proof-of-concept' proved that LSPIV could have discharge measurement accuracy similar to conventional techniques under certain conditions. The culmination of the information collected in the laboratory dramatically aided the development of an accurate field prototype.

4.2 Field Results and Discussion

The objective of the field experiments was to adapt the laboratory prototype for measuring flow rates in low-order streams by constructing a field prototype, developing an operation procedure, and conducting an accuracy analysis under varying field conditions. The development of the prototype and operating procedure are explained in detail in Chapter 3. LSPIV discharge measurements were collected in two low-order streams in the Blacksburg area. In addition, discharge measurements were made with a permanent control structure and Marsh-McBirney Flo-Mate 2000 current meter. An accuracy analysis was performed using these measurements as references. Finally, the measurement uncertainty was estimated for the prototype.

4.2.1 Results

The discharge measurements were made at a variety of conditions using a non-uniform sampling scheme (Table 12). A total of 20 measurements were collected from September 8th to November 1st, 2004. The measurements were collected under various illumination, wind, and stage conditions. Measurements were taken throughout the day; however, high surface glare conditions were avoided. Light sensitivity is a problem that was also encountered in previous LSPIV applications (Creutin et al., 2003). During the measurement period, three tropical storms passed through the area providing high flows and windy conditions. Stage measurements were made at both the LSPIV field-of-view and at the weir. Therefore, for clarity in the discussion, "stage" will refer to depth measurements made in the LSPIV field-of-view exclusively. Fourteen discharge measurements were collected at Stroubles Creek at the Duck Pond site on the Virginia Tech campus. Stage at Stroubles Creek varied from 0.31 to 1.85 ft during the monitoring period, with a corresponding range of discharge from 0.12 to 39.90 cfs. Six measurements were

collected at Crab Creek located in Christiansburg, Virginia. Crab Creek had stage measurements from 0.68 to 1.84 ft and discharges from 0.69 to 62.96 cfs. Two weir measurements at the Duck Pond site were discarded because the weir was not operational.

Table 12. Discharge measurements made during field experiments using a weir, Flo-Mate 2000 current meter, and LSPIV prototype. Twenty points were collected at two sites over two months. Stage refers to depth measurements made in the LSPIV field-of-view.

Date and Time	Stage (ft)	Weir Discharge (cfs)	Flo-Mate 2000 Discharge (cfs)	LSPIV Prototype Discharge
Stroubles Creek at the Duck Pond				
9/8/04 10:00 AM	1.85	39.90	30.10	28.62
9/8/04 12:00 PM	1.06	10.80	10.90	8.76
9/8/04 1:00 PM	0.81	4.40	4.30	4.40
9/9/04 9:00 AM	0.62	0.80*	1.10	1.00
10/13/04 10:00 AM	0.60	1.62	1.51	1.75
10/28/04 9:00 AM	0.50	1.87	3.10	1.80
9/7/04 11:00 AM	0.49	0.10*	0.40	0.50
10/20/04 5:00 PM	0.48	0.58	1.03	0.78
10/22/04 9:00 AM	0.46	0.42	0.91	0.31
10/19/04 8:30 AM	0.42	1.11	1.88	1.25
10/23/04 12:00 PM	0.39	0.35	0.88	0.31
10/31/04 4:00 PM	0.32	0.14	0.64	0.20
11/1/04 8:00 AM	0.31	0.12	0.58	0.12
Average	**0.64**	**5.57**	**4.41**	**3.83**
Crab Creek				
9/28/2004 11AM	1.84	62.96	13.65	53.71
9/29/2004 8 AM	1.02	5.60	4.61	5.06
9/29/2004 5:30 PM	0.98	2.39	2.46	3.11
9/30/2004 8:30 AM	0.86	2.11	1.27	1.86
9/30/2004 6:30 PM	0.86	2.05	1.36	1.67
9/29/2004 9:30 AM	0.85	3.11	2.54	2.63
10/05/2004 8:30 AM	0.68	0.69	0.66	0.60
Average	**1.01**	**11.27**	**3.79**	**9.81**

* These weir measurements were taken when significant leaking was present. The measurements were not used in statistical analyses.

4.2.2 Error and Bias Versus the Current Meter

The LSPIV discharge measurements were accurate over a variety of conditions, compared to current meter measurements. Discharge measurements at the Duck Pond site were under-predicted by LSPIV at high flows, compared to the current meter (Figure 33). The current meter measured higher discharge values than LSPIV over all stages, at the Duck Pond site. However, the current meter estimated higher discharge values than LSPIV only at low stages at the Crab Creek site (Figure 34). Therefore, there was a trend of under-prediction during low stage at both sites; however, they were more pronounced at the Duck Pond. This could be because more measurements were taken at baseflow conditions at the Duck Pond. It is possible the current meter would continue to over-estimate discharge at Crab Creek if more low-flows had been measured. Bradley et al. (1998) found an error of -6.0%, versus current meter measurements, for a single discharge measurement of 6.7 cfs (37,000 acre drainage area). The under-prediction is consistent with the results found in this study; LSPIV showed median error of -7.0% and mean error of -11.0% compared to the current meter discharge measurements. Therefore, the results indicate LSPIV is similar in accuracy to current meters for these measuring conditions.

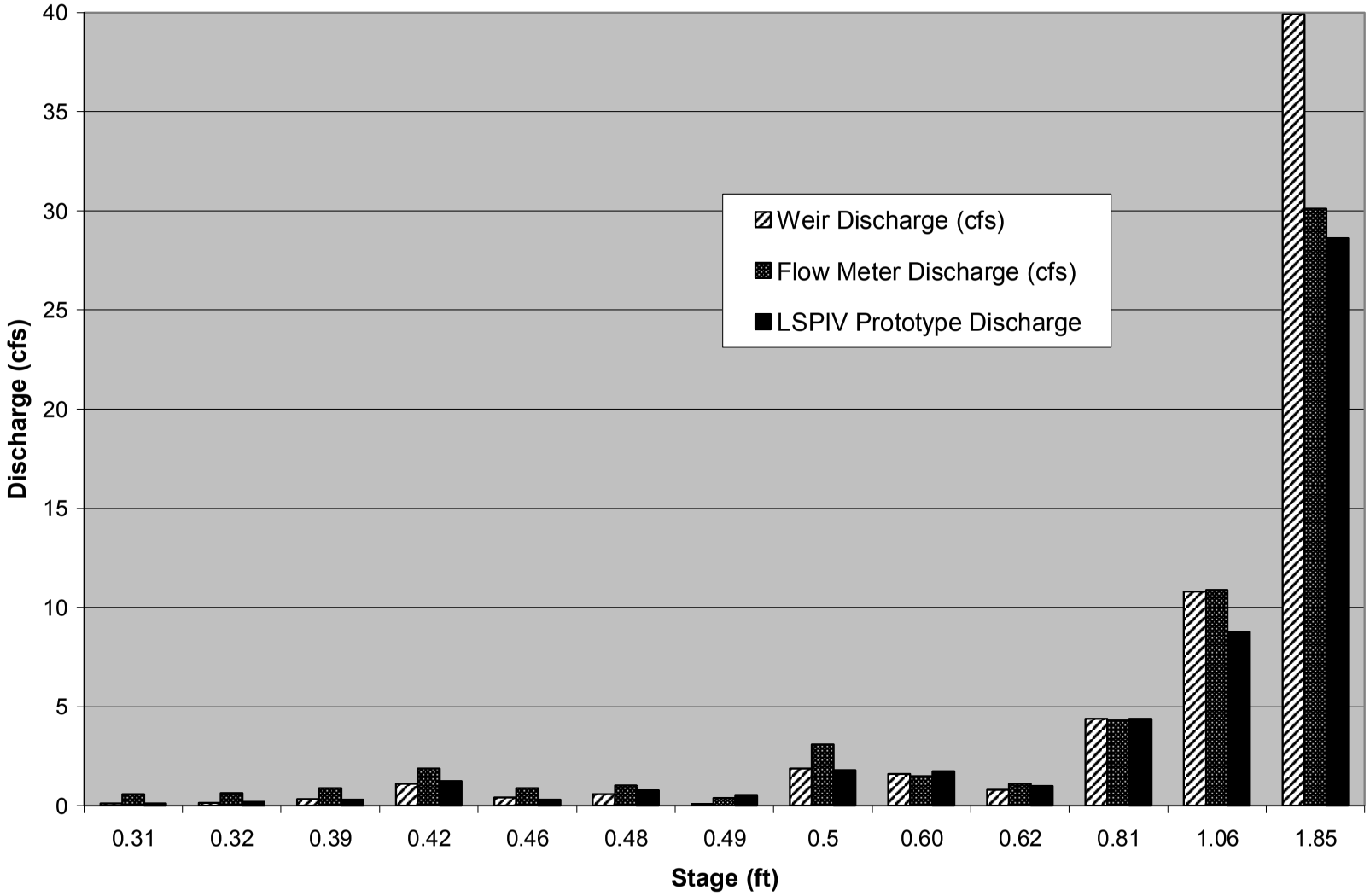

Figure 33. Discharge measurements made at Stroubles Creek at the Duck Pond in Blacksburg, Virginia. Measurements were made with a LSPIV prototype, concrete weir, and Flo-Mate 2000 current meter.

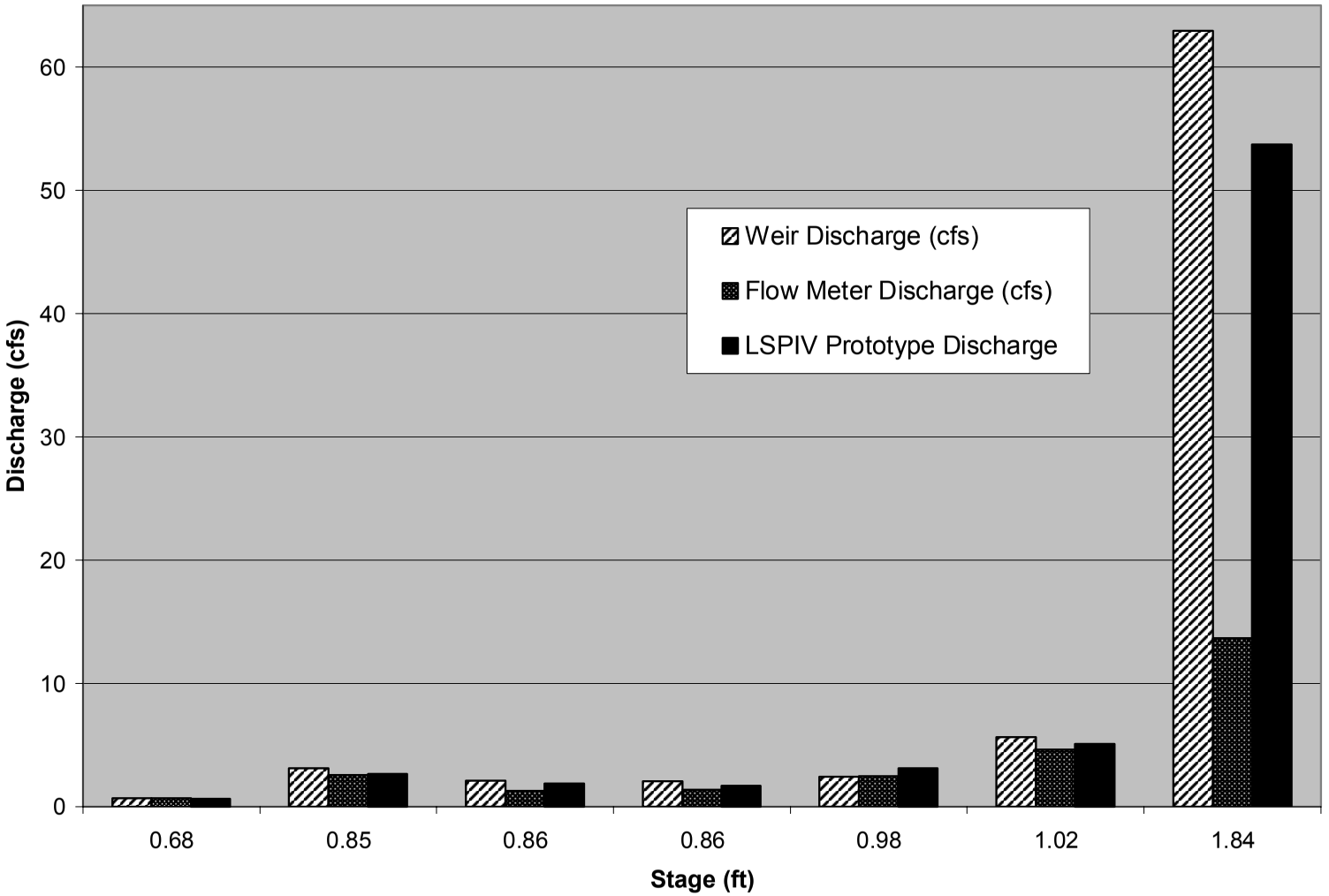

Figure 34. Discharge measurements made at Crab Creek in Christiansburg, VA. Measurements were made with a LSPIV prototype, concrete weir, and Flo-Mate 2000 current meter.

4.2.3 Error and Bias Versus Weir

The LSPIV error was determined using a calibrated weir as the baseline (control) for both sites. The Duck Pond site is ideal in many ways for LSPIV application because of the simplicity of the channel, lack of major disturbances, and minimal glare problems. Therefore, it is not surprising that the site showed good accuracy, with a median relative error of 0.0% and a mean error of 0.9%. The error was greatest at moderate stages, ranging from -26.2% to 34.5% (Figure 35). The LSPIV measurements underpredicted discharge at the higher stage measurements. Maintaining a constant seeding density over all image pairs was difficult during high stage. As a result, poor seeding density may have produced artificially-low velocities and underpredicted discharge. In addition, the conditions at high stage may have caused surface disturbances and out-of-plane displacement losses. For this reason, the effect of Froude number is reviewed subsequently. Crab Creek had more difficult measuring conditions and consequently more error was found in LSPIV discharge measurements.

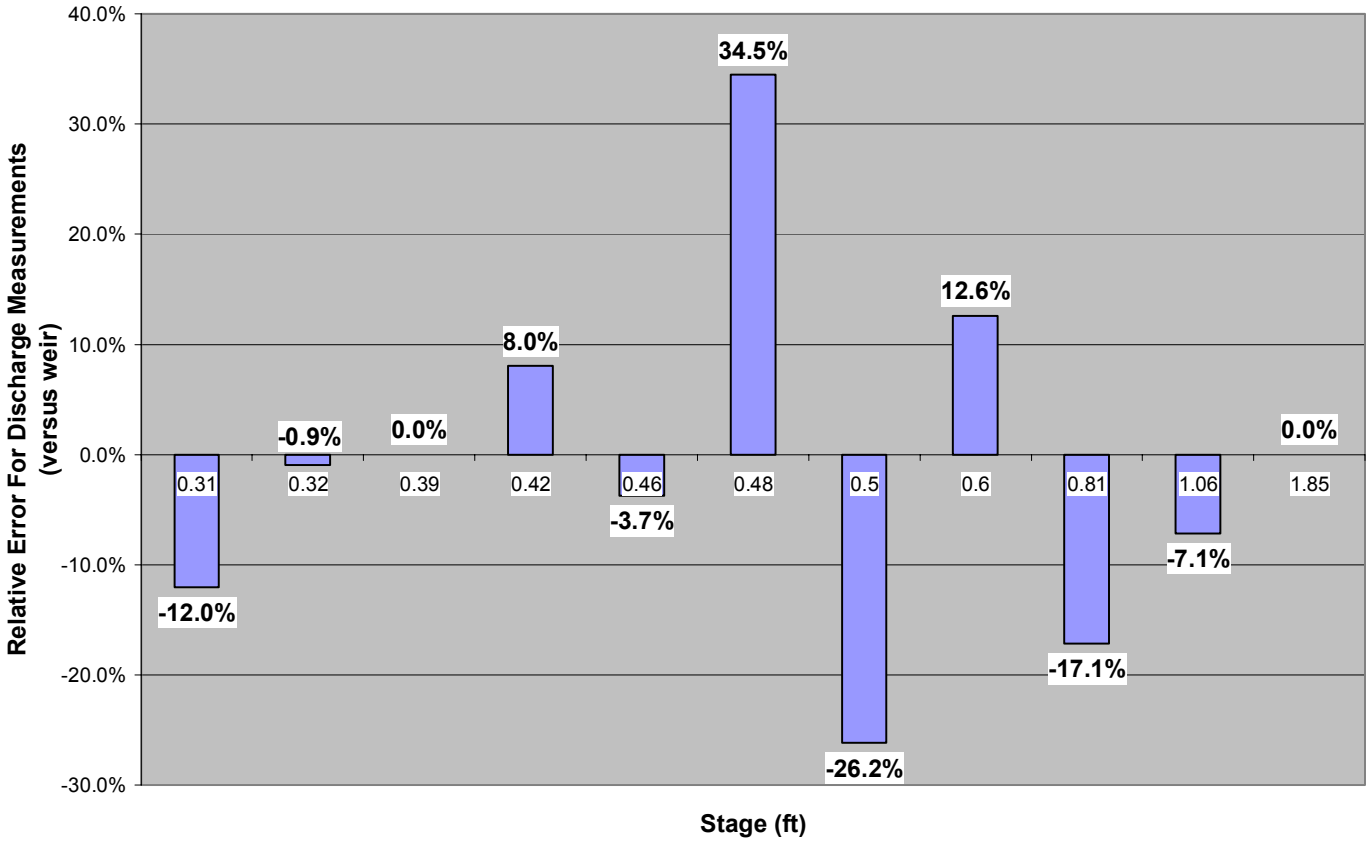

Figure 35. LSPIV discharge measurements compared to a weir at the Stroubles Creek, Duck Pond site. No clear trends are present; however, LSPIV under-predicts discharge at low and high stages.

The LSPIV discharge measurements from Crab Creek under-predicted the discharge values compared with weir measurements at most stages (Figure 36). LSPIV had a median relative error of -13.0% and a mean error of -7.6% compared to the weir using six measurements. There may be several explanations for the systematic under-prediction of discharge using LSPIV. The most likely explanation is that the excavation done at the Crab Creek site prior to the measurements altered the rating curve which was originally developed for the site. If this was the case, staff gauge measurements would be artificially elevated across all stages, as is evident in the results. This explanation is supported by the current meter measurements, which

also consistently under-predicted the discharge values measured by the weir (Figure 34 and Figure 36). The current meter also over-predicted the weir measurements for the 0.98 stage measurement; however, it offers no explanation for the discrepancy in this measurement. It is possible, however unlikely, that a misreported staff gauge measurement could lead to this outlier. Excluding this outlier, LSPIV had a bias error of approximately -10% at this site. Therefore, out-of-plane losses were investigated (using Froude number) as a source of this bias.

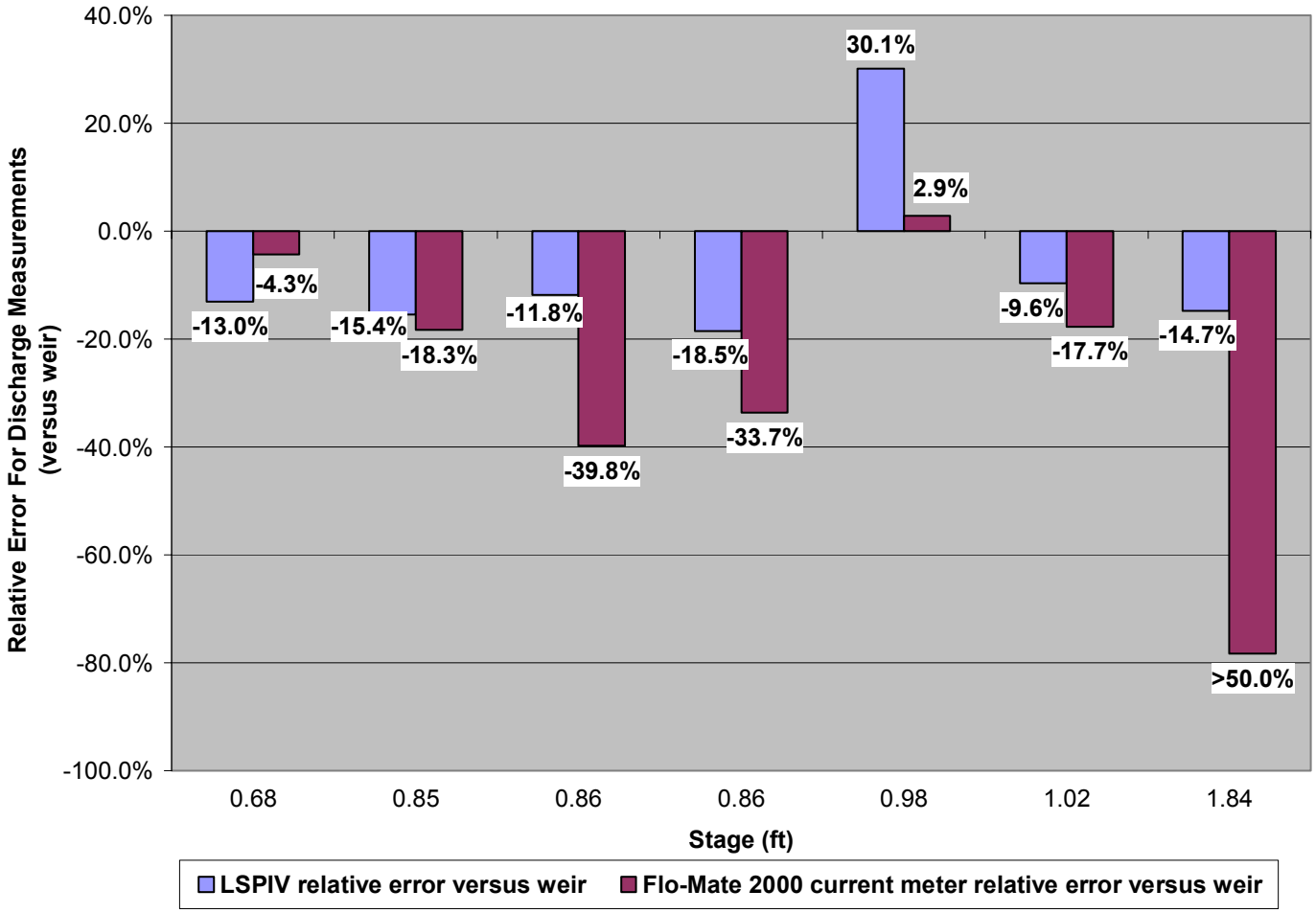

Figure 36. LSPIV discharge measurements compared to a weir at the Crab Creek site. Additionally, current meter relative error versus a weir is shown. The LSPIV and current meter discharge measurements show systematic under-predictions over all stages.

High Froude numbers correspond to high surface disturbances, which may cause out-of-plane losses and reduced velocity measurements (Figure 37). LSPIV underpredicted

discharge, compared to the weir, at the six highest Froude numbers. This trend is in agreement with the data collected from the laboratory, which also consistently underpredicted discharge at high Froude numbers (0.25 and 0.35). It is hypothesized that the under-predictions are due to out-of-plane losses, low seeding densities, or displacements occurring outside of the ROI. A sensitivity analysis showed little sensitivity in the field discharge measurements to larger ROI sizes (Appendix H Region-of-Interest and Grid Spacing Sensitivity Analysis). The LSPIV measurements also underpredicted the weir measurements at low stages, which may have been due to agglomeration of the particles. Consistent LSPIV discharge under-prediction across the range of stages would probably indicate that out-of-plane losses are not responsible for the poor accuracy. Instead, low seeding densities are the probable cause of the LSPIV discharge under-predictions. Seeding properly at high velocities (Froude numbers) was more difficult; therefore, surface effects were not the likely cause of LSPIV under-predictions. Additionally, adequate seeding distribution at small velocities (low Froude numbers) can be compromised due to agglomeration. Use of bias offset to correct for low LSPIV discharge measurements was impractical because seeding density is determined at the discretion of the field technician. The importance of obtaining accurate discharge measurements at high flows may necessitate future research into particle dispensing devices capable of applying high seeding densities.

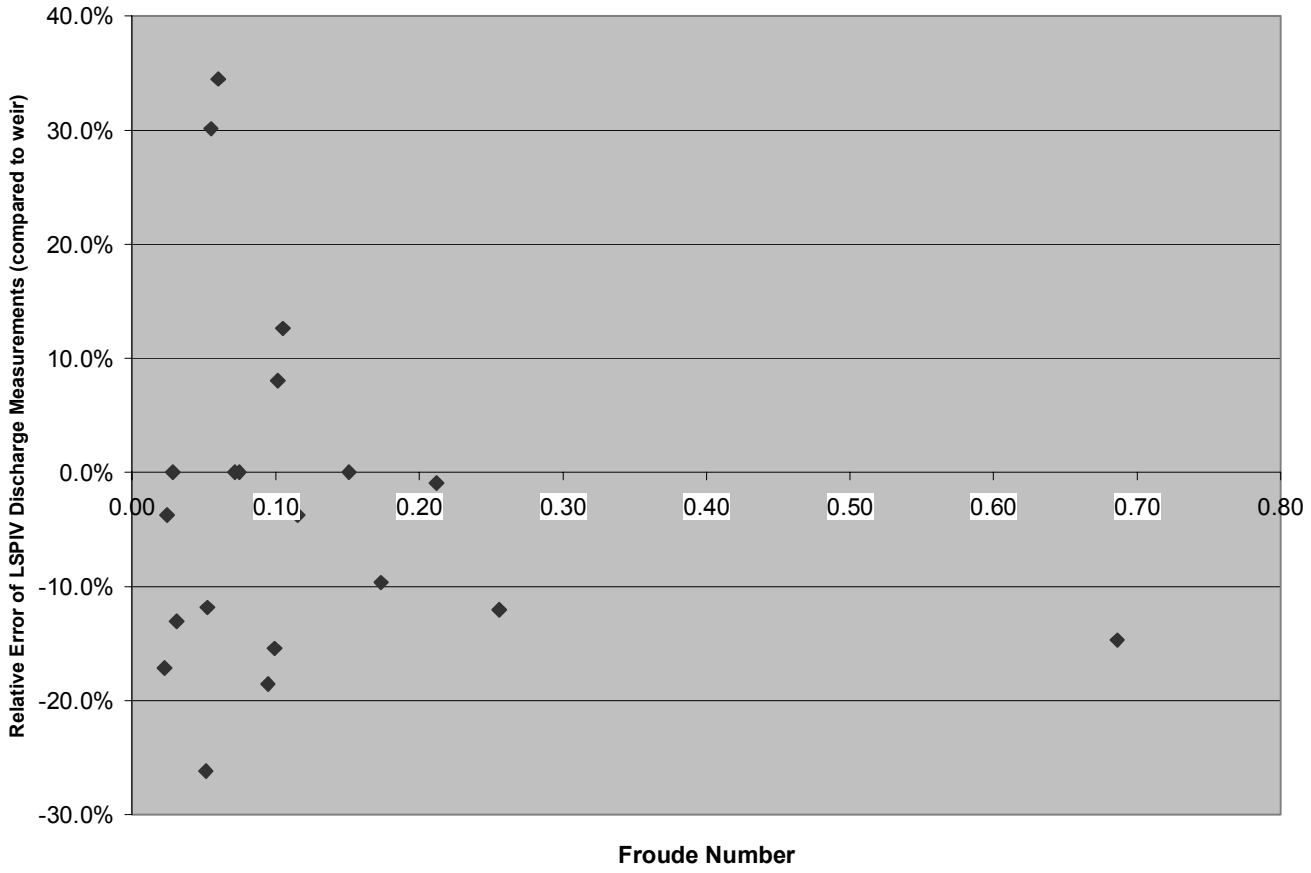

Figure 37. Relative error for LSPIV discharge measurements compared to a weir as a function of Froude number. The data show under-predictions at high Froude numbers, but no bias offset could be easily determined.

The overall LSPIV error was reasonable compared to both the current meter and weir for the 20 discharge measurements collected. The LSPIV data tended to under-predict the weir measurements over the range of discharges measured. This trend is in agreement with the work of Cruetin et al. (2003) which measured discharges from 1,700 to 10,000 cfs. Additionally, they found 'random' outliers that greatly overpredicted flow discharge (up to 39%). The LSPIV data from Crab Creek, and to a lesser extent those from Stroubles Creek, also had unexplained discharge over-predictions. Overall, the LSPIV discharge measurements had a median relative error of -10.5% and a mean error of -1.7%, compared to weir. The LSPIV discharge errors are similar to those found by Cruetin et al. (1998), which showed a small error compared to a weir.

Additionally, Fujita et al. (1998) found error measurement with ± 5% accuracy. However, these measurements were taken at much larger discharges. The increased number of data points collected in this investigation, compared with previous studies prompted testing statistical differences between treatments.

4.2.4 Statistical Differences

Statistical analyses were used to detect differences between treatments. Dependent group t-tests (one-way ANOVA) were used to detect differences between paired samples, using SAS Version 9.1 (SAS, 2004). This test was most appropriate because the discharge measurements from the three treatments were not independent. Dependent group t-tests assume the data were randomly drawn from normally distributed populations with unknown parameters. This assumption was tested prior to the analysis using a normal probability plot (Appendix D Statistical Analysis Programs). The differences between the treatments were shown to be normally distributed, by demonstrating a linear relationship (linear R^2 >0.98). After the assumptions were validated, two investigations were made to test the differences between the treatments and compare the LSPIV prototype against the weir measurements at extreme low and high flows.

The statistical analysis did not show a significant difference between treatments, using 18 to 20 discharge measurements. The measurement data were compared using three hypothesis tests (Table 13). The weir discharge measurements (control) did not show statistical differences from the Flo-Mate 2000, using a 0.95 level of significance. The high current meter accuracy is in agreement with the stated manufacturer velocity accuracy (± 2%). Furthermore, the current meter may show high accuracy because flow meters were used to develop the rating curve for the weir at the Crab Creek site. The difference between the current meter and LSPIV discharge

measurements were not statistically different from zero. Finally, the statistical results showed no difference in the LSPIV discharge measurements from the weir. These results suggest that LSPIV had accuracy comparable to conventional methods for the conditions measured.

Table 13. Statistical analysis from t-tests comparing the discharge measurements between all three treatments. The results show no statistical differences between the treatments.

Difference	N	Mean	Standard Error	Degrees of Freedom	t-value	p-value
Control - Current Meter discharge	20	3.214	2.77	19	1.16	0.2620^0
Current Meter - LSPIV discharge	18	-1.78	2.024	17	-0.85	0.4038^0
Control - LSPIV discharge	18	1.293	0.784	17	1.65	0.1175^0

Superscripts refer to level of significance of the results: 0 – not significant, 1 – moderately significant, 2 – highly significant, 3 – very highly significant.

The ability to measure extreme flow events is crucial in NPS water quality monitoring. Therefore, the LSPIV discharge measurements were separately compared to the weir for high and low-flow conditions (Table 14). This required separating the data points into high and low classifications. For a small data set this was difficult, but division based on quartiles was used. The upper and lower quartile represented high and low-flow conditions, respectively. The results show no difference between the LSPIV and weir discharge measurements at either quartile. The t-value is smaller for the low-flow quartile suggesting LSPIV may be more appropriate for measuring discharge at low-flow conditions. This is in agreement with the results from the laboratory, which also showed improved accuracy at lower flows and Froude numbers. High accuracy from LSPIV at low-flows is advantageous because water quality standards are often violated at these conditions. Additionally, current meters perform poorest at these low-flow conditions (ISO, 1997). Statistical differences are important for evaluating the

prototype; however, measurement uncertainty is ultimately more important for future water monitoring applications use of LSPIV to measure discharge.

Table 14. Statistical results from t-tests using the upper and lower discharge quartiles as a proxy for high and low flow conditions. The LSPIV discharge measurements were not statistically different from the weir measurements for both high and low flow conditions.

Conditions	Difference	N	Mean	Standard Error	Degrees of Freedom	t-value	p-value
High-Flow	Control - LSPIV discharge	5	4.622	2.35	4	1.97	0.1206^0
Low-Flow	Control - LSPIV discharge	5	-0.062	0.089	4	-0.7	0.5240^0

Superscripts refer to level of significance of the results: 0 – not significant, 1 – moderately significant, 2 – highly significant, 3 – very highly significant.

4.2.5 Uncertainty Estimation

Estimating the uncertainty of single discharge measurements is critical for determining the relative accuracy and assessing the methods and equipment used. Additionally, the individual uncertainties are used to derive the uncertainty of a stage-discharge relationship and estimate confidence levels in models used by water resources decision makers. Uncertainties in discharge measurements are due to the culmination of random and systematic uncertainties. The uncertainties in a single determination of discharge using LSPIV come from three primary sources: velocity measurements, averaging velocity in space and time, and measuring cross-section area (Pelletier, 1988). Therefore, estimating the overall uncertainty requires accounting for all of these sources.

Uncertainties were evaluated using procedures from International Standards Organization (ISO): 5168 Measurement of fluid flow – Evaluation of uncertainties (1998) (Appendix I Uncertainty Analysis). Uncertainty was estimated using both the additive and root sum-square models (section 2.3.1 Error and Accuracy). The assumptions made and corresponding references are given in Table 15. Using these assumptions, based on previous research data, the uncertainty

in a single LSPIV discharge value was estimated (Table 16). The uncertainty is relatively high at approximately 14% of the discharge value. In comparison, measurements from the Flo-Mate 2000 current meter had an uncertainty of 12% (Appendix I Uncertainty Analysis). The high LSPIV measurement uncertainty is due to several assumptions inherent in using LSPIV in low-order streams. The method can only measure surface velocities; therefore, the error due to the number of points in the vertical velocity profile will be high. Additionally, measuring more than 12 verticals in a small (6-10 ft wide) streams may not reduce uncertainty (Pelletier, 1988). However, a large number of verticals (>25) would reduce uncertainty following ISO standards. Additional improvements could be made by increasing the number of images and thereby using a longer exposure time. This would require increasing the efficiency of the image pre-processing tasks, which is possible. This uncertainty is likely too high for widespread application of LSPIV. However, improvements suggested for future research could reduce the LPSIV uncertainty.

Table 15. Errors sources and estimates used for estimating LSPIV discharge uncertainty following ISO: ISO/TR 5168 1998.

Error source	Units	Relative random uncertainty (95% confidence interval)	Relative systematic uncertainty (95% confidence interval)	Reference for error estimate
Number of verticals	N/A	6.0%	N/A	Pelletier (1988) Figure 8
Segment width	Ft	1.0%	0.5%	Pelletier (1988)
Segment depth	Ft	1.0%	0.5%	ISO 7178
Number of points in the vertical	ft/sec	7.5%	N/A	ISO 7178
Exposure time	ft/sec	8.0%	N/A	Pelletier (1988) Figure 7
Error from velocity measuring instrument (LSPIV)	ft/sec	3.0%	N/A	Adrian (1991) and Buchave (1992)

Table 16. LSPIV discharge uncertainty estimated using both root-sum-square and following ISO 5168: 1998.

Discharge uncertainty	Percent error (cfs)
(Combined) uncertainty Root-sum-square model	13.4%
(Combined) uncertainty Additive model	14.1%
Random uncertainty	13.7%
Systematic uncertainty	0.7%

Summary

The LSPIV prototype was used to make twenty discharge measurements at two low-order streams in the Blacksburg, Virginia area. The flow and conditions significantly varied over the two month data collection period; discharge values were measured from 0.12 to 62.96 cfs. Measurements using a Marsh-McBirney Flo-Mate 2000 and a weir were taken as reference values. The LSPIV discharge measurements showed similar trend to those found by Creutin et al. (2003) with consistent under-prediction and occasional extreme over-prediction. LSPIV had a median relative error of -10.5% and mean error of -1.7% compared to the weir discharge measurements. The overall error rates were similar to those found by most previous LSPIV research (Cruetin et al., 2003, Bradely et al., 2002, and Fujita et al., 1998). Additionally, the measurement methods did not show any statistical differences from one another, using t-tests (α=0.95). Furthermore, t-tests showed that LSPIV may be more accurate at low flows versus high flows. Finally, the overall uncertainty for the LSPIV discharge values was found to be relatively high, at approximately 14%. However, several methods may exist for reducing uncertainty in future work.

CHAPTER 5 SUMMARY AND CONCLUSIONS

5.1 Summary

Current limitations of conventional discharge measurement techniques were the impetus for investigating the potential for using Large-Scale Particle Image Velocimetry (LSPIV). LSPIV is a system capable of measuring surface velocity by collecting and analyzing recorded images of the flow field (the stream surface). The LSPIV system tracks the movement of 'tracers' on the water surface through successive images to determine velocity. The surface velocity field is used to estimate discharge using the channel dimensions. The overall goal of the study was to evaluate the accuracy and viability of using LSPIV to measure discharge in low-order streams of upland watersheds. The specific goals were to develop and test a prototype under varying conditions in a laboratory, adapt the prototype for field use, test the accuracy of the prototype, and assess and recommend improvements for LSPIV operation as a stream discharge measuring device. The study tested the null hypothesis that the LSPIV prototype will provide discharge measurements with accuracy comparable to those of current meters and control structures (weir).

The laboratory experiments tested the accuracy of LSPIV using a Marsh-McBirney Flo-Mate 2000 and flume manometers as references. The experiments found that LSPIV accuracy was influenced by camera angle, surface disturbances, flow regime (Froude number), and particle seeding density. Camera angle was optimum around 15 degrees in the laboratory; at this angle, there was no difference in discharge measurements using LSPIV and the flume manometers. However, larger camera angles showed error due to image distortion. Conditions at high Froude numbers likely produced out-of-plane displacement losses due to surface disturbances, which caused under estimations of discharge. Discharge rate was also under-

predicted at flow regimes with low Froude numbers, which were likely due to agglomeration of the tracer particles at low velocities. Finally, the laboratory results demonstrated seeding densities below three particles per interrogation window could significantly reduce LSPIV accuracy. The laboratory investigations refined the prototype components for subsequent field studies. The camera selected for the study was monochrome, high resolution, and had features to improve quality in low-light conditions. The prototype included equipment to digitize and save the images and make instantaneous stage measurements. Additionally, the equipment was mounted on a stand and was weatherproofed for field conditions. The camera angles ranged from 15 to 25 degrees from vertical.

The LSPIV prototype was tested at two low-order streams after developing robust operating procedures. The operating procedures acquired consistent images, performed the necessary image processing, and established rules for estimating input parameters. The accuracy of LSPIV was evaluated using a Flo-Mate 2000 current meter and a permanent weir with an established stage-discharge relationship. Overall, twenty discharge measurements were taken with each measuring device at Stroubles Creek and Crab Creek over a two month period. The measuring conditions varied considerably over the testing period. The discharges measured ranged from 0.12 to 63 cfs, which corresponded to a large range of velocities with both simple and complex flow patterns. Diverse illumination conditions were also encountered over the measurement period, including glare and shadows.

The LSPIV prototype was accurate over most measuring conditions. The LSPIV discharge measurements tended to under-predict discharge at high stages compared to the weir measurements. The LSPIV discharge measurements also had greater error at moderate flows, similar to the results of Creutin et al. (2003). However, at low flow conditions LSPIV showed

improved discharge accuracy over the current meter, in comparison to the weir measurements. The discharge values, using all twenty data points, were not statistically different from either the current meter or weir ($\alpha = 0.05$). Finally, the LSPIV discharge measurements had an uncertainty of approximately ±14% (at a 95% confidence interval). The uncertainty is relatively high for widespread application, but could be reduced in future work by using a closer grid spacing and measuring more verticals in the cross-section.

5.2 Conclusions

Based on the analysis of the data collected in this study, several conclusions can be drawn concerning the application of LSPIV to measure discharge in low-order streams:

- Conditions at a variety of Froude numbers affect the accuracy of LSPIV discharge measurements. At Froude numbers above 0.25, LSPIV may show out-of-plane displacement losses, which will cause underestimation of the actual discharge. At Froude numbers below 0.10, tracer particles are more likely to agglomerate and reduce the LSPIV measurement accuracy by up to 15%.
- Improper camera angles can be a source of error in LSPIV discharge measurements. Operating the camera orthogonal to the water surface may exacerbate out-of-plane losses; however, image distortion will worsen at angles above 30 degrees from vertical in the laboratory.
- Adequate seeding density is an extremely important factor in obtaining accurate LSPIV measurements. Seeding densities above three particles per interrogation window should produce satisfactory results. However, variance in LSPIV measurements can be drastically reduced using seeding densities above five particles per interrogation window.
- The LSPIV measurements had poor accuracy at high flows (40 to 60 cfs), with errors of up to 25%, compared to the control structure. High-flow conditions produce complex flow patterns, which may invalidate some of the velocity distribution assumptions used in area-velocity discharge estimation methods. Additionally, maintaining good seeding density and distribution can be more difficult at high flows.

- LSPIV resulted in satisfactory discharge accuracy at low-flow conditions (0.1 to 0.7 cfs). The results were improved over measurements made using a Marsh-McBirney Flo-Mate 2000 current meter.
- The LSPIV discharge measurements were similar to weir and current meter measurements, for the flow conditions tested in this study. A mean error of less than 5% resulted, compared to the weir, which is consistent with previous LSPIV research.
- The 'proof-of-concept' showed that LSPIV is capable of providing accurate discharge measurements in low-order streams. Additionally, the LSPIV system shows promise for replacing conventional discharge measuring techniques with a less-labor intensive alternative. However, improvements in automation and reducing measurement uncertainty are necessary for widespread application and/or commercial viability.
- The development of an accurate and cost-effective LSPIV system could improve and expand the surface water monitoring networks. Additionally, LSPIV has the potential for real-time open-channel flow monitoring. The possible benefits of a successful LSPIV system should encourage future work into resolving the limitations found in this study.

5.3 Study Limitations

Although the laboratory and field experiments were carefully planned, some limitations were observed. The results from the laboratory experiments were hindered by a lack of significant digits in the flume manometer measurements. This problem, combined with small discharge measurements, reduced the strength of the LSPIV accuracy analysis in the laboratory. Additionally, the Flo-Mate 2000 was operated at the limits of its depth operating range, in order to achieve high Froude numbers. Therefore, the current meter may have been a poor reference

for the LSPIV discharge measurements. Finally, the tracer particles averaged 5-12 pixels in diameter, which was larger than the optimum size.

Collecting more streams and data points during the field experiments would have assisted with a more robust evaluation of LSPIV performance. There is also a need to test the technology in higher order streams. More discharge measurements may have improved the statistical analysis and allowed investigation into the repeatability of the LSPIV measurements. Field data should be collected over a longer time period, to allow for measurements in a broader range of climatic conditions. In practical applications, flow data are collected year round. Finally, the results suggest there may have been systematic errors present in the weir's stage-discharge relationships at Crab Creek. These problems could have been alleviated by using a gauging station that was more recently in operation.

5.4 Future Research Needs

The results of this study do not constitute a complete evaluation of LSPIV for measuring discharge in open-channels. This study focused on testing in low-order streams, which is only one possible area for the application of LSPIV. Several important factors affecting LSPIV accuracy will require subsequent investigation. The effect of out-of-plane losses at high Froude numbers necessitates further investigation. The hypothesis that significant surface disturbances can reduce discharge accuracy could not be fully confirmed by this study. Further research could also improve image acquisition at high glare conditions, by using camera filters or more advanced image processing techniques. Additionally, the methods and prototype developed in this study were specific to conducting a 'proof-of-concept' and not for developing a final design.

LSPIV has the potential to reduce costs and labor compared to conventional methods. However, this will require improving the prototype used in this study by automating several of

its components. The design of an effective automated particle dispenser is necessary for full automation of LSPIV. Additionally, the computer processing and parameter selection methods could be automated. A more robust design would, therefore, be capable of measuring discharge without the assistance of a field technician. However, an economic analysis is necessary to compare the costs of LSPIV to conventional technologies. In conclusion, an improved design shows promise for widespread monitoring application and commercial viability.

References

Abiven, C. and P. Vlachos. 2002. Comparative study of established DPIV algorithms for planar velocity measurements. In Proceeding of ASME IMECE 2002. New Orleans, L.A.: American Society of Mechanical Engineers.

Abiven, C. and P. Vlachos. 2002. Super spatio-temporal resolution, digital PIV system for multi-phase flows with phase differentiation and simultaneous shape and size quantification. In Proceeding of ASME IMECE 2002. New Orleans, L.A.: American Society of Mechanical Engineers.

Ackers, P., W.R. White, J.A. Perkins, and A.J.M. Harrison. 1978. *Weirs and Flumes for Flow Measurement*. Chichester: John Wiley & Sons.

Adrian, R. 1991. Particle-image techniques for experimental fluid mechanics. Annual Review of Fluid Mechanics. 23: 261-304.

Bradley, A. A., A. Kruger, and M Muste. 2002. Flow measurement in stream using video imagery. Water Resources Research. 38(12): 512-518.

Buchanan, T.J. and W.P. Somers. 1984. Discharge measurements at gaging stations. In *U.S. Geol. Survey Techniques Water-Resources Inv.*, book 3, chap. A8, 64.

Buchave, P. 1992. Particle image velocimetry – Status and trends. Experimental Thermal Fluid Sciences. 5: 586-604.

Campbell Scientific, Inc. 2001. CR510 Datalogger Opearators Manual. Logan, U.T.

Carneal, J. 2004. Personal Communication. May and September 2004.

Carr, J.C., and J.B. Burford. 1967. Descriptive notes of Crab Creek and Thorne Springs Branch watersheds.

Cheng, R., Costa, J., Haeni, P., Melcher, N., and E. Thurman. In In Search of Technologies for Monitoring River Discharge, 203-219. Denver, CO: Colorado Water Resources Publications.

Costa, J.E., K. R. Spicer, R.T.Cheng, P.F. Haeni, N.B. Melcher, and M.E. Thurman. Measuring stream discharge by non-contact methods: A proof-of-concept experiment. Geophysical Research Letters. 27(4): 553-556.

Creutin, J.D., M. Muste, A.A. Bradley, S.C. Kim, and A. Kruger. River gauging using PIV techniques: a proof of concept experiment on the Iowa River. Journal of Hydrology. 277: 182-194.

Engineering Laboratory Designs (ELD), Inc. 1987. B-16 Hydraulic Demonstration Channel –

Installation, operation, and maintenance manual. Lake City, M.N.

Etterma, R., I. Fujita, M. Muste, and A. Kruger. 1997. Particle-image velocimetry for whole-field measurement of ice velocities. Cold Region Science and Technology. 26: 97-112.

Fujita, I., and T. Kaizu. 1995. Correction method of erroneous vectors in PIV. Journal of Flow Visualization and Image Processing. 2: 173-185.

Fujita, I., A. Shiro, and T. Deguchi. 1997. Surface velocity measurement of river flow using video images of an oblique angle. In *Proc. 27th Congress of the International Association for Hydraulic Research*, theme B. San Francisco, California.

Fujita, I., M. Muste, and A. Kruger. 1998. Large-scale particle image velocimetry for flow analysis in hydraulic engineering applications. Journal of Hydraulic Research. 38(3): 397-414.

Grant, I. 1997. Particle image velocimetry: A review. Prco. Istn. Mech. Engrs. 211 Part C: 55-76.

Grover, N.C., and J.C. Hoyt. Accuracy of stream-flow data. USGS Water Supply Paper 400-D. 53-59. Washington D.C.:USGS.

Gui, L., and W. Merzkirch. 2000. A comparative study of the MQD method and several correlation-based PIV evaluation algorithms. Experiments in Fluids. 28: 36-44.

Herschy, R.W. 2002. Editorial to: Open channel flow measurement. Flow Measurement and Instrumentation. 12: 189-190.

Holstein, G. 2004. Personal Communication. March.

ISO. 1997. ISO/TR 8363Measurement of liquid flow in open channels - General guidelines for selection of method. . Genvea, Switzerland: ISO.

ISO. 1986. ISO 8363. Liquid flow measurement in open channels - General guidelines for the selection of methods. Genvea, Switzerland: ISO.

ISO. 1997. ISO 748.Measurement of liquid flow in open channels - Velocity area methods. Genvea, Switzerland: ISO.

ISO. 1998. ISO 1100-2. Measurement of liquid flow in open channels - Part 2: Determination of the stage discharge relationship. Genvea, Switzerland: ISO.

Kruger, A., L.J. Weber, M.V. Muste, and I. Fujita. 1999. Real-Time Measurements of Free-Surface Velocity Using Imaging Techniques. Avaliable at: http://www.iihr.uiowa.edu/projects/realpiv/realpiv.pdf. Accessed 12 November 2003.

Leica Geosystems. 2003. User Manual TC(R)407 Version 1.1. Switzerland.

Lloyd, M.P., D.J. Ball, and P.K. Stansby. 1995. Unsteady surface-velocity field measurement using particle tracking velocimetry. Journal of Hydraulic Research. 33(4):519-534.

Marsh-McBirney. 1990. Model 2000 Operations and Instructions Manual. Frederick, M.D.

Mathworks. 2004. Matlab Version 7.0 Help. Natick, M.A.

Melcher, N.B., R.T. Cheng, and F.P. Haeni. 2000. Investigating technologies to monitor open-channel discharge by direct measurement of cross-sectional area and velocity of flow. In 28th Congress . Graz, Austria: International Association for Hydraulic Research.

Melcher, N.B., J.E. Costa, F.P. Haeni, R.T. Cheng, E.M. Thurman, M. Buursink, K.R. Spicer, E. Hayes, W.J. Plant, W.C. Keller, and K. Hayes. 2002. River discharge measurements by using helicopter-mounted radar. Geophysical Research Letters. 29(22): 411-414.

Melling, A. Velocity profiles for particles and liquid in open-channel flow with suspended sediment. Measurement Science and Technology. 8: 1406-1414.

Merk, C. 2004. Personal Communication. 10 February.

Mitchem, C.J. 1997. A Comparative Study of Stream-Gaging Methods Employed in Nonpoint Source Pollution Studies in Small Streams. M.S. Thesis. Blacksburg, V.A.: Virginia Polytechnic Institute, Department of Biological Systems Engineering.

Novak, C.E. 1985. WRD data reports preperation guide: US Gelogical Survey publication. Washington, D.C.: USGS.

NRC. 2002. The Twenty Needs Report: How Research Can Improve the TMDL Program. Washington, D.C.: NAS.

Pelletier, P. 1988. Uncertainties in the single determination of river discharge: a literature review. Canadian Journal of Civil Engineering. 15: 834-850.

Petrou, M. and P. Bosdogianni. 1999. *Image Processing: The Fundementals*. New York, N.Y.: John Wiley and Sons.

Pressure Systems Inc. 2003. KPSI™ Level and Pressure Transducers User's Manual. 10th Edition. Hampton, V.A.

Rantz, S. E., et al., Measurement and computation of streamflow, Volume 2, Computation of Discharge, U. S. Geological Survey Water Supply Paper 2175, 1982b.

Raffel, M., C. Willert, and J. Kompenhans. 1998. Particle image velocimetry – A practical guide. New York, N.Y.: Springer.

SAS. 2004. SAS 9 Online Help. Cary, N.C.

Stevens, C., and M. Coates. 1994. Applications of a maximized cross-correlation technique for resolving velocity fields in laboratory experiments. Journal of Hydraulic Research. 32: 195-212.

Thye, Brian. 2003. Virginia Tech Duck Pond Retrofit for Improved Water Quality in Stroubles Creek. M.S. Thesis. Blacksburg, V.A.: Virginia Polytechnic Institute, Department of Civil Engineering.

Toràn, F., D. Ramierez. A.E. Navarro, S. Casans, J. Pelegri, and J.M. Espi. Design of a virtual instrument for water quality monitoring across the Internet. Sensors and Actuators: B. 76: 281-285.

Usera, G. 1999. Adaptive algorithms for PIV image analysis. In 5th Annual Meeting. Groupo De Trabajo Sobre Hidromeanica.

USGS. 1999. Statements of Need: Explanation of USGS Needs for Wireless Data Telemetry Equipment. Mississippi: Hydrologic Instrumentation Facility.

Walpole, R. , R. Myers, S. Myers, K. Ye. 2002. *Probability & Statistics for Engineers & Scientists*. Seventh Edition. Upper Saddle River, N.J.: Prentince Hall.

Weitbrecht, V., G. Kuhn, and G.H. Jirka. 2002. Large scale PIV-measurements at the surface of shallow water flows. Flow Measurement and Instrumentation. 13: 237-245.

Westerweel, J. 2000. Theroretical analysis of the measurement precision in particle image velocimetry. Experiments in Fluids. S3-S12.

Westerweel, J., D. Dabiri, and M. Gharib. 1997. The effect of a discrete window offset on the accuracy of cross-correlation analysis of digital PIV recordings. Experiments in Fluids. 23: 20-28.

Willert, C.E., and M. Gharib. 1991. Digital particle image velocimetry. Experiments in Fluids. 10: 191-193.

Wynn, J. 2004. Personal Communication. 12 January.

Yagow, G. 2004. Personal Communication. 4 November.

York, T.H. and K.A. Oberg. 2002. Measuring river velocity and discharge with acoustic Doppler profilers. Flow Measurement and Instrumentation. 13: 191-195.

Zhou, Daquan. 2004. Restoring Our Urban Streams: A Study Plan for Restoring/Rehabilitating Stroubles Creek in Blacksburg, Virginia. M.S. Thesis. Blacksburg, V.A.: Virginia Polytechnic Institute, Department of Urban Affairs and Planning.

Appendix

Appendix A: Comparison of Equipment and Image Processing Parameters Used in Previous Research

Laboratory Experiments

	Fujita et al. (1998)	Fujita et al. (1998)	Etterma et al. (1997)	Weitbrecht et al. (2002)
Title	Aeration Process	Ice conveyance through river confluences	Particle-image velocimetry for whole-field measurement of ice velocities	LSPIV-measurements at the surface of shallow flows
Camera	CCD	CCD	Sony EVO video (8-mm focal length lens)	Sensicam with 1/2 in. CCD sensor (15-mm Nikon f-mount lens)
Image size	640 X 480 pixel (8-bit grey-level)	640 X 480 pixel	640 X 480 pixel	1280 X 1024 pixel
Field of view	0.95 - 1.1.5 m^2	5.65 X 4.14 m	4.1 - 5.7 m^2	1.5 - 1.2 m
Distance to image	1.5 -1.8 m	5.4 m	5.4 m	3 m
Sampling rate/length	30 Hz	1 Hz / 100 images	1 Hz / 100 images	7 Hz / 595 images
Tracer	2-mm diameter platic beads	3-mm diameter platic beads	Polypropylene beads	Black, 2.5 mm diameter PE and PP coated with lacquer
PC and software	Custom software used to: control frame grabbing, image processing, and the presentation of the vector plots	Custom software used to: control frame grabbing, image processing, and the presentation of the vector plots	133 MHz PC - custom software was written in the C language to control the VCR and frame grabber during play back and framing	PIV package from La Vision with PC (1 GB Ram), frame-grabber, camera, and software
Transformation	Not required	706 X 518 corrected image	Grid of known spacing over the imaged area (706 X 518 pixel corrected image)	Not required
Evaluation Method	Cross-correlation	Cross-correlation	Cross-correlation	Cross-correlation
Interrogation Area	33 X 33 pixels	31 X 31 pixel	15 X 10 pixel	16 X 16 pixel
Search area	N/A	N/A	N/A	N/A
Pixel size	3 X 3 cm	8 X 8 mm	8 X 8 mm	1.2 X 1.2 mm
Velocities recorded	0.01 - 3 m/s	0.02 - 0.16 m/s	0.02 - 0.16 m/s	N/A

Field Experiments

	Bradley et al. (2002)	Fujita et al. (1998)	Cruetin et al. (2003)
Title	Flow measurement in streams using video imagery	Velocity mapping in flood plains	River gauging using PIV techniques: a proof of concept experiment on the Iowa River
Camera	Panasonic Palmcorder PV IQ405 (video)	CCD	Sony DCR-TV V320
Image size	500 X 650 pixel	512 X 512 pixel (8-bit grey-level)	
Field of view	5 m cross-section	140.4 X 320 m	> 5000 m^2
Distance to image	On a bridge above stream	65 m	14 m
Sampling rate/length	1Hz / 60 images	1 Hz / 60 images	1 Hz / 600 images
Tracer	Leaves added by hand	Natural foam and surface wake	Natural bubbles
PC and software	200 MHz Pentium PC with framegrabber and computer controlled VCR	PC with a frame-grabber and video cassette recorder	PC not specified
Transformation	Ten points measured with total station	351 X 800 corrected image	Used fixed ground reference points
Evaluation Method	Cross-correlation	Cross-correlation	Cross-correlation
Interrogation Area	25 X 25 pixels	25 X 25 pixels	64 X 64 pixels
Search area	48 X 48 pixels	N/A	24 pixels
Pixel size	8 X 8 mm	40 X 40 cm	6.5 pixel / m
Velocities recorded	0.01 - 0.2 m/s	0.02 - 4 m/s	0.01 - 3 m/s

Appendix B Data Collection Sheets

LSPIV Laboratory Data Collection Sheet:

General Information:

Names:
Date:
Time:
Camera:
Lens:
Distance from lens to the bottom of flume: _____ ft.
Conversion to physical space:
Depth1 = 0 in. Horizontal Distance (D1) = _____ ft.
Depth2 = _____ ft Horizontal Distance (D2)= _____ ft.
pix0= D1 / 640 pixels = b =
pix1 = D2/640 pixels
pix1 = m(Depth2) +b
m =
Conversion Equation y=mx+b = _____
1 pixel = ____ ft.
Particle diameter = _0.01969_ in.
Notes:
Camera angle: _____°

Sample B___A 1 BLOCK __
Froude number = ____ using average velocity
Headgate distance to bottom of flume = _____ in.
Tailgate angle = _____°
Flume slope = _____°
Manometer: Pump #1 H1 = ____ ft - ____ ft = _____ ft
Pump #2 H2 = ____ ft - ____ ft = _____ ft
Q1 = 0.0646(H1)^0.5 = ____ cfs
Q2 = 0.2009(H2)^0.5 = ____ cfs
DischargeMan = Q1 + Q2 = _____ cfs
M-M Meter:
Depth=

Distance from edge (in.)	1.5	3	5	7	9	10.5
Velocity @ 6/10 depth (ft/s)						

Discharge = _____ cfs
Average Velocity = _____ fps

LSPIV:
Depth: _____ - 0.621 ft = _____ ft
Discharge = _____ cfs
Average velocity = _____ fps

LSPIV Prototype Field Data Collection Sheet

Location:
Date:
Time:
Operators:
Weather:
Comments:

M-M Meter:

Distance from water edge (ft)	Depth (ft)	Velocity (ft/s)	Distance from water edge (ft)	Depth (ft)	Velocity (ft/s)
0	0	0			

Discharge = _____ cfs

Weir (if applicable)
Height = _____
Discharge = _____ cfs

LSPIV Prototype
Camera Rate = _____ Hz
Stage (pressure-transducer) = _____ ft
Discharge = ____ cfs

Comments:

Appendix C Matlab Image Processing Programs

Laboratory Image Acquisition Program

```
clear
framerate = 1;
numberofimages = 10;

vid = videoinput('winvideo',1,'SP44_320x240');
src = getselectedsource(vid);

%preview(vid)

set(vid,'FramesPerTrigger',numberofimages);
set(vid,'FrameGrabInterval',framerate);

start(vid);
numAvail = vid.FramesAvailable
frames =getdata(vid,numberofimages);

start(vid);
wait(vid);
[f,t] = getdata(vid);

for x=1:numberofimages
rgb = (f(:,:,:,x));
I = rgb2gray(rgb);
filename = sprintf('pic%1.0f.tif',x);
imwrite(I,filename,'tiff');
end
```

Laboratory Image Enhancement Program

```
clear
close all

depth=0.35; %ft
pixsize = -.00627*depth+0.0090625; %ft
numberofimages=25;

 input_points0 =[12 108;
   75 276;
   163 129;
   293 241;
   407 172;
   525 300;
   583 54;
   627 289;
   89 257;
   248 105;
   511 196;
   612 106;
   12 307;
   339 331];

base_points_raw0 = [5 1;
    10 10;
    15 4;
    21 8;
```

```
    26 5;
    32 11;
    36 0;
    39 11;
    12 9;
    19 2;
    31 6;
    38 1;
    5 12;
    23 12];

 input_points15=[24 73;
    26 336;
     635 272;
     117 108;
    561 149;
    605 224 ;
    339 174;
    435 294;
    491 106;
    532 247;
    580 166 ;
    624 196;
    204 152;
        594 153;
        625 133;
        508 178;
       480 159;
       618 197;
       434 196];

    base_points_raw15=[0;
        0 12;
         40 12;
         5 2;
        30 3;
        35 8;
        15 5;
        20 11;
        24 1;
        27 9;
        32 4;
        38 6;
          9 4 ;
         39 1;
        25 5;
        28 4;
        37 6;
        20 6];

        input_points30 =[38 79;
        123 349;
        519 143;
        524 247;
        280 201;
        479 180;
        377 105;
        319 308;
        483 237;
        502 170;
        452 244;
        492 202;
        127 211;
        526 190;
        519 209;
        512 251;
        101 352;
        529 246;
        452 118;
        466 267;
        498 234;
        401 137;
        437 275];
    base_points_raw30 = [0 0;
        1 12;
        40 1;
        39 12;
        10 6;
        30 5;
        23 0;
        13 12;
        30 10;
        35 4;
        25 8;
        32 7;
        2 6;
        40 6;
        37 8;
        36 12;
        0 12;
        40 12;
        28 0;
        27 12;
        33 10;
        20 2;
        23 12];

    input_points45 =[82 91;
        112 327;
        389 132;
        402 226;
        397 179;
        91 208;
        305 139 ;
        290 239;
        162 147;
        245 236;
        365 200;
        323 173;
        380 139;
        386 171;
           391 211];

      base_points_raw45 = [0;
        0 12;
        40 0;
        40 12;
        40 6;
        0 6;
        20 2;
        16 10;
        5 3;
        11 9;
        30 8;
        23 5;
        37 1;
        37 5;
        37 11];


base_points = base_points_raw15./pixsize.*12; %Change for angle
TFORM = CP2TFORM(input_points15,base_points,'lwm'); %Change for angle
```

```
for count=1:numberofimages
   filename = sprintf('pic%0.4i.tif',count);
   q=imread(filename);

  x_2 = imadjust(q);

xstart=231;
ystart=109+160;
xfinish=xstart+392+64;
yfinish=ystart+402-224;
cropped=imcrop(x_2,[xstart ystart xfinish yfinish]); % for 0 degrees only A1

fprintf('Writing image %1.0f ...\n',count)
imwrite(cropped,filename,'tiff');

end
```

Laboratory Post-Processing Program

```
clear
close all
threshold = 0.05; %(1.0%)
avgTime=1/25; %sec
depth=(0.548+.61)/2; %ft
%pixsize = -.008451*depth+0.013125; %ft
pixsize = 1/448;
numberofimages=24;

for ii = 1:numberofimages

% oupen input file for reading -- filename will need to be replaced with a
% variable
filename = sprintf('pic%0.4i.plt',ii);
inputfile = fopen(filename);
% oupen output file for reading and writing, erase the file (w+)
outputfile = fopen('outputpic.txt','w+');
% read & discard the first three lines
textline = fgetl(inputfile);
textline = fgetl(inputfile);
textline = fgetl(inputfile);
% loop through the file, reading a line, writing a line
while 1
   textline = fgetl(inputfile);
   if ~ischar(textline), break, end %bail if EOF
   fwrite(outputfile,textline);
   fwrite(outputfile,13);
```

```
   fwrite(outputfile,10);
   %disp(textline)
end
% clean up after ourselves
fclose(inputfile);
fclose(outputfile);

   filename = sprintf('outputpic.txt',ii);
         A(:,:,ii) = load(filename);
          %A(:,:,ii) = load('outputpic.txt');

end

psize = size(A(:,:,ii));
hold1 = psize(1,1);
hold2 = A(1,1);
hold3= A(hold1,1);
hold4 = (hold3-hold2)/64+1;

for pic=1:numberofimages
totalcount=A(1,2,pic);
x=1;
xcount=1;

while totalcount>63
midpt=mean(A(xcount:(xcount+hold4-1),1,pic));
y=mean(A(xcount:(xcount+hold4-1),2,pic));

number=0;
total=0;

minimum = min(A(xcount:(xcount+hold4-1),3,pic));
for count2=0:(hold4-1)
if A((count2+xcount),3,pic) <= (threshold)*(minimum)
   total = total + A((count2+xcount),3,pic);
   number = number+1;
end
end
xvel1=total/number;

%xvel1=min(A(xcount:(xcount+hold4-1),3,pic));
xvel=xvel1/avgTime*pixsize;
yvel=mean(A(xcount:(xcount+hold4-1),4,pic));
yvel=yvel/avgTime*pixsize;
B(x,1,pic)=midpt;
B(x,2,pic)=y;
```

```
B(x,3,pic)=xvel;
B(x,4,pic)=yvel;
xcount=xcount+hold4;
x=x+1;
totalcount=y;
end;
pic=pic+1;
end;

x2=1;
y2=1;
for temp2=1:4
for temp=1:(x-1)
C(temp,temp2)=mean(B(temp,temp2,:));
end
end

        hold on
        quiver(A(:,1,1),A(:,2,1),A(:,3,1),A(:,4,1));
    hold on
   D = zeros(80,1);
        quiver(C(:,1),C(:,2),C(:,3),C(:,4));

verticalcorrcoef = .94;
      avgvelocity = verticalcorrcoef.*mean(C(:,3));
discharge=avgvelocity*(depth);

y=[pixsize,threshold,avgTime];
fid=fopen('data.txt','w');
fprintf(fid,'Pixel Size    Threshold   Frame Rate');
fprintf(fid,'\n %1.5f        %1.3f       %1.4f    ',y);
fclose(fid);

fid=fopen('C.txt','w');
fprintf(fid,'          x       y       u         v  ');
fprintf(fid,'\n      %1.5f   %1.5f    %1.5f    %1.5f',C);
fclose(fid);
```

Field Image Acquisition Program

```
clear

vid = videoinput('winvideo',1,'UYVY_640x480');
src = getselectedsource(vid);

numberofimages = 40; %sets the number of frames to acquire ***Cannot be 1
```

```
set(vid,'Timeout',50);
set(vid,'TriggerFrameDelay',1);
set(vid,'FramesPerTrigger',numberofimages);
set(src,'FrameRate','2.0000') %Specify frame rate here. Possible values:[ {30.0000} | 29.9700 |
29.0000 | 28.0001 | 27.0000 | 26.0000 | 25.0000 | 24.0000 | 23.0000 | 22.0000 | 21.0000 | 20.0000
| 19.0000 | 18.0000 | 17.0000 | 16.0000 | 15.0000 | 14.0000 | 13.0000 | 12.0000 | 11.0000 |
10.0000 | 9.0000 | 8.0000 | 7.0000 | 6.0000 | 5.0000 | 4.0000 | 3.0000 | 2.0000 | 1.0000 ]

fprintf('Gathering images in 1 second...\n')
start(vid);
%numAvail = vid.FramesAvailable;
wait(vid);
[f,t] = getdata(vid);

fprintf('Writing images...\n')
for x=1:numberofimages
rgb = (f(:,:,:,x));
I = rgb2gray(rgb);
filename = sprintf('pic%0.4i.tif',x);
imwrite(I,filename,'tiff');
end

fprintf('Done \n')
```

Field Image Enhancement Program

```
clear
close all

numberofimages=40;

base_points = [-18.97429996 70.81183766;
-19.13327412  66.10756707;
-18.36239679  59.1389481;
-18.32338177  52.88675094;
-19.02529407  47.61385628;
-19.25583892  41.71819452;
-28.50788811  40.80998709;
-26.80556365  46.30352349;
-26.53829569  49.49556587;
-26.2206439    53.19215285;
-26.18104706  58.09657032;
-24.92474205  64.29153674];

input_points = [58 115;
85 131;
```

```
125 178;
200 243;
320 305;
498 404;
598 211;
471 182;
406 152;
328 130;
254 104;
181 83];

for j=1:12
    base_points(j,1)=base_points(j,1)
   base_points(j,2)=base_points(j,2)-40.22;
end

TFORM = CP2TFORM(input_points,base_points,'affine'); %Change for angle

for count=1:numberofimages
    filename = sprintf('pic%0.4i.tif',count);
    q=imread(filename);

Rp = imtransform(q,TFORM);

 cropped=imcrop(Rp,[290 400 600 650]); % for 0 degrees only A1
x_eq = histeq(cropped);

background = imopen(cropped,strel('disk',15));
x2 = imsubtract(cropped,background);
x2_imadjust = imadjust(x2)


fprintf('Writing image %1.0f ...\n',count)
 imwrite(x2_imadjust,filename,'tiff');

  end

   figure, imshow(cropped)
   figure, imshow(x2_imadjust);
title('Imadjust2');
```

Field Post-Processing Program

```
clear
close all
surface_correction=0.93;
avgTime=1/2; %sec USER INPUT
```

```
numberofimages=39; %USER INPUT

for ii = 1:numberofimages

% oupen input file for reading -- filename will need to be replaced with a
% variable
filename = sprintf('First Order DWO PIV_pic%0.4i.plt',ii);
inputfile = fopen(filename);
% oupen output file for reading and writing, erase the file (w+)
outputfile = fopen('outputpic.txt','w+');
% read & discard the first three lines
textline = fgetl(inputfile);
textline = fgetl(inputfile);
textline = fgetl(inputfile);
% loop through the file, reading a line, writing a line
while 1
   textline = fgetl(inputfile);
   if ~ischar(textline), break, end %bail if EOF
   fwrite(outputfile,textline);
   fwrite(outputfile,13);
   fwrite(outputfile,10);
   %disp(textline)
end
% clean up after ourselves
fclose(inputfile);
fclose(outputfile);

   filename = sprintf('outputpic.txt',ii);
         A(:,:,ii) = load(filename);
          %A(:,:,ii) = load('outputpic.txt');

end

psize = size(A(:,:,ii));
hold1 = psize(1,1);
hold2 = A(1,1);
hold3= A(hold1,1);

count3=0;
for pic=1:numberofimages

count3=count3+1;
count4=1;
xcount=hold2;

while xcount<=hold3
```

```
   x=1;
   count=1;
   while x<=hold1
if A(x,1,pic)==xcount
   y(count)=A(x,4,pic);
   count=count+1;
end;
  x=x+1;
   end;

numofxvel=((hold3-hold2)/32)+1;

xvel1(count3,count4)=mean(y);
%mean_yvel(count3,count4) = mean(y);
count4=count4+1;
xcount=xcount+32;
end;
   pic=pic+1;
end;

xcount2=32;
for avgcount=1:numofxvel;
avg_vel(avgcount,1)=xcount2;
xcount2=xcount2+32;
avg_vel(avgcount,2)=mean(A(:,2,1));
   avg_vel(avgcount,4)=abs(mean(xvel1(:,avgcount)));
avg_vel(avgcount,3)=mean(A(:,3,1));
end

% quiver(A(:,1,5),A(:,2,5),A(:,3,5),A(:,4,5));
% hold on
imshow('pic0001.tif');
hold on
quiver(avg_vel(:,1),avg_vel(:,2),avg_vel(:,3),avg_vel(:,4));

clc
depth_correction=0;
actual_depth=1.06-depth_correction;   %USER INPUT

distance_master = [0.00;          3.05;          6.55;
%USER INPUT                       3.56;          7.05;
0.53;                             4.06;          7.56;
1.06;                             4.56;          8.07;
1.55;                             5.05;          8.56;
2.03;                             5.55;          9.04;
2.54;                             6.05;          9.55;
```

```
10.05;                  26.15;                  0.20;
10.57;                  26.62;                  0.17;
11.09;                  27.09;                  0.13;
11.56;                  28.13];                 0.09;
12.03;                                          0.04;
12.57;                  depth_master = [3.65;   0.02;
13.11;                  %USER INPUT             0.00;
13.58;                  3.60;                   0.09;
14.05;                  3.55;                   0.18;
14.55;                  3.48;                   0.21;
15.04;                  3.40;                   0.24;
15.60;                  3.30;                   0.42;
16.15;                  3.20;                   0.59;
16.64;                  3.09;                   0.86;
17.12;                  2.98;                   1.13;
17.63;                  2.89;                   1.38;
18.14;                  2.80;                   1.62;
18.64;                  2.69;                   1.84;
19.13;                  2.58;                   2.06;
19.68;                  2.48;                   2.20;
20.22;                  2.37;                   2.33;
20.68;                  2.34;                   2.43;
21.14;                  2.30;                   2.52;
21.66;                  2.09;                   2.63;
22.17;                  1.88;                   2.73;
22.66;                  1.68;                   2.91;
23.14;                  1.47;                   3.09;
23.64;                  1.08;                   3.28;
24.14;                  0.69;                   3.47;
24.67;                  0.56;                   3.65];
25.19;                  0.43;
25.67;                  0.32;
count8=1;
count9=1;
while actual_depth < depth_master(count8)
   count8=count8+1;
end
      ratio=(actual_depth-depth_master(count8))/(depth_master(count8-1)-
depth_master(count8));
      starting_distance = distance_master(count8-1)+ratio*(distance_master(count8)-
distance_master(count8-1));
      distance(count9) = 0;
      depth(count9) = 0;
      count9=count9+1;
while actual_depth >= depth_master(count8)
      distance(count9)=distance_master(count8)-starting_distance;
```

```
        depth(count9)=actual_depth-depth_master(count8);
        count8=count8+1;
        count9=count9+1;
        end
depth(count9)=0;
ratio=(actual_depth-depth_master(count8))/(depth_master(count8-1)-depth_master(count8));
finishing_distance = (distance_master(count8-1)+ratio*(distance_master(count8)-
distance_master(count8-1)))-starting_distance;
distance(count9)=finishing_distance;

number_of_piv_vectors=14; %USER INPUT
count10=size(distance);
count10=count10(1,2);
total_distance=distance(count10);
PIVdistance(1)=0;

for count11=2:number_of_piv_vectors;
   PIVdistance(count11)=(total_distance/(number_of_piv_vectors-1))+PIVdistance(count11-1);
end

pixelPIVdistance = 32; %pixels
pixsize = [PIVdistance(2)-PIVdistance(1)]/pixelPIVdistance;
pixsize=(total_distance)/((number_of_piv_vectors)*32);
%convert avgvel to physical size:
for count5=1:numofxvel
   avg_vel_corrected(count5)=avg_vel(count5,4)/avgTime*pixsize*surface_correction;
end

count1=1;
count2=1;

psize = size(PIVdistance(:,:));
distancecount=size(distance(:,1));
distancecount=distancecount(1);
totalcount = psize(1,2);
carryover=0;

while PIVdistance(count2)<PIVdistance(totalcount)
   area(count2)=carryover;
%     if distance(count1)<(distancecount-1);
   while round(distance(count1+1)*1000)< round(PIVdistance(count2+1)*1000)
      if depth(count1) <= depth(count1+1)
         area(count2)=area(count2)+[(distance(count1+1)-
distance(count1))*depth(count1)]+[(1/2)*(distance(count1+1)-
distance(count1))*(depth(count1+1)-depth(count1))];
      else
```

```
          area(count2)=area(count2)+[(distance(count1+1)-
distance(count1))*(depth(count1+1))]+[(1/2)*(distance(count1+1)-
distance(count1))*(depth(count1)-depth(count1+1))];
          end
         count1=count1+1;
         end

       if depth(count1) >= depth(count1+1)
          depthint=[[(PIVdistance(count2+1)-distance(count1))/(distance(count1+1)-
distance(count1))]*(abs(depth(count1+1)-depth(count1)))]+depth(count1);
          area(count2)=area(count2)+[(PIVdistance(count2+1)-
distance(count1))*depth(count1)]+[(1/2)*(PIVdistance(count2+1)-distance(count1))*(depthint-
depth(count1))];
          carryover=[(distance(count1+1)-
distance(count1))*depth(count1)]+[(1/2)*(distance(count1+1)-
distance(count1))*(depth(count1+1)-depth(count1))]-[[(PIVdistance(count2+1)-
distance(count1))*depth(count1)]+[(1/2)*(PIVdistance(count2+1)-distance(count1))*(depthint-
depth(count1))]];
       else
          depthint=[[(PIVdistance(count2+1)-distance(count1))/(distance(count1+1)-
distance(count1))]*(abs(depth(count1+1)-depth(count1)))]+depth(count1+1);
          area(count2)=area(count2)+[(PIVdistance(count2+1)-
distance(count1))*depth(count1+1)]+[(1/2)*(PIVdistance(count2+1)-
distance(count1))*(depth(count1)-depthint)];
          carryover=[(distance(count1+1)-
distance(count1))*(depth(count1+1))]+[(1/2)*(distance(count1+1)-
distance(count1))*(depth(count1)-depth(count1+1))]-[[(PIVdistance(count2+1)-
distance(count1))*depth(count1+1)]+[(1/2)*(PIVdistance(count2+1)-
distance(count1))*(depth(count1)-depthint)]];
       end
             count1=count1+1;
             count2=count2+1;
          end
          area(count2-1)=area(count2-1)+carryover;

% end
 %The following code calculates discharge from avg_vel_corrected and area
 starting_PIV_vector =2; %USER INPUT   What is the first vector in the water plane
 water_edge = [starting_PIV_vector,number_of_piv_vectors+starting_PIV_vector-3]; %%USER
INPUT       The inside and outside points from avg_vel_corrected for water's edge
 start_point = water_edge(1);
 count6=water_edge(2)-water_edge(1)+1;
 discharge = 0;
 %calculate discharge with mean velocity method
 for count7=1:count6
```

```
discharge=discharge+area(count7)*[(avg_vel_corrected(start_point)+avg_vel_corrected(start_po
int+1))/2];
```

Appendix D Statistical Analysis Programs using SAS

First Laboratory Experiment

ANACOVA Input File

Obs	A	B	C	sub	D	Y
1	1	1	1	1	1	0.10
2	1	1	1	1	1	0.11
3	1	1	1	2	2	0.07
4	1	1	1	2	2	0.09
5	1	1	1	3	3	0.07
6	1	1	1	3	3	0.07
7	1	1	2	4	1	0.10
8	1	1	2	4	1	0.11
9	1	1	2	5	2	0.07
10	1	1	2	5	2	0.09
11	1	1	2	6	3	0.09
12	1	1	2	6	3	0.09
13	1	1	3	7	1	0.10
14	1	1	3	7	1	0.11
15	1	1	3	8	2	0.07
16	1	1	3	8	2	0.09
17	1	1	3	9	3	0.09
18	1	1	3	9	3	0.10
19	1	1	4	10	1	0.10
20	1	1	4	10	1	0.11
21	1	1	4	11	2	0.07
22	1	1	4	11	2	0.09
23	1	1	4	12	3	0.10
24	1	1	4	12	3	0.06
25	1	1	5	13	1	0.10
26	1	1	5	13	1	0.10
27	1	1	5	14	2	0.07
28	1	1	5	14	2	0.07
29	1	1	5	15	3	0.10
30	1	1	5	15	3	0.10
31	2	1	1	16	1	0.15
32	2	1	1	16	1	0.15
33	2	1	1	17	2	0.14
34	2	1	1	17	2	0.13
35	2	1	1	18	3	0.07
36	2	1	1	18	3	0.07
37	2	1	2	19	1	0.15
38	2	1	2	19	1	0.15
39	2	1	2	20	2	0.14
40	2	1	2	20	2	0.13
41	2	1	2	21	3	0.10
42	2	1	2	21	3	0.06
43	2	1	3	22	1	0.15
44	2	1	3	22	1	0.15
45	2	1	3	23	2	0.14
46	2	1	3	23	2	0.13
47	2	1	3	24	3	0.08
48	2	1	3	24	3	0.08
49	2	1	4	25	1	0.15
50	2	1	4	25	1	0.15
51	2	1	4	26	2	0.14
52	2	1	4	26	2	0.13
53	2	1	4	27	3	0.09
54	2	1	4	27	3	0.09
55	2	1	5	28	1	0.15
56	2	1	5	28	1	0.15
57	2	1	5	29	2	0.14
58	2	1	5	29	2	0.13
59	2	1	5	30	3	0.09
60	2	1	5	30	3	0.09
61	1	2	1	31	1	0.10
62	1	2	1	31	1	0.11
63	1	2	1	32	2	0.09
64	1	2	1	32	2	0.13
65	1	2	1	33	3	0.03
66	1	2	1	33	3	0.07
67	1	2	2	34	1	0.10
68	1	2	2	34	1	0.11
69	1	2	2	35	2	0.09
70	1	2	2	35	2	0.13
71	1	2	2	36	3	0.03
72	1	2	2	36	3	0.11
73	1	2	3	37	1	0.10
74	1	2	3	37	1	0.11
75	1	2	3	38	2	0.09
76	1	2	3	38	2	0.13

77	1	2	3	39	3	0.13
78	1	2	3	39	3	0.12
79	1	2	4	40	1	0.10
80	1	2	4	40	1	0.11
81	1	2	4	41	2	0.09
82	1	2	4	41	2	0.13
83	1	2	4	42	3	0.13
84	1	2	4	42	3	0.11
85	1	2	5	43	1	0.10
86	1	2	5	43	1	0.11
87	1	2	5	44	2	0.09
88	1	2	5	44	2	0.13
89	1	2	5	45	3	0.10
90	1	2	5	45	3	0.14
91	2	2	1	46	1	0.16
92	2	2	1	46	1	0.16
93	2	2	1	47	2	0.13
94	2	2	1	47	2	0.14
95	2	2	1	48	3	0.12
96	2	2	1	48	3	0.12
97	2	2	2	49	1	0.16
98	2	2	2	49	1	0.16
99	2	2	2	50	2	0.13
100	2	2	2	50	2	0.14
101	2	2	2	51	3	0.12
102	2	2	2	51	3	0.13
103	2	2	3	52	1	0.16
104	2	2	3	52	1	0.16
105	2	2	3	53	2	0.13
106	2	2	3	53	2	0.14
107	2	2	3	54	3	0.11
108	2	2	3	54	3	0.15
109	2	2	4	55	1	0.16
110	2	2	4	55	1	0.16
111	2	2	4	56	2	0.13
112	2	2	4	56	2	0.14
113	2	2	4	57	3	0.12
114	2	2	4	57	3	0.14
115	2	2	5	58	1	0.16
116	2	2	5	58	1	0.16
117	2	2	5	59	2	0.13
118	2	2	5	59	2	0.14
119	2	2	5	60	3	0.13
120	2	2	5	60	3	0.13

SAS ANACOVA Analysis Program

```
data test;
infile 'E:\Lab Tests\labtest1.xls';
input A B C rep D Y;
proc print;
run;
proc mixed data=test;
class A B C sub D;
model Y=A|B|C|D/ddfm=satterth;
random sub(A*B*C) D*sub(A*B*C);
*contrast 'A1 v. A2' A 1 -1;
*contrast 'D1 v. D2' D 1 -1 0;
*contrast 'A1D1 v. A1D2' D 1 -1 0 A*D 1 -1 0 0 0 0;
*lsmeans A B C D;
run;

proc mixed data=test;
class A B C sub D;
model Y=A B C D A*D B*D C*D A*B*D/ddfm=satterth;
random sub(A*B*C) D*sub(A*B*C);
*contrast 'A1 v. A2' A 1 -1;
contrast 'D1 v. D2' D 1 -1 0;
```

```
contrast 'D2 v. D3' D 0 1 -1;
contrast 'D1 v. D3' D 1 0 -1;
*contrast 'A1D1 v. A1D2' D 1 -1 0 A*D 1 -1 0 0 0 0;
*lsmeans A B C D;
run;
```

Second Laboratory Experiment

Input File

Obs	A	B	sub	D	Y
1	1	1	1	1	0.11
2	1	1	1	1	0.11
3	1	1	1	1	0.11
4	1	1	1	1	0.11
5	1	1	1	1	0.11
6	1	1	2	2	0.08
7	1	1	2	2	0.08
8	1	1	2	2	0.10
9	1	1	2	2	0.11
10	1	1	2	2	0.07
11	1	1	3	3	0.11
12	1	1	3	3	0.12
13	1	1	3	3	0.13
14	1	1	3	3	0.11
15	1	1	3	3	0.12
16	2	1	4	1	0.16
17	2	1	4	1	0.16
18	2	1	4	1	0.16
19	2	1	4	1	0.15
20	2	1	4	1	0.15
21	2	1	5	2	0.13
22	2	1	5	2	0.12
23	2	1	5	2	0.14
24	2	1	5	2	0.14
25	2	1	5	2	0.13
26	2	1	6	3	0.15
27	2	1	6	3	0.15
28	2	1	6	3	0.15
29	2	1	6	3	0.14
30	2	1	6	3	0.15
31	3	1	7	1	0.20
32	3	1	7	1	0.20
33	3	1	7	1	0.20
34	3	1	7	1	0.20
35	3	1	7	1	0.20
36	3	1	8	2	0.18
37	3	1	8	2	0.18
38	3	1	8	2	0.18
39	3	1	8	2	0.19
40	3	1	8	2	0.18
41	3	1	9	3	0.17
42	3	1	9	3	0.17
43	3	1	9	3	0.17
44	3	1	9	3	0.17
45	3	1	9	3	0.20
46	4	1	10	1	0.24
47	4	1	10	1	0.23
48	4	1	10	1	0.23
49	4	1	10	1	0.23
50	4	1	10	1	0.23
51	4	1	11	2	0.22
52	4	1	11	2	0.20
53	4	1	11	2	0.21
54	4	1	11	2	0.23
55	4	1	11	2	0.20
56	4	1	12	3	0.12
57	4	1	12	3	0.19
58	4	1	12	3	0.17
59	4	1	12	3	0.18
60	4	1	12	3	0.14
61	1	2	13	1	0.11
62	1	2	13	1	0.11
63	1	2	13	1	0.11
64	1	2	13	1	0.11
65	1	2	13	1	0.11
66	1	2	14	2	0.11
67	1	2	14	2	0.09
68	1	2	14	2	0.11
69	1	2	14	2	0.11
70	1	2	14	2	0.07
71	1	2	15	3	0.13
72	1	2	15	3	0.13
73	1	2	15	3	0.12

74	1	2	15	3	0.13
75	1	2	15	3	0.09
76	2	2	16	1	0.16
77	2	2	16	1	0.16
78	2	2	16	1	0.15
79	2	2	16	1	0.16
80	2	2	16	1	0.15
81	2	2	17	2	0.14
82	2	2	17	2	0.14
83	2	2	17	2	0.14
84	2	2	17	2	0.15
85	2	2	17	2	0.13
86	2	2	18	3	0.17
87	2	2	18	3	0.14
88	2	2	18	3	0.15
89	2	2	18	3	0.16
90	2	2	18	3	0.18
91	3	2	19	1	0.20
92	3	2	19	1	0.20
93	3	2	19	1	0.20
94	3	2	19	1	0.20
95	3	2	19	1	0.20
96	3	2	20	2	0.17
97	3	2	20	2	0.18
98	3	2	20	2	0.18
99	3	2	20	2	0.20
100	3	2	20	2	0.16
101	3	2	21	3	0.19
102	3	2	21	3	0.18
103	3	2	21	3	0.20
104	3	2	21	3	0.19
105	3	2	21	3	0.20
106	4	2	22	1	0.23
107	4	2	22	1	0.23
108	4	2	22	1	0.23
109	4	2	22	1	0.23
110	4	2	22	1	0.23
111	4	2	23	2	0.19
112	4	2	23	2	0.26
113	4	2	23	2	0.22
114	4	2	23	2	0.23
115	4	2	23	2	0.20
116	4	2	24	3	0.21
117	4	2	24	3	0.22
118	4	2	24	3	0.21
119	4	2	24	3	0.22
120	4	2	24	3	0.20
121	1	3	25	1	0.11
122	1	3	25	1	0.11
123	1	3	25	1	0.11
124	1	3	25	1	0.11
125	1	3	25	1	0.11
126	1	3	26	2	0.07
127	1	3	26	2	0.08
128	1	3	26	2	0.08
129	1	3	26	2	0.09
130	1	3	26	2	0.08
131	1	3	27	3	0.22
132	1	3	27	3	0.09
133	1	3	27	3	0.09
134	1	3	27	3	0.11
135	1	3	27	3	0.09
136	2	3	28	1	0.16
137	2	3	28	1	0.15
138	2	3	28	1	0.16
139	2	3	28	1	0.15
140	2	3	28	1	0.16
141	2	3	29	2	0.13
142	2	3	29	2	0.13
143	2	3	29	2	0.13
144	2	3	29	2	0.13
145	2	3	29	2	0.12
146	2	3	30	3	0.13
147	2	3	30	3	0.15
148	2	3	30	3	0.12
149	2	3	30	3	0.14
150	2	3	30	3	0.11
151	3	3	31	1	0.20
152	3	3	31	1	0.20
153	3	3	31	1	0.20
154	3	3	31	1	0.20
155	3	3	31	1	0.20
156	3	3	32	2	0.16
157	3	3	32	2	0.18
158	3	3	32	2	0.18
159	3	3	32	2	0.18
160	3	3	32	2	0.16
161	3	3	33	3	0.17
162	3	3	33	3	0.13
163	3	3	33	3	0.15
164	3	3	33	3	0.19
165	3	3	33	3	0.12

166	4	3	34	1	0.23
167	4	3	34	1	0.23
168	4	3	34	1	0.23
169	4	3	34	1	0.23
170	4	3	34	1	0.23
171	4	3	35	2	0.21
172	4	3	35	2	0.21
173	4	3	35	2	0.22
174	4	3	35	2	0.22
175	4	3	35	2	0.20
176	4	3	36	3	0.19
177	4	3	36	3	0.18
178	4	3	36	3	0.15
179	4	3	36	3	0.17
180	4	3	36	3	0.19
181	1	4	37	1	0.11
182	1	4	37	1	0.11
183	1	4	37	1	0.11
184	1	4	37	1	0.11
185	1	4	37	1	0.11
186	1	4	38	2	0.09
187	1	4	38	2	0.08
188	1	4	38	2	0.11
189	1	4	38	2	0.11
190	1	4	38	2	0.07
191	1	4	39	3	0.11
192	1	4	39	3	0.09
193	1	4	39	3	0.09
194	1	4	39	3	0.10
195	1	4	39	3	0.08
196	2	4	40	1	0.15
197	2	4	40	1	0.16
198	2	4	40	1	0.15
199	2	4	40	1	0.16
200	2	4	40	1	0.16
201	2	4	41	2	0.14
202	2	4	41	2	0.13
203	2	4	41	2	0.15
204	2	4	41	2	0.15
205	2	4	41	2	0.12
206	2	4	42	3	0.13
207	2	4	42	3	0.12
208	2	4	42	3	0.12
209	2	4	42	3	0.11
210	2	4	42	3	0.12
211	3	4	43	1	0.20
212	3	4	43	1	0.20
213	3	4	43	1	0.20
214	3	4	43	1	0.20
215	3	4	43	1	0.20
216	3	4	44	2	0.18
217	3	4	44	2	0.18
218	3	4	44	2	0.19
219	3	4	44	2	0.17
220	3	4	44	2	0.17
221	3	4	45	3	0.15
222	3	4	45	3	0.15
223	3	4	45	3	0.16
224	3	4	45	3	0.15
225	3	4	45	3	0.16
226	4	4	46	1	0.23
227	4	4	46	1	0.23
228	4	4	46	1	0.23
229	4	4	46	1	0.23
230	4	4	46	1	0.23
231	4	4	47	2	0.20
232	4	4	47	2	0.21
233	4	4	47	2	0.22
234	4	4	47	2	0.20
235	4	4	47	2	0.21
236	4	4	48	3	0.18
237	4	4	48	3	0.18
238	4	4	48	3	0.18
239	4	4	48	3	0.18
240	4	4	48	3	0.19

SAS Analysis Program

```
data test;
infile 'E:\Lab Tests\labtest2.xls';
input A B rep D Y;
proc print;
run;
proc mixed data=test;
```

```
class A B sub D;
model Y=A|B|D/ddfm=satterth;
random sub(A*B) D*sub(A*B);
*contrast 'A1 v. A2' A 1 -1;
*contrast 'D1 v. D2' D 1 -1 0;
*contrast 'A1D1 v. A1D2' D 1 -1 0 A*D 1 -1 0 0 0 0;
*lsmeans A B D;
run;
proc mixed data=test;
class A B sub D;
model Y=A B D A*D B*D A*B*D/ddfm=satterth;
random sub(A*B) D*sub(A*B);
contrast 'A1 v. A2' A 1 -1;
contrast 'A2 v. A3' A 0 1 -1;
contrast 'A3 v. A4' A 0 0 1 -1;
contrast 'B1 v. B2' B 1 -1;
contrast 'B2 v. B3' B 0 1 -1;
contrast 'B3 v. B4' B 0 0 1 -1;
contrast 'D1 v. D2' D 1 -1 0;
contrast 'D2 v. D3' D 0 1 -1;
contrast 'D1 v. D3' D 1 0 -1;
*contrast 'A1D1 v. A1D2' D 1 -1 0 A*D 1 -1 0 0 0 0;
*lsmeans A B C D;
run;
```

Sample T-Test Input File

sub	Control	LSPIV
1	0.11	0.11
2	0.16	0.15
3	0.2	0.17
4	0.24	0.12
5	0.11	0.12
6	0.16	0.15
7	0.2	0.17
8	0.23	0.19
9	0.11	0.13
10	0.16	0.15
11	0.2	0.17
12	0.23	0.17
13	0.11	0.11
14	0.15	0.14
15	0.2	0.17
16	0.23	0.18
17	0.11	0.12
18	0.15	0.15
19	0.2	0.2

20 0.23 0.14

SAS T-test Analysis Program

```
proc print;
proc ttest data=test1; PAIRED Control*LSPIV;
run;
proc ttest data=test2; PAIRED Control*LSPIV;
run;
proc ttest data=test3; PAIRED Control*LSPIV;
run;
proc ttest data=test4; PAIRED Control*LSPIV;
run;
```

Field Experiment

Input File (Sample)

sub	Control	LSPIV
1	39.9	28.62
2	10.8	8.76
3	4.4	4.40
4	1.62	1.75
5	1.87	1.80
6	0.58	0.78
7	0.42	0.31
8	1.11	1.25
9	0.35	0.31
10	0.14	0.20
11	0.12	0.12
12	62.96	53.71
13	5.6	5.06
14	2.39	3.11
15	2.11	1.86
16	2.05	1.67
17	3.11	2.63
18	0.69	0.60

SAS T-Tests Program

```
proc ttest data=MmvslsPIV;
PAIRED MM*LSPIV;
run;
proc ttest data=Weirvsmm;
PAIRED Control*MM;
```

```
run;
proc ttest data=WeirvsPIV;
PAIRED Control*LSPIV;
run;
```

Appendix E Laboratory Results

First Laboratory Experiment

Number of Particles Per Window	*Control (manometer)*	*M-M Meter*	*LSPIV Prototype*	*Control (manometer)*	*M-M Meter*	*LSPIV Prototype*
	First Repetition			*Second Repetition*		
	Low Froude number and 0 degree camera angle					
1	0.104	0.07	0.065	0.11	0.09	0.068
2	0.104	0.07	0.09	0.11	0.09	0.091
3	0.104	0.07	0.085	0.11	0.09	0.096
4	0.104	0.07	0.097	0.11	0.09	0.058
5	0.104	0.07	0.101	0.11	0.09	0.109
	High Froude number and 0 degree camera angle					
1	0.153	0.135	0.071	0.154	0.134	0.07
2	0.153	0.135	0.098	0.154	0.134	0.058
3	0.153	0.135	0.079	0.154	0.134	0.075
4	0.153	0.135	0.085	0.154	0.134	0.085
5	0.153	0.135	0.085	0.154	0.134	0.085
	Low Froude number and 30 degree camera angle					
1	0.104	0.085	0.028	0.108	0.134	0.068
2	0.104	0.085	0.029	0.108	0.134	0.107
3	0.104	0.085	0.134	0.108	0.134	0.115
4	0.104	0.085	0.131	0.108	0.134	0.114
5	0.104	0.085	0.101	0.108	0.134	0.143
	High Froude number and 30 degree camera angle					
1	0.156	0.133	0.118	0.157	0.144	0.122
2	0.156	0.133	0.124	0.157	0.144	0.133
3	0.156	0.133	0.111	0.157	0.144	0.152
4	0.156	0.133	0.124	0.157	0.144	0.142
5	0.156	0.133	0.128	0.157	0.144	0.132

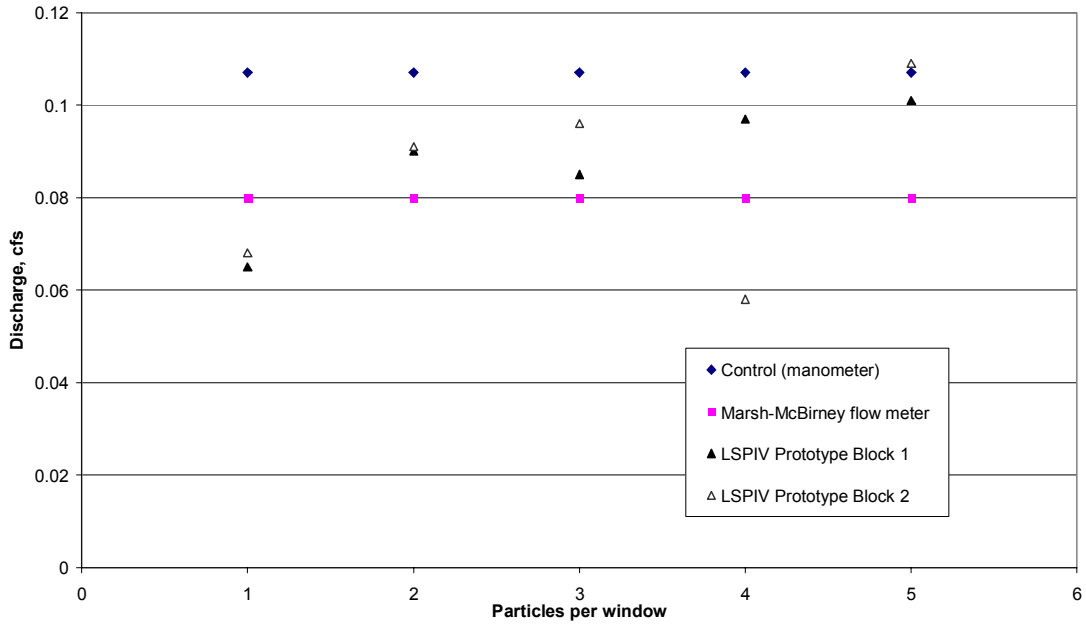

Figure 38 Discharge measurements for all three treatments for a zero degree camera angle and low Froude number are shown. The LSPIV prototype had a median error of -8.20 % and the current meter had an average error of -25.4 %, compared to the flume manometer.

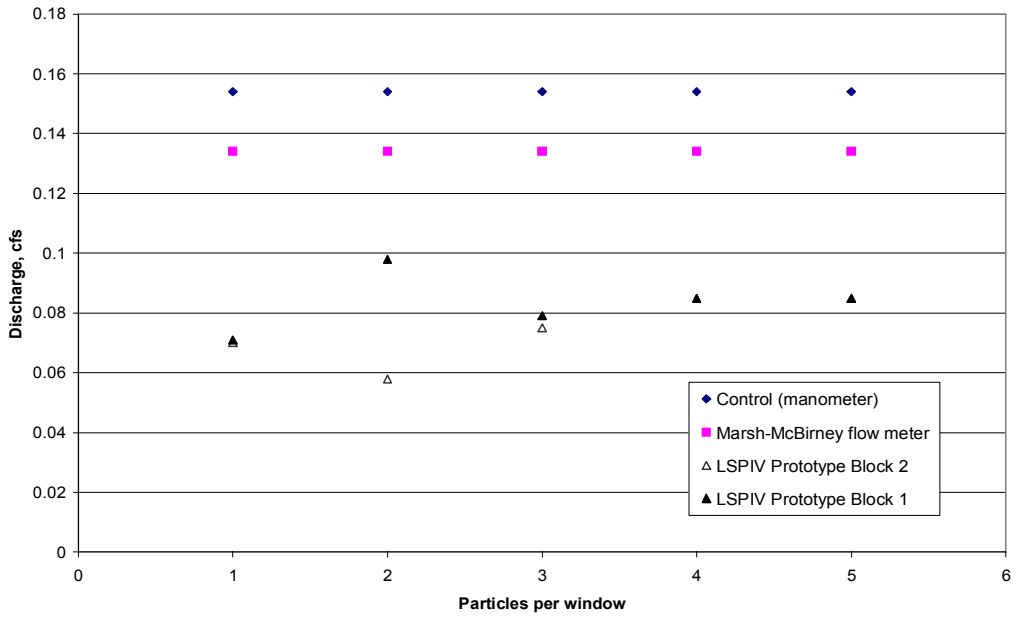

Figure 39 Discharge measurements for all three treatments using a zero degree camera angle and high Froude number are shown. The median error was -46.6 % for the LSPIV prototype and -12.4 % for the current meter. The large error was likely due to out-of-plane losses and static input parameters.

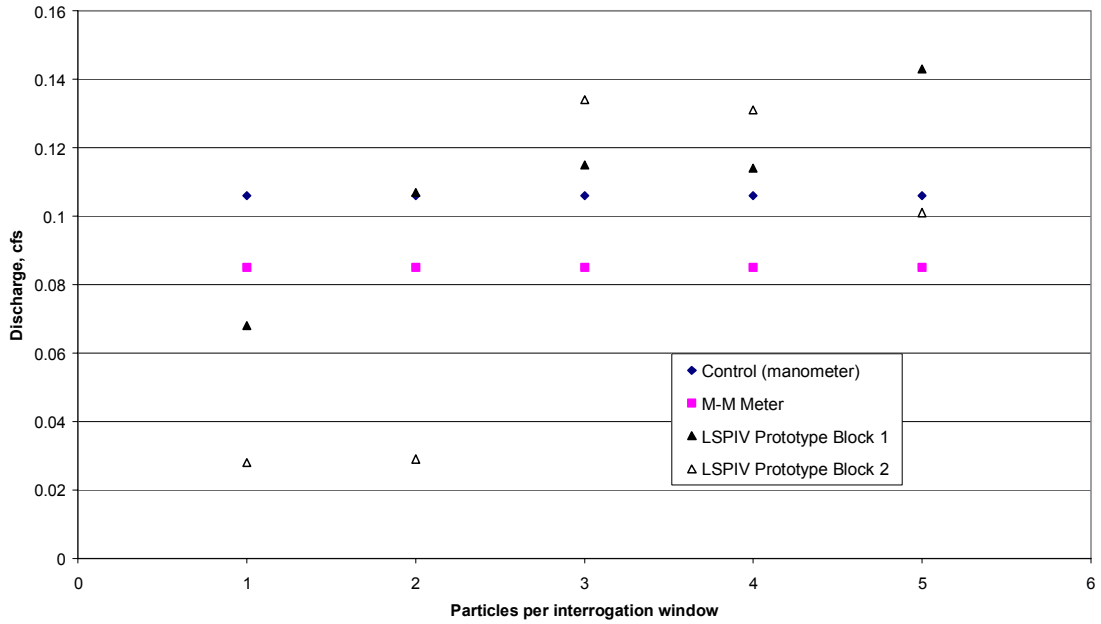

Figure 40 Discharge measurements for all three treatments using a 30 degree camera angle and low Froude number are shown. The LSPIV prototype had a relative error from -70.0 % to 28.9 %, with a median of 2.31 %.

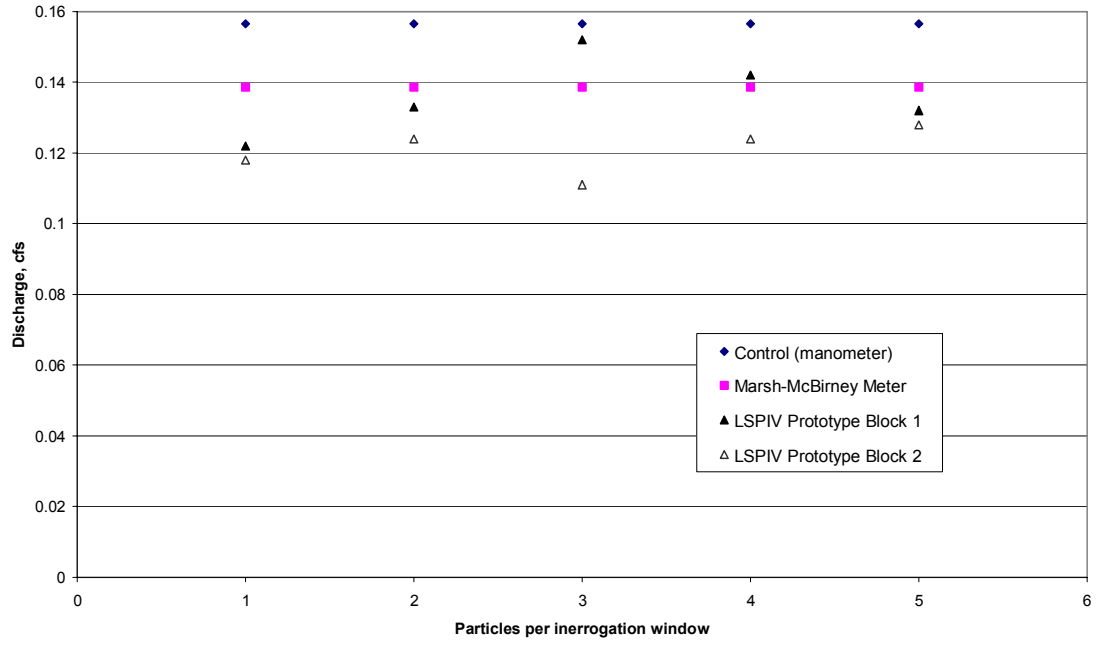

Figure 41 Discharge measurements for all three treatments using a 30 degree camera angle and high Froude number are shown.

Second Laboratory Experiment

		Block 1			Block 2			Block 3			Block 4			Block 5		
0 Degrees	Froude Number	Control (manometer)	M-M Meter	LSPIV Prototype	Control (manometer)	M-M Meter	LSPIV Prototype	Control (manometer)	M-M Meter	LSPIV Prototype	Control (manometer)	M-M Meter	LSPIV Prototype	Control (manometer)	M-M Meter	LSPIV Prototype
	0.05	0.112	0.08	0.112	0.108	0.083	0.124	0.108	0.097	0.128	0.108	0.111	0.106	0.112	0.07	0.122
	0.15	0.157	0.13	0.154	0.156	0.123	0.145	0.156	0.137	0.151	0.152	0.14	0.139	0.154	0.131	0.151
	0.25	0.2	0.176	0.171	0.199	0.181	0.17	0.201	0.176	0.17	0.197	0.193	0.171	0.198	0.178	0.197
	0.35	0.239	0.222	0.124	0.23	0.204	0.189	0.23	0.211	0.169	0.231	0.225	0.18	0.227	0.199	0.143
15 degrees	Froude Number	Control (manometer)	M-M Meter	LSPIV Prototype	Control (manometer)	M-M Meter	LSPIV Prototype	Control (manometer)	M-M Meter	LSPIV Prototype	Control (manometer)	M-M Meter	LSPIV Prototype	Control (manometer)	M-M Meter	LSPIV Prototype
	0.05	0.106	0.111	0.132	0.11	0.089	0.134	0.11	0.106	0.124	0.108	0.11	0.129	0.108	0.073	0.091
	0.15	0.157	0.137	0.168	0.157	0.14	0.141	0.154	0.139	0.154	0.156	0.149	0.157	0.154	0.125	0.175
	0.25	0.201	0.169	0.194	0.2	0.179	0.184	0.199	0.182	0.203	0.199	0.196	0.188	0.201	0.164	0.197
	0.35	0.231	0.194	0.211	0.229	0.258	0.218	0.231	0.222	0.213	0.23	0.228	0.219	0.231	0.2	0.204
15 degrees	Froude Number	Control (manometer)	M-M Meter	LSPIV Prototype	Control (manometer)	M-M Meter	LSPIV Prototype	Control (manometer)	M-M Meter	LSPIV Prototype	Control (manometer)	M-M Meter	LSPIV Prototype	Control (manometer)	M-M Meter	LSPIV Prototype
	0.05	0.108	0.073	0.217	0.11	0.08	0.091	0.108	0.082	0.086	0.11	0.088	0.108	0.114	0.076	0.094
	0.15	0.156	0.134	0.13	0.154	0.132	0.145	0.156	0.132	0.119	0.154	0.133	0.143	0.156	0.124	0.108
	0.25	0.201	0.157	0.172	0.2	0.179	0.13	0.198	0.184	0.148	0.2	0.179	0.19	0.2	0.163	0.117
	0.35	0.231	0.205	0.192	0.231	0.21	0.178	0.231	0.218	0.146	0.232	0.22	0.165	0.232	0.2	0.189
15 degrees	Froude Number	Control (manometer)	M-M Meter	LSPIV Prototype	Control (manometer)	M-M Meter	LSPIV Prototype	Control (manometer)	M-M Meter	LSPIV Prototype	Control (manometer)	M-M Meter	LSPIV Prototype	Control (manometer)	M-M Meter	LSPIV Prototype
	0.05	0.108	0.088	0.107	0.11	0.082	0.092	0.108	0.105	0.092	0.11	0.111	0.096	0.11	0.074	0.08
	0.15	0.154	0.14	0.129	0.156	0.132	0.117	0.154	0.15	0.123	0.158	0.153	0.107	0.157	0.122	0.123
	0.25	0.2	0.177	0.15	0.2	0.175	0.145	0.201	0.193	0.162	0.197	0.169	0.154	0.201	0.169	0.157
	0.35	0.23	0.201	0.183	0.23	0.209	0.179	0.232	0.22	0.175	0.233	0.198	0.18	0.231	0.207	0.19

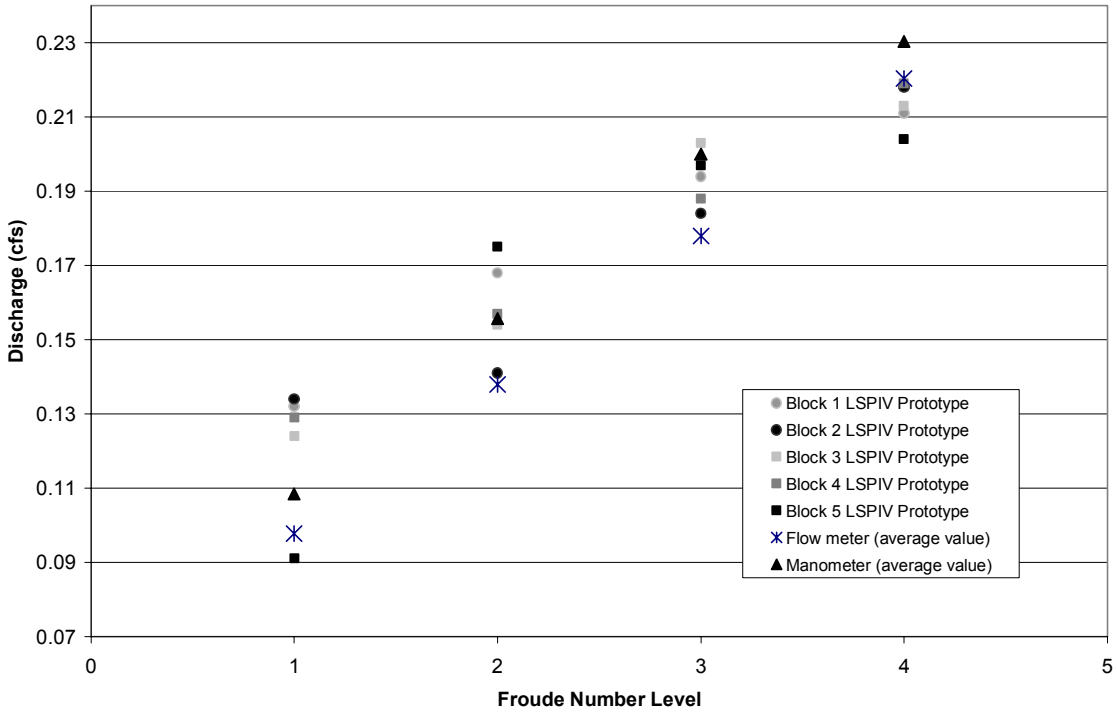

Figure 42 Discharge measurements for 15 degree camera angle and a range of Froude numbers. The LSPIV prototype showed relative errors from -15.74 % to 24.4 %, with a median of -2.74 %.

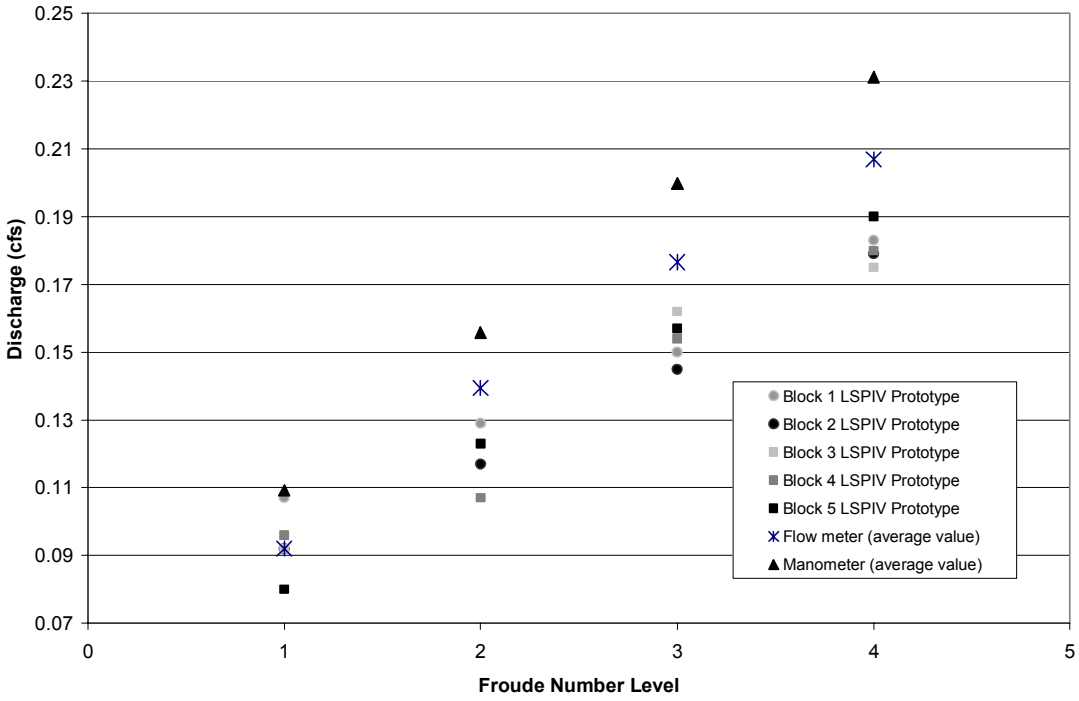

Figure 43 Discharge measurements for 45 degree camera angle and a range of Froude numbers. The LSPIV prototype showed relative errors from -27.3 % to -9.1 %, with a median of -21.8 %.

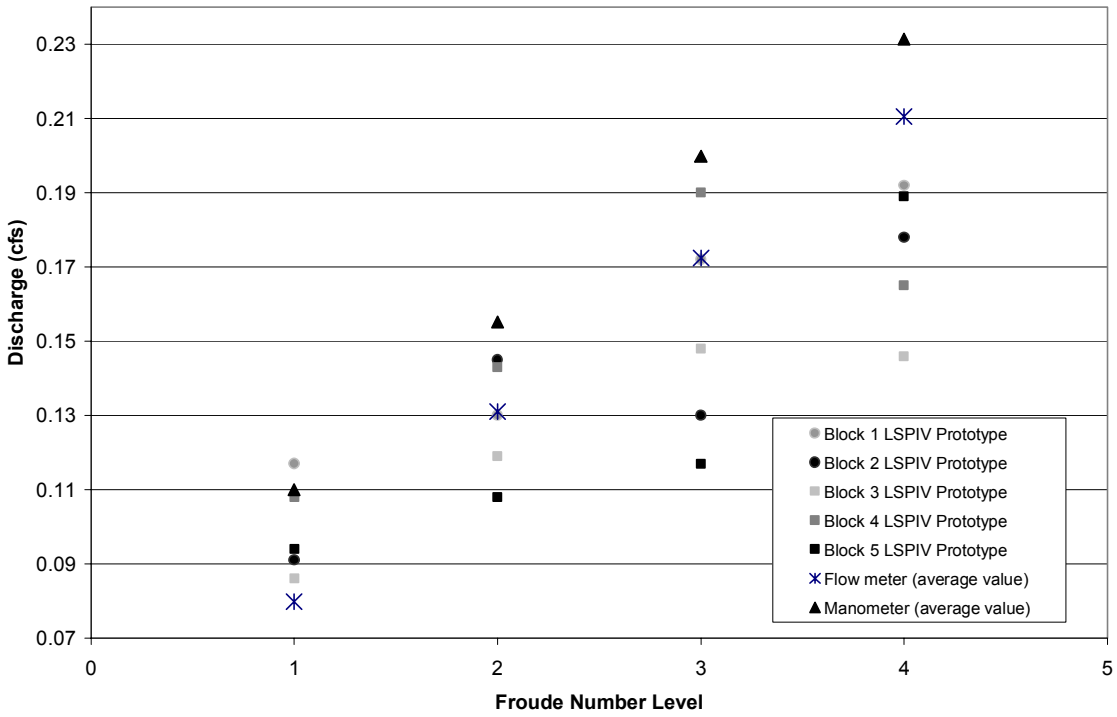

Figure 44 Discharge measurements for 30 degree camera angle and a range of Froude numbers. The LSPIV prototype showed relative errors from -41.5 % to -5.7 %, with a median of -18.0 %.

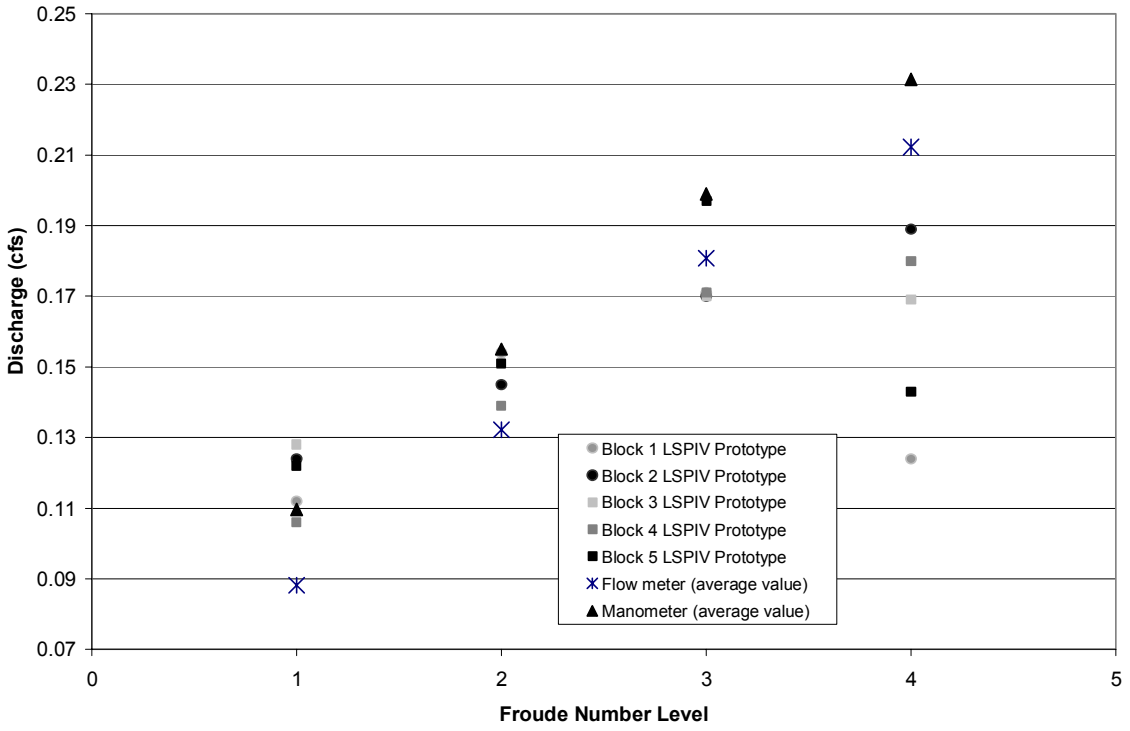

Figure 45 Discharge measurements for zero degree camera angle and a range of Froude numbers. The LSPIV prototype showed relative errors from -28.6 % to 0.0 %, with a median of -8.2 %.

Appendix F Results from Statistical Analysis and Tests of Normality

Laboratory Experiments

Normal Probability Plot (Example)

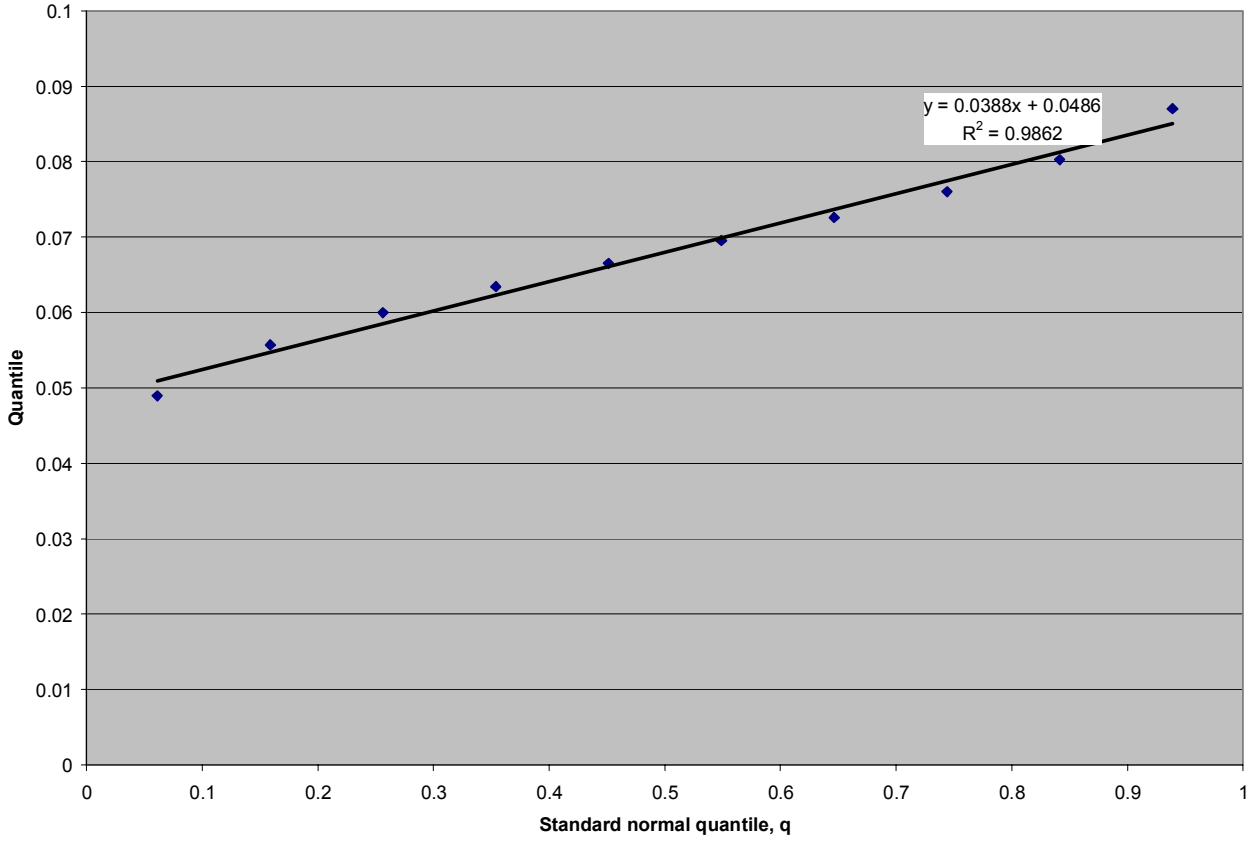

Figure 46. Normal probability plot to test the assumption that the differences are normally distributed. This is an example using discharge difference between LSPIV and control. The linear relationship indicates the data are normally distributed (R^2=0.9862).

SAS ANACOVA Output for First Experiment

The Mixed Procedure
Model Information

Data Set	WORK.TEST
Dependent Variable	Y
Covariance Structure	Variance Components
Estimation Method	REML
Residual Variance Method	Profile
Fixed Effects SE Method	Model-Based
Degrees of Freedom Method	Satterthwaite

Class Level Information

Class	Levels	Values
A	4	1 2 3 4
B	4	1 2 3 4
sub	48	1 2 3 4 5 6 7 8 9 10 11 12 13 14 15 16 17 18 19 20 21 22 23 24 25 26 27 28 29 30 31 32 33 34 35 36 37 38 39 40 41 42 43 44 45 46 47 48
D	3	1 2 3

Dimensions

Covariance Parameters	3
Columns in X	84
Columns in Z	96
Subjects	1
Max Obs Per Subject	240
Observations Used	240
Observations Not Used	0
Total Observations	240

Iteration History

Iteration	Evaluations	-2 Res Log Like	Criterion
0	1	-1015.38837749	
1	1	-1015.38837749	0.00000000

Convergence criteria met but final hessian is not positive definite.

The Mixed Procedure

Covariance Parameter Estimates

Cov Parm	Estimate
sub(A*B)	0
sub*D(A*B)	0
Residual	0.000198

Fit Statistics

-2 Res Log Likelihood	-1015.4
AIC (smaller is better)	-1013.4
AICC (smaller is better)	-1013.4

BIC (smaller is better) -1011.5

Type 3 Tests of Fixed Effects

Effect	Num DF	Den DF	F Value	Pr > F
A	3	192	631.91	<.0001
B	3	192	10.83	<.0001
D	2	192	65.31	<.0001
A*D	6	192	16.79	<.0001
B*D	6	192	6.15	<.0001
A*B*D	27	192	1.50	0.0609

Contrasts

Label	Num DF	Den DF	F Value	Pr > F
A1 v. A2	1	192	232.77	<.0001
A2 v. A3	1	192	226.87	<.0001
A3 v. A4	1	192	107.90	<.0001
B1 v. B2	1	192	10.96	0.0011
B2 v. B3	1	192	23.71	<.0001
B3 v. B4	1	192	0.02	0.8968
D1 v. D2	1	192	85.02	<.0001
D2 v. D3	1	192	1.53	0.2176
D1 v. D3	1	192	109.37	<.0001

SAS ANACOVA Output for the Second Experiment

The Mixed Procedure
Model Information

Data Set	WORK.TEST
Dependent Variable	Y
Covariance Structure	Variance Components
Estimation Method	REML
Residual Variance Method	Profile
Fixed Effects SE Method	Model-Based
Degrees of Freedom Method	Satterthwaite

Class Level Information

Class	Levels	Values
A	2	1 2
B	2	1 2
C	5	1 2 3 4 5
sub	60	1 2 3 4 5 6 7 8 9 10 11 12 13

14 15 16 17 18 19 20 21 22 23
24 25 26 27 28 29 30 31 32 33
34 35 36 37 38 39 40 41 42 43
44 45 46 47 48 49 50 51 52 53
54 55 56 57 58 59 60

D 3 1 2 3

Dimensions

Covariance Parameters	3
Columns in X	52
Columns in Z	120
Subjects	1
Max Obs Per Subject	120
Observations Used	120
Observations Not Used	0
Total Observations	120

Iteration History

Iteration	Evaluations	-2 Res Log Like	Criterion
0	1	-497.95964874	
1	1	-497.95964874	0.00000000

Convergence criteria met.

The Mixed Procedure

Covariance Parameter Estimates

Cov Parm	Estimate
sub(A*B*C)	0
sub*D(A*B*C)	0
Residual	0.000199

Fit Statistics

-2 Res Log Likelihood	-498.0
AIC (smaller is better)	-496.0
AICC (smaller is better)	-495.9
BIC (smaller is better)	-493.9

Type 3 Tests of Fixed Effects

Effect	Num DF	Den DF	F Value	Pr > F
A	1	96	181.21	<.0001

B	1	96	40.23	<.0001
C	4	96	2.25	0.0692
D	2	96	49.89	<.0001
A*D	2	96	19.66	<.0001
B*D	2	96	6.09	0.0032
C*D	8	96	2.67	0.0108
A*B*D	3	96	9.76	<.0001

Contrasts

Label	Num DF	Den DF	F Value	Pr > F
D1 v. D2	1	96	23.38	<.0001
D2 v. D3	1	96	26.54	<.0001
D1 v. D3	1	96	99.74	<.0001

SAS T-Test Output for the Second Experiment

The TTEST Procedure

Statistics

Difference	N	Lower CL Mean	Mean	Upper CL Mean	Lower CL Std Dev	Std Dev	Upper CL Std Dev	Std Err
Control - LSPIV	20	0.0076	0.024	0.0404	0.0266	0.035	0.0511	0.0078

T-Tests

Difference	DF	t Value	Pr > |t|
Control - LSPIV	19	3.07	0.0064

Statistics

Difference	N	Lower CL Mean	Mean	Upper CL Mean	Lower CL Std Dev	Std Dev	Upper CL Std Dev	Std Err
Control - LSPIV	20	-0.005	0.003	0.0109	0.0128	0.0169	0.0247	0.0038

T-Tests

Difference	DF	t Value	Pr > |t|
Control - LSPIV	19	0.79	0.4368

The SAS System 10:06 Thursday, September 23, 2004 17

Statistics

Difference	N	Lower CL Mean	Mean	Upper CL Mean	Lower CL Std Dev	Std Dev	Upper CL Std Dev	Std Err
Control - LSPIV	20	0.01	0.029	0.048	0.0309	0.0406	0.0594	0.0091

T-Tests

Difference	DF	t Value	Pr > |t|
Control - LSPIV	19	3.19	0.0048

Statistics

Difference	N	Lower CL Mean	Mean	Upper CL Mean	Lower CL Std Dev	Std Dev	Upper CL Std Dev	Std Err
Control - LSPIV	20	0.0288	0.036	0.0432	0.0117	0.0154	0.0224	0.0034

T-Tests

Difference	DF	t Value	Pr > |t|
Control - LSPIV	19	10.48	<.0001

Field Experiments

Normal Probability Plot (Example)

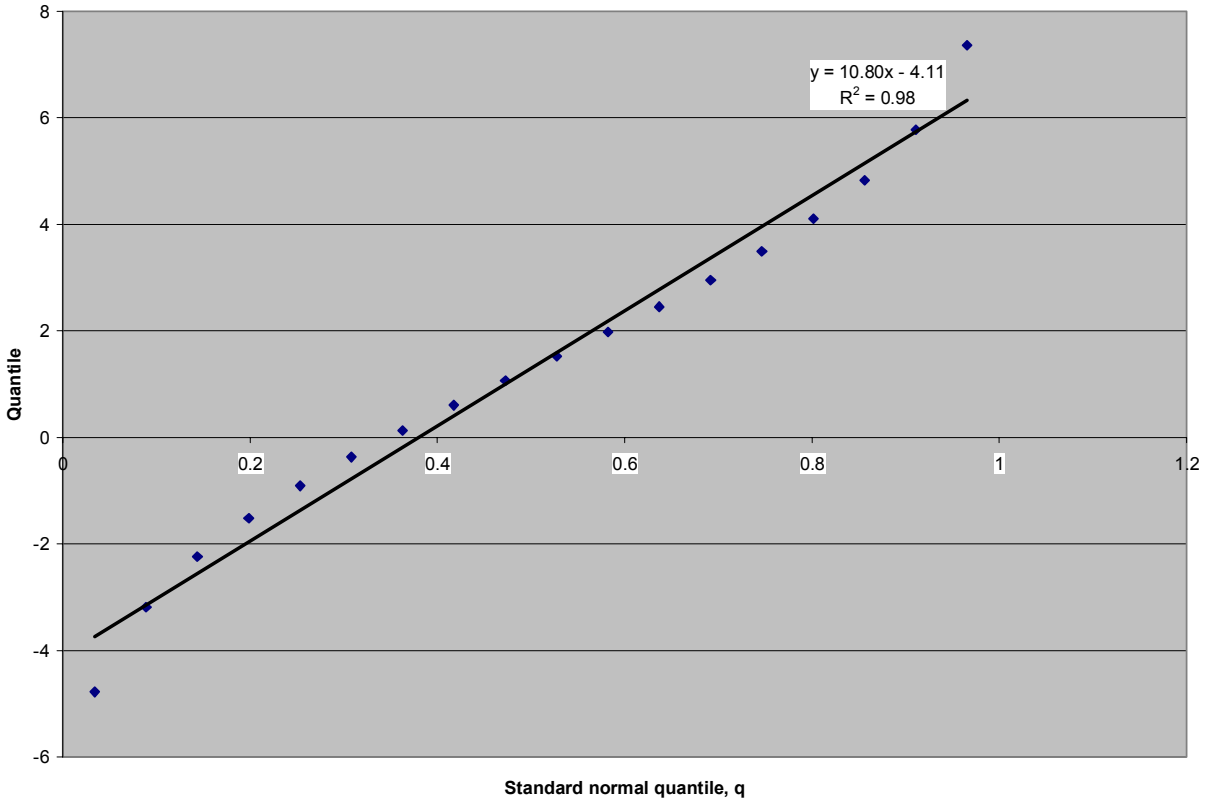

Figure 47. Normal probability plot to test the assumption that the differences are normally distributed. This is an example using discharge difference between LSPIV and weir. The linear relationship indicates the data are normally distributed (R^2=0.98).

SAS T-Test Output: Testing Difference Between Treatments

The TTEST Procedure

Statistics

Difference	N	Lower CL Mean	Mean	Upper CL Mean	Lower CL Std Dev	Std Dev	Upper CL Std Dev
MM - LSPIV	20	-5.964	-1.728	2.5077	6.8827	9.0503	13.219

Statistics

Difference	Std Err	Minimum	Maximum
MM - LSPIV	2.0237	-40.06	2.14

T-Tests

Difference	DF	t Value	Pr > |t|
MM - LSPIV	19	-0.85	0.4038

The SAS System 2

Statistics

Difference	N	Lower CL Mean	Mean	Upper CL Mean	Lower CL Std Dev	Std Dev	Upper CL Std Dev
Control - MM	18	-2.63	3.2133	9.057	8.8178	11.751	17.616

Statistics

Difference	Std Err	Minimum	Maximum
Control - MM	2.7697	-1.23	49.31

T-Tests

Difference	DF	t Value	Pr > |t|
Control - MM	17	1.16	0.2620

Statistics

Difference	N	Lower CL Mean	Mean	Upper CL Mean	Lower CL Std Dev	Std Dev	Upper CL Std Dev
Control - LSPIV	18	-0.361	1.2933	2.948	2.4968	3.3273	4.9881

Statistics

Difference	Std Err	Minimum	Maximum
Control - LSPIV	0.7843	-0.72	11.28

T-Tests

Difference	DF	t Value	Pr > |t|
Control - LSPIV	17	1.65	0.1175

SAS T-Test Output: Testing Difference Between Treatments at High/Low Quartiles

The TTEST Procedure

Statistics

Lower CL	Upper CL	Lower CL	Upper CL

Difference	N	Mean	Mean	Mean	Std Dev	Std Dev	Std Dev
Control - LSPIV	5	-1.902	4.622	11.146	3.1482	5.2545	15.099

Statistics

Difference	Std Err	Minimum	Maximum
Control - LSPIV	2.3499	0	11.28

T-Tests

Difference	DF	t Value	Pr > |t|
Control - LSPIV	4	1.97	0.1206

Statistics

	Lower CL	Upper CL	Lower CL	Upper CL		
Difference	N	Mean	Mean	Mean	Std Dev	Std Dev	Std Dev
Control - LSPIV	5	-0.309	-0.062	0.1848	0.1191	0.1988	0.5713

Statistics

Difference	Std Err	Minimum	Maximum
Control - LSPIV	0.0889	-0.4	0.11

T-Tests

Difference	DF	t Value	Pr > |t|
Control - LSPIV	4	-0.70	0.5240

Appendix G Prototype Operating Instructions

Equipment:

Stand: three tripod legs, triangle mount, two telescoping pieces, and camera mount

Camera and case (which should be attached to image acquisition box)

Camera sun-shade

Re-bar stakes

Battery and battery container

Solar panel

HP Laptop PC

Tape measure

Ruler

Staff gauge or pressure transducer

Locks and chain

Assembly/Maintenance:

¾" ratchet

¼" ratchet bit and wrench

Ampage/Voltage meter

Various screwdrivers

Wire clippers and mobile soldering device

Sledge-hammer

Laser survey equipment: station, tripod, pole, and prism

LOCATING AND ASSEMBLING STAND:

1. Select site based on channel characteristics and objectives of the study. Please see related literature for reach selection.
2. Locate the prototype stand:
    a. Choose a location to reduce the camera angle (e.g. the closer to the stream the better).
    b. Minimize reflections and shadows in the image-of-view.
    c. Evaluate potential hazards of high flow conditions.

d. Make sure the stand is balanced and secure.

3. Setup the stand:
    a. The three pieces of the trip fit 'inter-locking', use the color-coded top bracket to aid assembly.
    b. Screw in the bottom 3 nuts.
    c. Place the triangle mount piece on top of the tripod. CAREFUL! This is heavy and you ***cannot*** climb on the stand.
    d. Screw in the top 3 nuts that hold down the triangle mount piece.
    e. Make minor adjustments to the location of the stand.
    f. Use re-bar stakes to secure the bottom of the stand.
    g. Attach the next two pieces of the telescoping stand. ***Caution***, this will require you to get on the stand. All remaining pieces lock together by means of tension screws on the outside of the pieces. Extra care should be taken so that the pieces are secure as pinching of your hands is possible.
    h. The final stand piece will typically be the swivel mount with camera case attached. Therefore, it will be necessary to care for the wires as you are handling this.
4. Installing additional components to the stand:
    a. The equipment box is positioned on the second rung of the stand. It should be level and not pinching the wires coming in and out of it.
    b. One U-bolt holds the box on and a chain will be attached later for theft protection.
    c. The optimum location for the solar panel is determined. The panel should face south, but avoid a direction that is more likely to shady.
    d. The solar panel is attached via to U-bolts. This is a two person job requiring a wrench and a socket-wrench.
    e. The battery position must be dug into the ground at a position that is not subject to flooding.
5. Wiring the system:
    a. Make sure all of the connections are made within the box and the camera case.
    b. Turn AC inverter off.
    c. Attach wires from solar panel to the batter one at a time.

d. Attach the wires from the box one at a time. Double check the negative and positive wires correspond to the battery terminals. Be careful, do not touch the wires together or reverse the wires.
e. The system should turn on. Check the LED on the back of the camera, the green light on the A/D converter, and the inverter will turn on.

6. Powering-up the system:
   a. Turn on computer:
      Username: LSPIV project
      Password: watersh3d
   b. Start Matlab 7
   c. Run setup commands:

vid = videoinput('winvideo',1,'UYVY_640x480');

src = getselectedsource(vid);

   d. Check the camera preview:

preview(vid)

7. Testing the field-of-view:
   a. The stand can now be adjusted to set the field-of-view. Several objectives should be adhered to in adjusting the camera:
      i. The angle should be minimized by increasing the height.
      ii. The field-of-view should include the primary flood plain.
      iii. Additional view out of the flood plain should be minimized.
8. Optimizing camera parameters:
   a. After the field-of-view was established at the site, the camera was focused to the water surface. Additionally, the back focus was adjusted for resolution.
   b. The automatic gain setting can be used to adjust the gain for low-levels of illumination.
   c. The electronic shutter control and flickerless camera options can also be used to compensate for excessive light levels.
   d. Finally, the DC lens level adjustment was changed to provide maximum contrast. It should be noted that contrast levels should be adjusted for bright sunlight conditions or glare problems can be exacerbated.

9. Safety measures:
    a. Make sure that the prototype is well-marked to ward off children from playing on the structure. Contact information may also prove valuable.
    b. The equipment enclosure should be pad-locked and secured to the stand. Additional theft prevention measures may be necessary in some situations.

INSTALL STAGE MEASURING DEVICE

1. Installation of the pressure transducer is site-specific however, guidelines are given here for typical conditions.
2. Install the pressure-transducer mounting plate in the deepest part of the stream, in the center of the measurement reach. The mounting plate can be hammered into place if sufficient bed material is present.
3. Install the pressure transducer and secure it using the top portion of the mounting plate.
4. Discretely run the cable back to the prototype stand. Additional stakes or rocks may be necessary to secure the cable for high-flow conditions.
5. The pressure transducer can then be wired to the control unit (data logger). Specific instructions should be sought depending on the pressure transducer used.
6. Lastly, the data logger must be programmed and connected to the battery.

IDENTIFYING GROUND REFERENCE POINTS

1. Select a location for the laser-level that is in view of the reach of interest and adjacent flood plain.
2. Level the laser-level following user instructions.
3. Locate a minimum of ten distinct points in the field-of-view that can be surveyed with accuracy greater than one inch. The structures may be rocks, roots, trees, etc. If sufficient reference points are not present markers can be installed and used a semi-permanent control points.
4. Start the camera and obtain a ‘snap-shot’ of the image. Re-open this image in Microsoft Paint (or similar image editor). Also, turn on the live video preview.
5. As one technician moves the survey pole to each ground-refernce point, the other marks the location of the point in the image editor. After the point is marked on the image, the technician must obtain the physical coordinate with the laser-level equipment.

6. Repeat the previous step until sufficient GRPs are acquired for accurate image registration.

SURVEY CROSS-SECTION

1. Mark the upstream and downstream ends of the field-of-view using the preview command.
2. Make stream bathymetry measurements with a minimum of 18 points for cross-sections more than 10 meters in width and over 25 points for greater stream widths.

MAKING DISCHARGE MEASUREMENTS

Prepare GRPs for Registration and Transformation

1. Open up the LSPIV.xls Excel spreadsheet.
2. Copy and paste the horizontal (Hz),vertical (Vz) angle, and distance SDist.
3. Use the GRPs graph to adjust the angle correction (between 0-90 degrees) so that the corrected GRPs are parallel with the y-axis (northing).
4. Copy and past the corrected northing and easting into Enhance.m matlab file into the variable named base_points at the top of the file.
5. Open GRP image file with a program that allows identification of pixel locations (Microsoft Paint works).
6. Copy x and y pixel locations to the file named input_points in the Matlab file.
7. Save and run the Enhance .m file.
8. Using Figure 2 and the pixel selector find the optimum field of view. The field-of-view should have an equal pixel size (no distortion), minimum glare and shadows, a straight section with minimum disturbances, and be nearly bounded by the measured cross-sections.
9. Use the crop tool to input the crop location and size in the following format: [upper left corner x location, upper left corner y location, width, length].
10. Repeat this procedure until an adequate cropped image is found.
11. Change the number of images to 40 and run the program for all the images.

Prepare Cross-Section for Discharge Calculations

12. Open up the LSPIV.xls Excel spreadsheet.

13. Copy and paste the Northing (North), Easting (East), and elevation (Elev) for both upstream and downstream cross-sections into the corresponding places in the Cross-Section input sheet.
14. Check and make sure the Cross-Section graph is correct.
15. Copy and paste the cross-section distance and depth into distance_master and depth_master within the Averager.m file.

Appendix H Region-of-Interest and Grid Spacing Sensitivity Analysis

Table 17. Sensitivity analysis using different region-of-interest (ROI) window sizes. The analysis was performed for one set of images from 9/9/2004.

Window Sizes			Discharge	Relative Error Versus Control
1st Pass	2nd Pass	3rd Pass		
(16 256)	(8 256)	(16 16)	1.12	1.82%
(16 256)	(16 256)		1.18	7.27%
(32 128)	(32 64)	(16 16)	1.26	14.55%
(32 128)			1.07	-2.73%
(32 128)	(32 64)	(8 8)	1.24	12.73%
(32 256)	(16 256)	(32 32)	1.31	19.09%
(64 128)			1.15	4.55%
(64 256)	(32 128)	(16 64)	1.39	26.36%
(64 256)	(32 256)	(32 32)	1.39	26.36%
(64 256)			1.4	27.27%
(128 256)	(64 128)	(32 32)	1.14	3.64%
(128 256)	(64 256)	(32 32)	1.15	4.55%
(128 256)			1.15	4.55%
(16 256)	(8 256)	(16 16)	1.12	1.82%
(128 256)	(64 128)	(32 32)	1.14	3.64%
(128 256)	(64 256)	(32 32)	1.15	4.55%
(128 256)			1.15	4.55%
(64 128)			1.15	4.55%
(32 128)	(32 64)	(8 8)	1.24	12.73%
(32 128)	(32 64)	(16 16)	1.26	14.55%
(32 256)	(16 256)	(32 32)	1.31	19.09%
(64 256)	(32 128)	(16 64)	1.39	26.36%
(64 256)	(32 256)	(32 32)	1.39	26.36%
(64 256)			1.4	27.27%

Table 18. Sensitivity analysis using different grid spacing distances. The analysis was performed for one set of images from 9/9/2004.

Grid spacing (x,y)	First Pass	Second Pass	Discharge	Relative Error Versus Control
(4,16)	(128 256)		1.3	18.18%
(4,16)	(16 256)	(16 256)	1.04	-5.45%
(8,16)	(16 256)	(16 256)	1.09	-0.91%
(32, 32)	(16 256)	(16 256)	1.15	4.55%

Appendix I Uncertainty Analysis

LSPIV Uncertainty Analysis:

Error source	Units	Systematic Uncertainty Variable	Random Uncertainty Variable	Relative random uncertainty (95% confidence interval)	Relative systematic uncertainty (95% confidence interval)	Reference for error estimate
Number of verticals	N/A	s'_{F_m}	N/A	6.0%	N/A	Pelletier (1988) Figure 8
Segment width	Ft	s'^2_b	B'_b	1.0%	0.5%	Pelletier (1988)
Segment depth	Ft	s'^2_d	B'_d	1.0%	0.5%	ISO 7178
Number of points in the vertical	ft/sec	s'_p	N/A	7.5%	N/A	ISO 7178
Exposure time	ft/sec	s'_e	N/A	8.0%	N/A	Pelletier (1988) Figure 7
Error from velocity measuring instrument (LSPIV)	ft/sec	s'_c	N/A	3.0%	N/A	Adrian (1991) and Buchave (1992)

The overall random uncertainty is first determined:

$$s'_Q = \sqrt{s'^2_{F_m} + \frac{1}{m}\left(s'^2_b + s'^2_d + s'^2_p + s'^2_c + s'^2_e\right)}$$

$$= \sqrt{6^2 + \frac{1}{12}\left(1^2 + 1^2 + 7.5^2 + 8^2 + 3^2\right)} = 13.70\%$$

The overall systematic uncertainty is estimated:

$$B'_Q = \sqrt{B'^2_b + B'^2_d + B'^2_c}$$

$$= \sqrt{0.5^2 + 0.5^2 + 0^2} = 0.71\%$$

Combination of random and systematic uncertainty using the additive and root-sum square models:

$$U'_{Q_{RSS}} = \sqrt{\left(2s'_Q\right)^2 + \left(B'_Q\right)^2} = 13.40\%$$

$$U'_{Q_{ADD}} = B'_Q + 2s'_Q = 14.09\%$$

Flo-Mate 2000 Uncertainty Analysis:

Error source	Units	Systematic Uncertainty Variable	Random Uncertainty Variable	Relative random uncertainty (95% confidence interval)	Relative systematic uncertainty (95% confidence interval)	Reference for error estimate
Number of verticals	N/A	s'_{F_m}	N/A	5.5%	N/A	Pelletier (1988) Figure 8
Segment width	Ft	s'^2_b	B'_b	1.0%	0.5%	Pelletier (1988)
Segment depth	Ft	s'^2_d	B'_d	1.0%	0.5%	ISO 7178
Number of points in the vertical	ft/sec	s'_p	N/A	4.8%	N/A	ISO 7178
Exposure time	ft/sec	s'_e	N/A	6.0%	N/A	Pelletier (1988) Figure 7
Error from velocity measuring instrument (LSPIV)	ft/sec	s'_c	N/A	2.0%	1.0%	ISO 5168

The overall random uncertainty is first determined:

$$s'_Q = \sqrt{s'^2_{F_m} + \frac{1}{m}\left(s'^2_b + s'^2_d + s'^2_p + s'^2_c + s'^2_e\right)}$$

$$= \sqrt{5.5^2 + \frac{1}{15}\left(1^2 + 1^2 + 4.8^2 + 6^2 + 2^2\right)} = 11.76\%$$

The overall systematic uncertainty is estimated:

$$B'_Q = \sqrt{B'^2_b + B'^2_d + B'^2_c}$$

$$= \sqrt{0.5^2 + 0.5^2 + 1^2} = 1.22\%$$

Combination of random and systematic uncertainty using the additive and root-sum square models:

$$U'_{Q_{RSS}} = \sqrt{\left(2s'_Q\right)^2 + \left(B'_Q\right)^2} = 11.82\%$$

$$U'_{Q_{ADD}} = B'_Q + 2s'_Q = 12.98\%$$

Vita

Adrian Adam Harpold

Adrian Harpold was born in Seattle, Washington on February 4th, 1981 to Mindy S. Nichols. He moved around Western Washington quite a lot during his youth. He began to love being in nature as a child, especially enjoying family backpacking trips. His 5th grade year he moved and settled in Winston-Salem, North Carolina, where he went to high-school. Adrian attended Virginia Tech directly out of high-school and finished his Bachelor of Science in 2003. During his undergraduate he pursued many interests outside of classes including professional societies, honor societies, and university clubs. He also enrolled in a five-year Master's program at Tech, which he started in 2003. He plans to finish his Master's in Science in January 2005. His future looks wide-open; however, he will likely continue for his PhD in the fall of 2005. His passions are rock climbing, fly-fishing, mountain biking, and playing the guitar.